Check for updates

RESEARCH ARTICLE

Onshore surface–subsurface correlation of orogenic structures and the continuation of the late Paleozoic Gondwanides in the Tierra del Fuego fold-and-thrust belt, southern Patagonia

[version 1; peer review: awaiting peer review]

Jean-Baptiste P. Koehl[1], Rocio E. Gallardo Jara[2], Juan Ortiz[2], John Ballesteros Prada[3], Benjamín Sandoval-Leal[4], Sebastián Parra Irribarra[5]

[1]Grannes terrasse 107, Hafrsfjord, Rogaland, 4044, Norway
[2]Soil and Natural Resources, University of Concepción, Chillan, Ñuble, 3812120, Chile
[3]CONICET, IIDyPCa, National University of Río Negro, San Carlos de Bariloche, Río Negro, 8400, Argentina
[4]Faculty of Architecture, Geography and Urbanism, University of Concepción, Concepción, Bío Bío, 4070386, Chile
[5]Department of Earth Sciences, University of Concepción, Concepción, Bío Bío, 4070386, Chile

v1 **First published:** 24 Sep 2026, **6**:375
https://doi.org/10.12688/openreseurope.24310.1
Latest published: 24 Sep 2026, **6**:375
https://doi.org/10.12688/openreseurope.24310.1

Open Peer Review

Approval Status *AWAITING PEER REVIEW*

Any reports and responses or comments on the article can be found at the end of the article.

Abstract

Background

The Cretaceous–Cenozoic Tierra del Fuego fold-and-thrust belt in southern Patagonia exposes Paleozoic–Cenozoic rocks recording the protracted, subduction-dominated tectonic evolution of South America, from Cambrian–Ordovician magmatism to Permian metamorphism, Jurassic backarc basin formation, Cretaceous–Cenozoic contraction, and ongoing transtension.

Methods

High-resolution seismic reflection data were used to interpret tectonic structures in the subsurface and correlate them with surface outcrops and nearby exploration wellbores. The study leverages recent findings in the subsurface architecture and seismic facies of orogenic structures.

Results

Hundred-meter-scale asymmetric, thrust-related and parasitic folds

and related structures in surface outcrops are tied to equivalent structures in subsurface seismic data. Seismic structural mapping suggests that Paleozoic basement rocks in southern Patagonia were involved in more than one episode of contraction, including a pre-Jurassic episode and that Jurassic–Lower Cretaceous basins correspond to broad open synclines instead of fault-bounded (half-) grabens and recorded two phases of Cretaceous–Cenozoic contractional deformation.

Conclusions

The present study validates the seismic facies of hundred-meter- to km-scale orogenic structures in the subsurface, thus opening new avenues for detailed structural studies in intensely deformed crustal domains. The Permian Gondwanide Orogen extends to southern Patagonia, which should be considered as a single tectonic block with northern Patagonia, the Falkland Islands and Maurice Ewing Bank at least since the Permian and probably since the early Cambrian, thus providing valuable anchors for future plate reconstructions. Jurassic–Lower Cretaceous volcanosedimentary rocks were deposited during a period of tectonic quiescence, possibly in a passive backarc setting, and were later deformed (1) in the mid-Early to mid-Cretaceous and (2) mildly reworked in the Late Cretaceous–Paleogene during the formation of the Tierra del Fuego fold-and-thrust belt. Only tenuous traces of Cenozoic extension were found in the subsurface, thus suggesting a limited and/or localized impact of the ongoing transtensional tectonic regime.

Plain Language summary

The Tierra del Fuego fold-and-thrust belt in southern Patagonia reflects convergent tectonic plate movements dominated almost continuously by subduction of oceanic crust below the South America continental crust for the past ca. 550–500 Myr.

Using seismic imaging of regional crustal transects, previous field studies, and drilling results from exploration for natural resources in the Fuegian Andes, the present work attempts at providing a clearer understanding of the tectonic evolution of southern Patagonia and its long-term connection to nearby regions such as northern Patagonia, the Malvinas Basin, Maurice Ewing Bank, but also South Africa, Antarctica, New Zealand, Australia, and Indonesia.

The results show that the continental crust in southern Patagonia was part of a large mountain-chain building episode (plate collision) ca. 300–250 Myr ago. While subduction and convergence may have continued, the study area then experienced a period of quiescence until ca. 125–120 Myr ago, when renewed convergence resulted the formation of the Tierra del Fuego mountain range. The impact of ongoing lateral to divergent plate movements is, however, unclear and might be limited and/or restricted to narrow areas.

Keywords
Patagonia, Tierra del Fuego, Gondwanides, Thrust, Cenozoic, Cretaceous, Jurassic, Permian, Cambrian, Fold

This article is included in the Horizon 2020 gateway.

This article is included in the Marie-Sklodowska-Curie Actions (MSCA) gateway.

Corresponding author: Jean-Baptiste P. Koehl (jeanbaptiste.koehl@gmail.com)

Author roles: Koehl JBP: Conceptualization, Data Curation, Formal Analysis, Funding Acquisition, Investigation, Methodology, Project Administration, Resources, Validation, Visualization, Writing – Original Draft Preparation, Writing – Review & Editing; **Gallardo Jara RE**: Conceptualization, Investigation, Validation, Visualization, Writing – Review & Editing; **Ortiz J**: Investigation, Validation, Writing – Review & Editing; **Ballesteros Prada J**: Investigation, Validation, Writing – Review & Editing; **Sandoval-Leal B**: Investigation, Validation, Writing – Review & Editing; **Parra Irribarra S**: Investigation, Validation, Writing – Review & Editing

Competing interests: No competing interests were disclosed.

Grant information: This project has received funding from the [European Union's Horizon 2020 research and innovation programme under grant agreement No [101023439].
The funders had no role in study design, data collection and analysis, decision to publish, or preparation of the manuscript.

Copyright: © 2026 Koehl JBP *et al*. This is an open access article distributed under the terms of the Creative Commons Attribution License, which permits unrestricted use, distribution, and reproduction in any medium, provided the original work is properly cited.

How to cite this article: Koehl JBP, Gallardo Jara RE, Ortiz J *et al.* **Onshore surface–subsurface correlation of orogenic structures and the continuation of the late Paleozoic Gondwanides in the Tierra del Fuego fold-and-thrust belt, southern Patagonia [version 1; peer review: awaiting peer review]** Open Research Europe 2026, **6**:375 https://doi.org/10.12688/openreseurope.24310.1

First published: 24 Sep 2026, **6**:375 https://doi.org/10.12688/openreseurope.24310.1

Introduction

Despite decades of field studies, regional subsurface mapping, and exploration drilling, the long-term relationships of southern Patagonia and the Fuegian Andes with adjacent regions (e.g., Maurice Ewing Bank and northern Patagonia) remain elusive (Figure 1a). This is particularly well illustrated by the uncertain relationship of southern Patagonia with the rest of the South American continent in Precambrian–early Paleozoic plate reconstructions (e.g., Domeier & Torsvik, 2014; Ramos, 2008). This is partly related to the remoteness of the area and to the relatively young geological period reflected by accessible rocks in the area (up to early Cambrian magmatic protoliths in exploration wellbores; Barbeau Jr *et al.*, 2009; Hervé *et al.*, 2010a; Hervé *et al.*, 2010b).

The goal of the present study is to reexamine regional subsurface seismic reflection data in the light of recent advances in structural mapping (e.g., Koehl *et al.*, 2022; Koehl *et al.*, 2023a; Phillips *et al.*, 2016; Stewart & Salem, 2023) and recent results in the study area (e.g., Gallardo Jara *et al.*, 2019; Gallardo Jara *et al.*, 2022; Mosqueira González *et al.*, 2021; Torres Carbonell *et al.*, 2013; Torres Carbonell *et al.*, 2020; Zanella *et al.*, 2014) and nearby regions (e.g., McCarthy *et al.*, 2017; Ramos *et al.*, 2019; Stanca *et al.*, 2022). The study notably aims at tying hundred-meters- to km-scale orogenic structures (e.g., folds, thrusts, duplexes) in outcrops to their potential equivalent in seismic reflection data, refine the tectonic evolution of the Tierra del Fuego fold-and-thrust belt (Figure 1a) and compare it to that of nearby regions, and further showcase the use of seismic reflection data as a tool for detailed tectonic and structural studies.

The results have implications for subsurface exploration of natural resources, such as hydrocarbons (e.g., extent of continental crust in the subsurface; Angulo & Vargas, 2022) and natural hydrogen along major fault zones (e.g., Lefeuvre *et al.*, 2021; Moretti *et al.*, 2021; Osselin *et al.*, 2022; Wang *et al.*, 2023), e.g., with respect to up-dip segmentation of brittle faults for fluid pathways in the crust. The study also provides new anchors for Precambrian–Paleozoic plate reconstructions, which has implications for the energy transition (e.g., Wrobel-Daveau *et al.*, 2022), and further support for emerging new concepts such as Orogenic Bridge Theory (Koehl & Foulger, 2025), which is partly based on regional subsurface mapping of crustal- to hundred-meter-scale orogenic structures (e.g., Koehl, 2025; Koehl, 2026a).

Geological setting

The study area experienced a protracted tectonic history in the Phanerozoic, including (late Neoproterozoic?–) early Paleozoic magmatism, contractional deformation episodes in the Permian and Late Cretaceous–Cenozoic, and a Jurassic–Earliest Cretaceous rifting episode.

Precambrian (?) to early Paleozoic metamorphic basement rocks

Igneous basement rocks below the Tierra del Fuego fold-and-thrust belt in southern Patagonia are early Paleozoic in age. They are part of the Tierra del Fuego igneous and metamorphic complex and were possibly intruded during the Pampean Orogeny (Hervé *et al.*, 2010a; Hervé *et al.*, 2010b; Pankhurst *et al.*, 2003; Söllner *et al.*, 2000). They consist of migmatitic orthogneisses and peraluminous granitoids, some of which contain cordierite and garnet (i.e., high-pressure high-temperature metamorphism; Hervé *et al.*, 2010a). Igneous protoliths in orthogneiss from exploration well Gaviota 6 (San Sebastián Bay; Figure 1b) yielded U–Pb crystallization ages of 529 ± 7.5 Ma and 523 ± 5 Ma (Pankhurst *et al.*, 2003; Söllner *et al.*, 2000). Comparably, Hervé *et al.* (2010a) obtained U–Pb protolith crystallization ages of 523 ± 7 Ma (Águila 2 wellbore), 522 ± 6 Ma (Gaviota 6 wellbore), and 538 ± 6 Ma (María Emilia 2 wellbore) for orthogneisses, and ca. 525 Ma, and latest Mesoproterozoic–earliest Neoproterozoic and late Neoproterozoic ages for inherited zircons in a migmatite in the Monte Aymond 20 wellbore (Figure 1b). Two samples recovered near the bottom of exploration wells Lago Mercedes 1 and 2 yielded U–Pb crystallization ages of 527.2 ± 2.7 Ma (amphibolitic schist) and 536 ± 2.4 Ma (banded orthogneiss) with input from latest Mesoproterozoic–earliest Neoproterozoic and late Neoproterozoic detrital zircons (i.e., Grenvillian and Brasiliano orogens; Hervé *et al.*, 2010b; Figure 1b).

Farther southwest, early Paleozoic, up to amphibolite-facies, metasedimentary rocks of the Darwin Cordillera metamorphic complex are exposed in the core of the Tierra del Fuego fold-and-thrust belt (Betka *et al.*, 2022; Nelson *et al.*, 1980; Figure 1c). The deposition of the sediments is constrained to the (Cambrian?–) Ordovician–Early Devonian by U–Pb geochronology of detrital zircons (Hervé *et al.*, 2010b). Despite similar concentrations in Ordovician detrital zircons, the relatively low quantity of Cambrian zircons in metasedimentary rocks of the Darwin Cordillera metamorphic complex contrasts with the abundance of Cambrian zircons in rocks of the Tierra del Fuego igneous and metamorphic complex (Barbeau Jr *et al.*, 2009; Hervé *et al.*, 2010b). It was thus suggested that basement rocks of the Darwin Cordillera metamorphic complex are separated from the Tierra del Fuego igneous and metamorphic complex by a pre-Jurassic suture zone and belong to an exotic terrane (Hervé *et al.*, 2010b).

Cambrian–Ordovician ages indicate links to the Pampean and Famatinian orogenies farther north (e.g., Cristofolini *et al.*, 2014; Pankhurst *et al.*, 1998; Ramos *et al.*, 2014; Ramos *et al.*, 2015; Rapela *et al.*, 1998; Schwartz *et al.*, 2008; Steenken

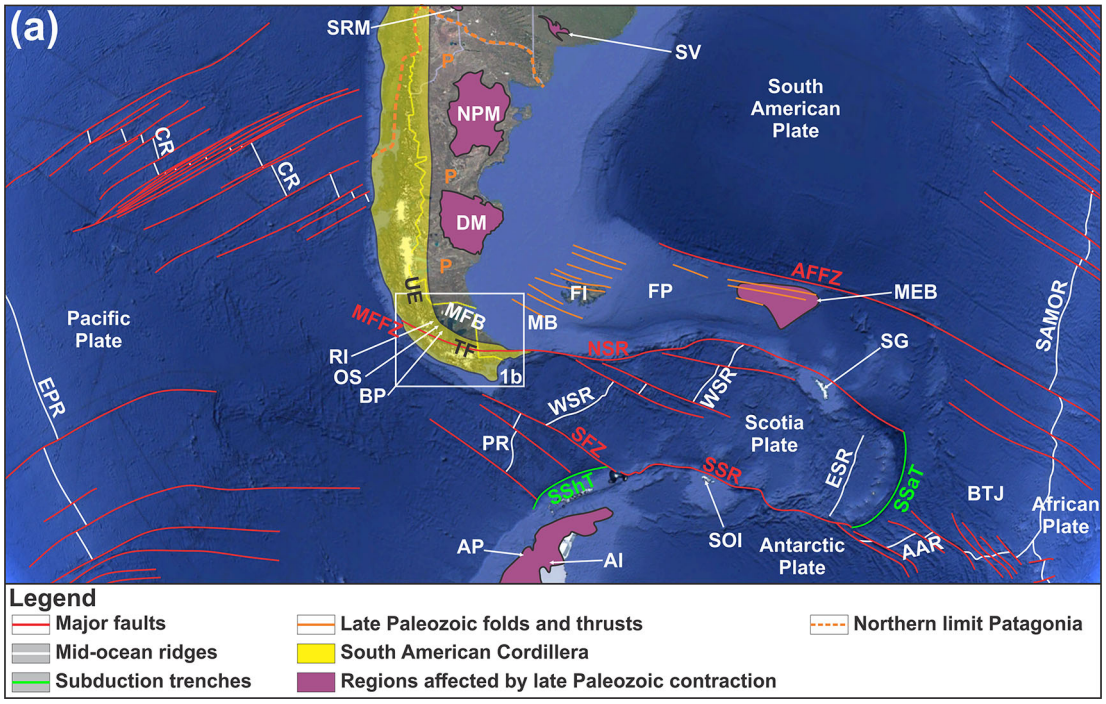

Figure 1. (a) Regional tectonic map of Patagonia and nearby regions. The late Paleozoic structures of the Cape Fold Belt in the Malvinas Basin, Falkland Islands, Falkland Plateau, and Maurice Ewing Bank are from McCarthy *et al.* (2017), Ramos *et al.* (2019), and Stanca *et al.* (2022). The basemap is from © Google Earth. Abbreviations: AAR: American–Antarctic Ridge; AFFZ: Agulhas–Falkland fault zone; AI: Adie Inlet; AP: Antarctic Peninsula; BP: Brunswick Peninsula; BTJ: Bouvet Triple Junction; CR: Chile Ridge; DM: Deseado Massif; EPR: East Pacific Rise; ESR: East Scotia Ridge; FI: Falkland Islands; FP: Falkland Plateau; MB: Malvinas Basin; MEB: Maurice Ewing Bank; MFB: Magallanes foreland basin; MFFZ: Magallanes–Fagnano Fault Zone; NPM: North Patagonian Massif; NSR: North Scotia Ridge; OS: Otway Sound; P: Patagonia; PR: Phoeniz Ridge; RI: Riesco Island; SAMOR: South Atlantic mid-ocean ridge; SFZ: Shackleton fault zone; SG: South Georgia; SOI: South Orkney Island; SRM: San Rafael Massif; SSaT: South Sandwich Trench; SShT: South Shetland Trench; SSR: South Scotia Ridge; SV: Sierra de la Ventana fold-and-thrust belt; TF: Tierra del Fuego fold-and-thrust belt; UE: Última Esperanza province; WSR: West Scotia Ridge. (b) Structural map of the Tierra del Fuego fold-and-thrust belt showing regional seismic reflection profiles and major structures. Major fault zones are from Álvarez-Marrón *et al.* (1993), Betka *et al.* (2022), Gallardo Jara *et al.* (2022), Muller *et al.* (2020), Torres Carbonell *et al.* (2013), Torres Carbonell *et al.* (2020), and Zanella *et al.* (2014). The thick yellow line shows the location of seismic profile PR-1 (Figure 3a–h). The locations of regional seismic reflection profiles, exploration wellbores, and Jurassic–Lower Cretaceous synclines are from Gallardo Jara *et al.* (2022) and those of the seismic stations from Buffoni *et al.* (2018). Note that the northern thrust front interpretation is from Torres Carbonell *et al.* (2013) and Torres Carbonell *et al.* (2020), whereas the southern interpretation is from Malkowski *et al.* (2015) and Muller *et al.* (2020). Abbreviations: Ag: Aguíla 2 wellbore; Av: Avutarda 1A wellbore; BC: Beagle Channel; BP: Brunswick Peninsula; Cb: Cachimba 1 wellbore; Ci: Cisne 1 wellbore; Co: Cormorán 1 wellbore; Cr: Carmen 1 wellbore; Ct: Catalina 1 wellbore; DC: Darwin Cordillera; DeS: Delfin syncline; DI: Dawson Island; DoS: Dorado syncline; DuS: Dungeness syncline; ETF: Eastern Tobífera fault zone; Ev: Evans 1 wellbore; Fa: Flamenco 4 wellbore; FS: Fueguino syncline; G: Gaviota 1 & 6 wellbores; GS: Gaviota syncline; IB: Inútil Bay; LB: Lago Blanco; LF: Lago Fagnano; LM: Lago Mercedes 1 & 2 wellbores; LPF: La Pera fault zone; MA: Monte Aymond 20 wellbore; MaS: Manantiales syncline; ME: María Emilia 2 & 3 wellbores; MFFZ: Magallanes–Fagnano fault zone; MP: Mitre Peninsula; MS: Magellan Strait; MSZ: Magallanes shear zone; MuS: Munición syncline; Mz: Manzano 7 wellbore; NS: Neptuno syncline; OrS: Oriental/Ostión/Calafate syncline; OS: Otway Sound; OvS: Olivos syncline; PA: Punta Arenas; PB: Punta Baja 1 wellbore; RC: Río Chico 1 wellbore; RF: Rocallosa fault zone; RG: Río Grande; RI: Riesco Island; SA: Sierra de Apen; SB: Sierra de Beauvoir; SSB: San Sebastián Bay; TF: Thrust Front; To: Tolhuin; Us: Ushuaia; VF: Vicuña fault zone; VS: Vania syncline; V1: Vicuña 1 wellbore; V2: Vicuña 2 wellbore. (c) Geological map of the study area in Isla Grande de Tierra del Fuego. The thick black line shows the location of seismic profile PR-1 (Figure 3a–h). Tectonic structures are from Álvarez-Marrón *et al.* (1993); Gallardo Jara *et al.* (2022), Lozano *et al.* (2020), Torres Carbonell *et al.* (2013), Torres Carbonell *et al.* (2016), Torres Carbonell *et al.* (2020), and Zanella *et al.* (2014). The rock units are modified after Sáez Moreno (2017), Sánchez *et al.* (2010), and Torres Carbonell *et al.* (2020). The northern and southern interpretations of the Colo-Colo fault zone are from Álvarez-Marrón *et al.* (1993) and Zanella *et al.* (2014) respectively. Abbreviations: AMF: Apen–Malvinera fault system; Ag: Aguíla 2 wellbore; AS: Aurelia Syncline; Av: Avutarda 1A wellbore; BAA: Buenos Aires Anticline; BBF: Bahia Bell fault zone; BS: Ballena Syncline; CA: Constancia Anticline; Cb: Cachimba 1 wellbore; CCF: Colo-Colo fault zone; Ci: Cisne 1 wellbore; Co: Cormorán 1 wellbore; Cr: Carmen 1 wellbore; Ct: Catalina 1 wellbore; DA: Despedida Anticline; DC: Darwin Cordillera; DeS: Delfin syncline; DoS: Dorado syncline; Ev: Evans 1 wellbore; Fa: Flamenco 4 wellbore; FS: Fueguino syncline; G: Gaviota 1 & 6 wellbores; GS: Gaviota syncline; IB: Inútil Bay; LB: Lago Blanco; LCS: Los Cerros Syncline; LF: Lago Fagnano; LM: Lago Mercedes 1 & 2 wellbores; MaS: Manantiales syncline; McF: Mercedes fault zone; ME: María Emilia 2 & 3 wellbores; MF: Mercedes fault zone; MFFZ: Magallanes–Fagnano fault zone; MiA: Miraflores Anticline; MoA: Moneta Anticline; MrF: Marinelli fault zone; MS: Magellan Strait; OrS: Oriental/Ostión/Calafate syncline; OvS: Olivos syncline; PA: Pilarica Anticline; PB: Punta Baja 1 wellbore; RA: Ruby Anticline; RC: Río Chico 1 wellbore; RG: Río Grande; RJD: Río Jackson Detachment; RPF: Río Paralelo–Rocha fault zone; SA: Sierra de Apen; SB: Sierra de Beauvoir; SJA: San Justo Anticline; SSB: San Sebastian Bay; TF: Thrust Front; To: Tolhuin; Us: Ushuaia; VF: Vicuña fault zone; V1: Vicuña 1 wellbore; V2: Vicuña 2 wellbore; YF: Yartou fault zone.

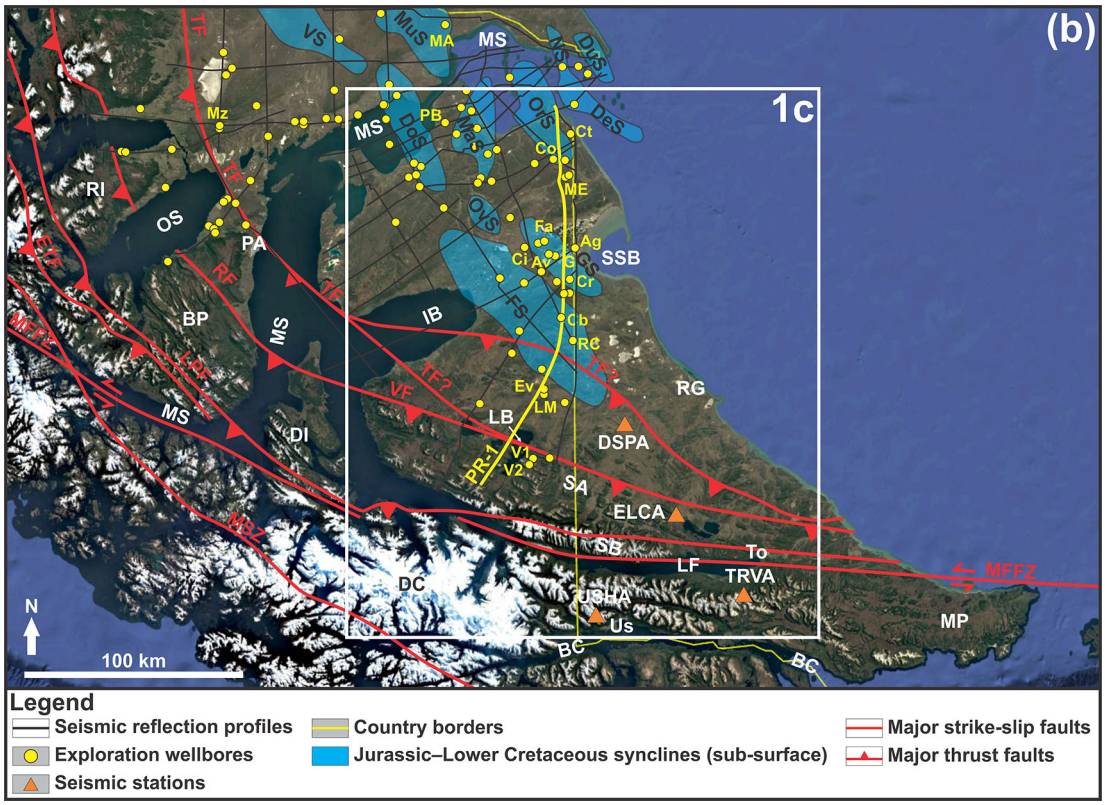

Figure 1. (continued)

et al., 2011; Verdecchia *et al.*, 2011; von Gosen *et al.*, 2002). However, the southern extent of these orogens remains uncertain.

Permian Gondwanides

The Tierra del Fuego igneous and metamorphic complex was later affected by a thermal event in the Permian, which resulted in high-grade metamorphism and anatexis in the Permian (ca. 292–254 Ma; Halpern, 1973; Hervé *et al.*, 2010a) and related post-orogenic magmatism at ca. 255 Ma (Castillo *et al.*, 2017). Notably, Hervé *et al.* (2010a) obtained a 267 ± 3 Ma U–Pb zircon age for metamorphism in the Punta Baja area (Figure 1b) with associated P-T conditions of 2–3 kbar and 760–770°C. Thus, the tectonomagmatic record of southern Patagonia is comparable to that of the Antarctica Peninsula (e.g., 258 ± 3 Ma U–Pb zircon age for metamorphism in migmatitic gneiss in Adie Inlet; Curtis, 2001; Elliott *et al.*, 2019; Millar *et al.*, 2002; Riley *et al.*, 2022; Figure 1a) and the Cape Fold Belt in South Africa (e.g., ca. 276–261 Ma ^{40}Ar–^{39}Ar ages for the onset of deformation and ca. 255–248 Ma ages for post-deformation cooling and exhumation; Hansma *et al.*, 2016), i.e., suggesting a common tectonic history.

Jurassic–Early Cretaceous Breakup of Gondwana

A thermal event occurred in the Middle–Late Jurassic as suggested by 161.6 ± 4.5 Ma and 178.4 ± 1.4 Ma Rb–Sr ages obtained for a greenschist-facies metamorphism in the Gaviota 6 wellbore (Figure 1b–c) potentially associated with the initial breakup of Gondwana and deposition of sedimentary rocks of the Rocas Verde basin, a possible backarc basin in southern Patagonia (Pankhurst *et al.*, 2000; Söllner *et al.*, 2000). This event is coeval with the deposition of silicic volcanics and clastic sedimentary rocks of the Tobífera Formation (Lemaire and Lapataia formations in Argentina; González Guillot *et al.*, 2016; Mosqueira González *et al.*, 2021) in NW–SE- to N–S-striking (half-) grabens on the Atlantic portion of Patagonia (e.g., Oriental/Ostión/Calafate, Fueguino, and Gaviota grabens; Gallardo, 2014; Gallardo Jara *et al.*, 2022 their fig. 9a; Miller *et al.*, 2022; Robbiano *et al.*, 1996; Figure 1b–c), calcalkaline volcanics of the Hardy Formation (Miller *et al.*, 1994; Suárez, 1979), and intrusion of Ordovician–Devonian metasedimentary rocks of the Darwin Cordillera metamorphic complex by a Late Jurassic granitic gneiss (Darwin Granite) on the Pacific side (Betka *et al.*, 2022; Figure 1b–c). Volcanics of the Tobífera Formation yielded latest Early–Middle Jurassic U–Pb (178.4 ± 1.4 – Gaviota 6 wellbore, and 171.8 ± 1.2 Ma – outcrop in western Patagonia; Pankhurst *et al.*, 2000) and Middle Jurassic–earliest Cretaceous (Valanginian) K–Ar ages (170 ± 5 Ma – Cisne 4 wellbore, 150 ± 5 Ma – Carmen 7 wellbore,

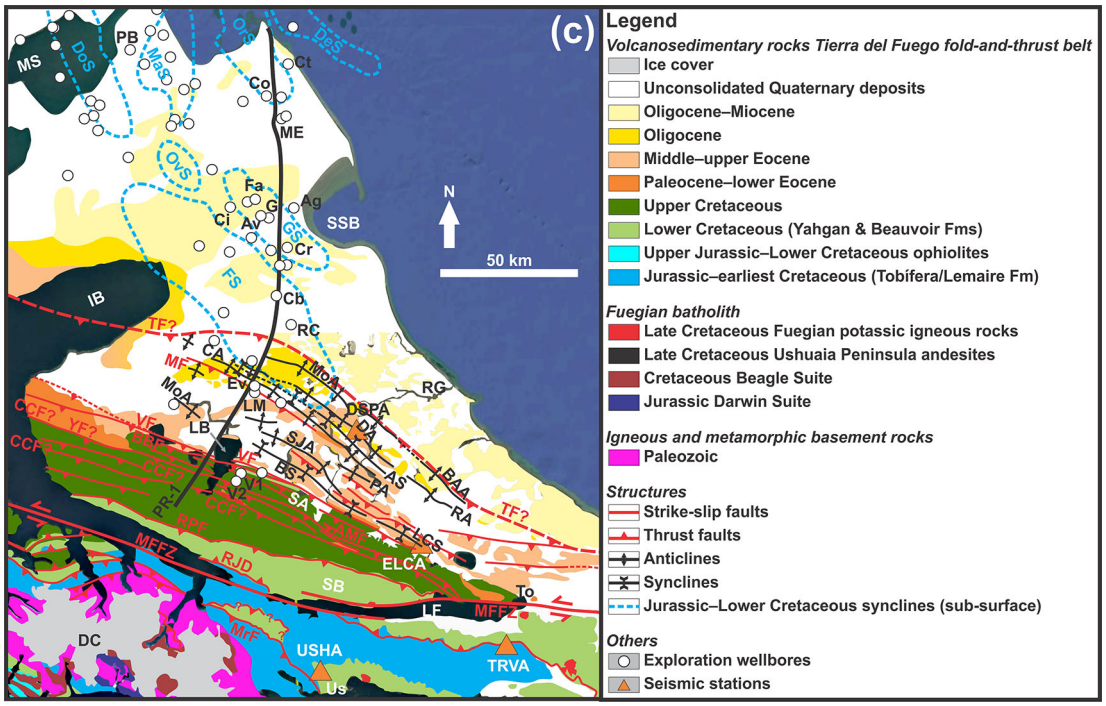

Figure 1. (continued)

135 ± 3 Ma – Avutarda 1A wellbore, and 134 ± 3 Ma – Flamenco 4 wellbore; ENAP, 1991; Gallardo Jara *et al.*, 2022), as well as a Late Jurassic maximum deposition age (ca. 160 Ma) based on detrital zircons (Muller *et al.*, 2020; Figure 1b and Figure 2).

Volcanosedimentary rocks of the Tobífera Formation are unconformably covered by lowermost Cretaceous, fluvial to shallow-marine clastic sediments of the Springhill Formation under the Magallanes foreland basin (Gallardo Jara *et al.*, 2022; Robbiano *et al.*, 1996) and upper Lower Cretaceous Zapata Formation in the west (maximum deposition age of ca. 125 Ma; Muller *et al.*, 2020; Figure 2). Deposition occurred during a period of global transgression and was diachronous in the study area, starting in the Berriasian (?) or Valanginian (i.e., partly coeval with the upper part of the Tobífera Formation volcanics; Gallardo Jara *et al.*, 2022) and ending in the Barremian (Quattrocchio *et al.*, 2006; Riccardi, 1977; Schwarz *et al.*, 2010).

In the south, latest Jurassic–earliest Cretaceous, mafic–intermediate volcanics of the Hardy Formation (partly coeval with the Tobífera Formation) interfinger with shale-rich marine sedimentary rocks of the Yaghan Formation, which were deposited onto the Darwin Cordillera metamorphic complex and yielded latest Jurassic–Early Cretaceous ages based on paleontological and detrital zircon studies, including a maximum deposition age of ca. 148 Ma (Halpern & Rex, 1972; Klepeis *et al.*, 2010; Muller *et al.*, 2020; Figure 1c and Figure 2), and a minimum deposition age of ca. 101 Ma for its time equivalent in the west (Zapata Formation; Fosdick *et al.*, 2011), i.e., coeval with the emplacement of Early–mid Cretaceous basalts (ca. 137–93 Ma) at the intersection of the North Scotia Ridge and northernmost West Scotia Ridge (Riley *et al.*, 2019; Figure 1a) and with the onset of seafloor spreading in the South Atlantic at ca. 125–100 Ma (e.g., Barker, 2001; Eagles, 2007; Scotchman *et al.*, 2010; Figure 2). In the study area, Lower Cretaceous sediments consist of tightly (isoclinally) folded and foliated (banded) shale–slate and metapelites of the Río Jackson Formation and Beauvoir Formation (Gallardo Jara *et al.*, 2022; Klepeis, 1994a; Zanella *et al.*, 2014). The Beauvoir Formation contains Aptian–Albian fossils (e.g., Martinioni *et al.*, 2013) and is a time correlative of the Zapata and Vicuña and La Paciencia formations in the subsurface and in western Pagatonia (Gallardo Jara *et al.*, 2022; Muller *et al.*, 2020). NW–SE-striking (transform- and/or ridge-push-related?) strike-slip faults have been postulated to explain potential basin segmentation along a N–S-trending axis based on stratigraphic variations (Ghiglione *et al.*, 2015).

Late Cretaceous–Cenozoic Tierra del Fuego fold-and-thrust belt and Cenozoic opening of the Drake Passage

In the Late Cretaceous–Paleocene, Jurassic–Early Cretaceous rift-related sedimentary rocks of the Rocas Verde basin (Hardy, Tobífera, Yaghan, and Zapata formations), related Late Jurassic intrusions (e.g., Darwin Granite), and underlying Ordovician–Devonian rocks of the Darwin Cordillera metamorphic complex were intensely sheared, imbricated, and thrust overall to the north-northeast along the Magallanes shear zone and Magallanes décollement (Betka *et al.*, 2022; Figure 1b). These rocks recorded greenschist–amphibolite-facies metamorphism, which culminated with the formation of the Tierra del Fuego fold-and-thrust belt (also known as Magallanes foreland fold-and-thrust belt) and Patagonian Orocline (Betka *et al.*, 2022; Gombosi *et al.*, 2009; Klepeis, 1994a; Poblete *et al.*, 2014).

In the foreland to the north, previous studies have shown evidence of a décollement level between Paleozoic basement rocks and overlying Mesozoic–Cenozoic volcanosedimentary rocks of the Rocas Verde and Magallanes foreland basins, illustrated by tens of km wide duplex structures and thrust imbricates (e.g., Álvarez-Marrón *et al.*, 1993). The initiation of foreland sedimentation in southern Patagonia is constrained to ca. 92 Ma by U–Pb ages on detrital zircon (Fildani *et al.*, 2003). This is consistent with the ca. 86–83 Ma U–Pb crystallization age for both deformed and undeformed intrusions, which indicate protracted deformation (i.e., various events of localized deformation), ca. 73–70 Ma ^{40}Ar–^{39}Ar ages for late (back?-) thrusting (Klepeis *et al.*, 2010; Muller *et al.*, 2020; Torres Carbonell *et al.*, 2020), and ca. 86–65 Ma ^{40}Ar–^{39}Ar ages for high-grade metamorphism in the Darwin Cordillera metamorphic complex (Kohn *et al.*, 1995). However, ca. 130–91 Ma K–Ar ages for brittle–ductile, mylonitic and cataclastic shear zones in southern Tierra del Fuego suggest that contractional deformation initiated as early as the mid-Early Cretaceous (Suárez *et al.*, 2000).

In the study area, the Tierra del Fuego fold-and-thrust belt is bounded to the north by the a 12–15 km wide system of imbricate brittle–ductile thrusts with top-NNE kinematics consisting from north to south of the Vicuña, Yartou and

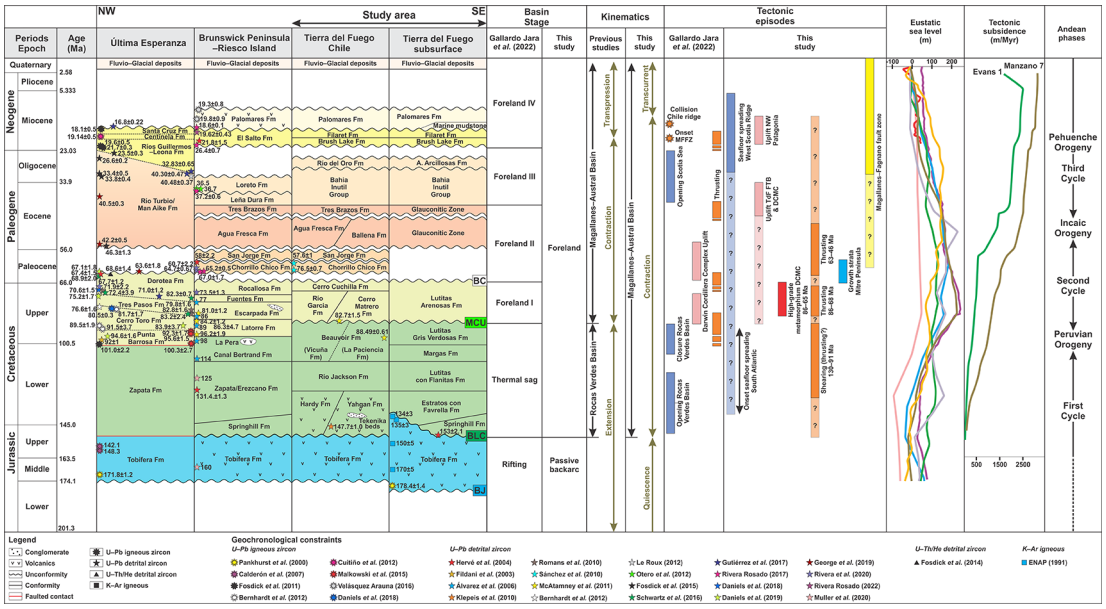

Figure 2. Stratigraphic chart of the study area (Tierra del Fuego) and nearby areas. The chart for Tierra del Fuego and the Brunswick Peninsula–Riesco Island area is after Gallardo Jara *et al.* (2022) and based on Fosdick *et al.* (2011) for the Última Esperanza area. Geochronological constraints on unit deposition is in Ma. ENAP ages are after Gallardo Jara *et al.* (2022). Eustatic sea level variation curves are from van der Meer *et al.* (2022; see references therein). The 20–12 Ma uplift in northwestern Patagonia is from Blisniuk *et al.* (2006) and Aramendía *et al.* (2022). Note that the Centinella Formation is the equivalent to the Estancia 25 de Mayo Formation (e.g., Gutiérrez *et al.*, 2017). Chronostratigraphic ages are from the Geological Time Scale 6.0 (Walker & Geissman, 2022). Geochronological ages are from Álvarez *et al.* (2006), Bernhardt *et al.* (2012), Calderón *et al.* (2007), Cuitiño *et al.* (2012), Daniels *et al.* (2018), Daniels *et al.* (2019), ENAP (1991), Fildani *et al.* (2003), Fosdick *et al.* (2011), Fosdick *et al.* (2014), Fosdick *et al.* (2015), George *et al.* (2019), Gutiérrez *et al.* (2017), Hervé *et al.* (2004), Klepeis *et al.* (2010), Le Roux (2012), Malkowski *et al.* (2015), McAtamney *et al.* (2011), Muller *et al.* (2020), Otero *et al.* (2012), Pankhurst *et al.* (2000), Rivera *et al.* (2020), Rivera Rosado (2017), Rivera Rosado (2022), Romans *et al.* (2010), Sánchez *et al.* (2010), Schwartz *et al.* (2016), and Velásquez Arauna (2016). Abbreviations: BC: Base Cenozoic horizon; BJ: Base Jurassic horizon; BLC: Base Lower Cretaceous horizon; MCU: Mid-Cretaceous Unconformity horizon; MFFZ: Magallanes–Fagnano fault zone.

Apen–Malvinera, Bahia Bell, Colo-Colo, and Río Paralelo and Rocha fault zones (Álvarez-Marrón *et al.*, 1993; Gallardo Jara *et al.*, 2019; Mosqueira González *et al.*, 2021; Rojas & Mpodozis, 2006; Torres Carbonell *et al.*, 2016; Zanella *et al.*, 2014; Figure 1c). There, upper Lower Cretaceous (Aptian–Albian) to Paleocene sedimentary rocks are deformed into moderately open to tight (e.g., chevron-type), inclined to overturned, up to 2–3 km wide, NNE-verging asymmetric folds and crosscut by undeformed intrusions, which yielded ca. 74–73 Ma ^{40}Ar–^{39}Ar and a ca. 68 Ma U–Pb ages (Mosqueira González *et al.*, 2021; Torres Carbonell *et al.*, 2020). Related moderately SSW-dipping foliation grades from intense and continuous in lower structural levels (e.g., Beauvoir Formation; Figure 2) to discontinuous and spaced in upper structural units (Mosqueira González *et al.*, 2021). Local brittle–ductile mylonitic shear zones are up to several hundreds of meters wide and display isoclinal folding of the foliation and cataclastic fault rocks (Esteban *et al.*, 2011; González Guillot *et al.*, 2010; Menichetti *et al.*, 2008; Mosqueira González *et al.*, 2021; Suárez *et al.*, 2000; Torres Carbonell *et al.*, 2020). Deformation in the Magallanes foreland basin is milder and include open upright folds and SSW-dipping low-angle thrusts, e.g., Mercedes fault zone (Gallardo Jara *et al.*, 2022), Constancia Anticline, Aurelia Syncline, and Despedida Anticline (Torres Carbonell *et al.*, 2016; Figure 1c).

Cenozoic opening of the Scotia Sea

The Magallanes–Fagnano fault system in southern Patagonia is a major transform plate boundary between the Scotia and the South American plates, which continues as the North Scotia Ridge fault in the east (Ghiglione *et al.*, 2008; Klepeis, 1994b; Restelli *et al.*, 2025; Riley *et al.*, 2019; Figure 1a). It has accommodated up to 55 km of Cenozoic left-lateral displacement in response to seafloor spreading at the now-extinct West Scotia Ridge and more recent (currently active) East Scotia Ridge from ca. 30 Ma to present (Barker, 2001; Eagles, 2007; Eagles, 2010; Hervé *et al.*, 2010b; Klepeis, 1994b; Riley *et al.*, 2019; Rossello, 2005; Torres Carbonell *et al.*, 2008; Figure 1a). Nevertheless, rifting and sinistral-normal movements along the Magallanes–Fagnano fault system probably initiated as early as 62 Ma, as suggested by paleomagnetic data (Gao *et al.*, 2025) and latest Paleocene–early Eocene normal faulting along related E–W-striking faults (Ghiglione *et al.*, 2008), i.e., coeval with an episode of rapid exhumation in the Tierra del Fuego fold-and-thrust belt at ca. 45–34 Ma (Gombosi *et al.*, 2009). Both extensional and contractional deformation mechanisms have been proposed for this cooling episode (e.g., Dalziel & Brown, 1989; Gombosi *et al.*, 2009). Despite moderate Cenozoic lateral displacement (≤ 55 km), the Magallanes–Fagnano fault system juxtaposes early Paleozoic blocks of seemingly different origin suggested by a relatively low concentration in Cambrian detrital zircons in Paleozoic rocks south of the fault. It was thus suggested that the Magallanes–Fagnano fault system may have formed along a pre-Jurassic suture zone (Hervé *et al.*, 2010b).

Methods

Seismic data

The present study uses existing seismic reflection data from the Chilean National Hydrocarbon Company (ENAP; e.g., Gallardo, 2014; Gallardo Jara *et al.*, 2022; Figure 1b), to map orogenic structures in the Tierra del Fuego fold-and-thrust belt in southern Patagonia with emphasis on the internal architecture of major thrust systems (e.g., Vicuña fault zone; Álvarez-Marrón *et al.*, 1993; Gallardo Jara *et al.*, 2019). The study builds on recent advances in interpreting orogenic structures in seismic reflection data, such as mylonitic surfaces (e.g., Fazlikhani *et al.*, 2017; Fountain *et al.*, 1984; Hurich *et al.*, 1985; Phillips *et al.*, 2016; Reeve *et al.*, 2013) and hundred-meter- to km-scale folds, duplexes, and thrust faults (e.g., Koehl, 2021; Koehl & Allaart, 2021; Koehl *et al.*, 2022; Koehl *et al.*, 2023a; Koehl *et al.*, 2023b; Koehl and Stokmo, 2025; Koehl, 2025; Koehl *et al.*, 2024; Koehl, 2026a). Interpreted structures and stratigraphic units in the subsurface are tied to nearby exploration wells, e.g., Lago Mercedes 1, Rio Chico 1, Cachimba 1, Carmen 1, Gaviota 1, Cisne 1, and María Emilia 3 (Gallardo Jara *et al.*, 2022; Hervé *et al.*, 2010a; Pankhurst *et al.*, 2003; Söllner *et al.*, 2000), and to surface outcrops in the study area (e.g., Klepeis, 1994a; Mosqueira González *et al.*, 2021; Torres Carbonell *et al.*, 2020) and are then compared to previous seismic mapping in the Tierra del Fuego fold-and-thrust belt (e.g., Álvarez-Marrón *et al.*, 1993; Gallardo Jara *et al.*, 2022; Miller *et al.*, 2022; Figure 1b–c). High-resolution versions of the figures necessary to examine the interpreted reflections and structures in detail are available on Zenodo (Koehl, 2026b; https://doi.org/10.5281/zenodo.20640160).

Data resolution

The data were acquired with a bin size of 13.5 m (CDP spacing) and 27 m (trace spacing; Aguirre, 2003), which equates to a 364.5 m wide Fresnel Zone (13.5 x 27), i.e., horizontal resolution near the surface. The structures mapped in the present study (e.g., asymmetric folds and duplexes) are typically ≥ 300 m wide and are, thus, well within the resolution of the data at shallow depth.

Well tie

Time conversion

For time conversion of the depth of key stratigraphic horizons in existing wellbores (Table 1), seismic velocities of Buffoni *et al.* (2018) in the Tierra del Fuego fold-and-thrust belt were used. The Tobífera Formation (Jurassic–earliest Cretaceous) was ascribed an average P-wave velocity of 5.65 km.s^{-1}. This velocity is derived from the 3.0–3.3 km.s^{-1} S-wave velocities (Buffoni *et al.*, 2018 their table 2) characterizing the 3-, 6-, and 9-second-depth (TWT) slices between stations TRCA and USHA in between which outcrops consist almost exclusively of rocks of the Tobífera Formation (Buffoni *et al.*, 2018; Figure 1b–c).

The Lower Cretaceous Yaghan and Beauvoir formations were assigned an average P-wave velocity of 5.05 km.s^{-1}, which was derived from average S-wave velocities of 2.6–2.9 km.s^{-1} (Buffoni *et al.*, 2018 their table 2). These values reflect the dominant velocities of the 3-, 6-, and 9-second (TWT) slices between stations ELCA and USHA and of the 9-second between stations ELCA and TRCA (Buffoni *et al.*, 2018; Figure 1b–c). Lower Cretaceous rocks of the Beauvoir and Yaghan formations crop out between these three stations and are likely to be found at intermediate depths and to be thickest between stations USHA and ELCA due to potential thrust-related repetitions in the Tierra del Fuego fold-and-thrust belt (e.g., Álvarez-Marrón *et al.*, 1993; Mosqueira González *et al.*, 2021; Figure 1b–c).

For Upper Cretaceous sedimentary rocks, an average P-wave velocity of 4.5 km.s^{-1} was used. This value is tied to 2.2–2.5 km.s^{-1} S-wave velocities (Buffoni *et al.*, 2018 their table 2), which characterize the 3- and 6-second (TWT) slices between stations DSPA and USHA in between which Upper Cretaceous rocks crop out and are likely found at shallow depth below deformed Cenozoic sediments (Buffoni *et al.*, 2018; Figure 1b–c).

Most outcrops between stations DSPA, ELCA, and TRCA consist of deformed Cenozoic sediments (Buffoni *et al.*, 2018; Figure 1b–c). Thus, an average P-wave velocity of 3.5 km.s^{-1} was used for deformed Cenozoic sediments in the southwest (Lago Mercedes 1 wellbore). This value corresponds with the lowest P-wave velocity estimate at near-surface depth in the study area (Buffoni *et al.*, 2018 their table 2). Farther northeast, intermediate average P-wave velocities of 2.5 and 2.2 km.s^{-1} were used for the area encompassing the Rio Chico 1, Cachimba 1, and Carmen 1 wellbores, i.e., intermediate to account for the gradually less undeformed character of the upper part of Cenozoic sediments away from the Tierra del Fuego fold-and-thrust belt. In the area including the Gaviota 1 and Cisne 1 wellbores, Cenozoic sediments are largely undeformed and up to c. 1.3 km thick (Gallardo Jara *et al.*, 2022). Thus, an average P-wave velocity of 1.95 km.s^{-1} (i.e., average velocity of wet sand; e.g., Earle, 2019) was used for Cenozoic rocks. In the northeasternmost wellbore (María Emilia 3), a velocity of 1.8 km.s^{-1} (lower estimate of average velocity of wet sand; Earle, 2019) was preferred because Cenozoic sediments there are thinnest (c. 1 km; Gallardo Jara *et al.*, 2022) and farthest from the deformation front of the Tierra del Fuego fold-and-thrust belt (Figure 1b–c and Figure 3a–h).

Seismic stratigraphy

The main seismic horizons interpreted in the present work were tied to the results of exploration wellbores in the area (Figure 3a–h and Table 1). The Base Tobífera–Lemaire/Lapataia formations horizon corresponds to the base of Jurassic volcanosedimentary units of the Tobífera and Lemaire/Lapataia formations and to the top of the Paleozoic igneous and metamorphic basement rocks. It is characterized by a generally positive, moderate- to high-amplitude seismic reflection (dark blue horizon in Figure 3a–h), which is consistent with a transition from volcaniclastic rocks with a relatively lower overall density to early Paleozoic igneous and metamorphic rocks with higher density (Figure 3a–h). This stratigraphic boundary was penetrated only by two exploration wellbores (Lago Mercedes 1 and María Emilia 3; Figure 3a–h).

In places, an Intra Jurassic unconformity occurs within the Tobífera Formation and is characterized by a dominantly positive, moderate- to high-amplitude reflection (light blue horizon in Figure 3a–h), which truncates underlying reflections resulting in toplap geometries. This horizon is more challenging to trace in the southwest, where Jurassic–Lower Cretaceous sedimentary units are thinner (Figure 3a–h; Gallardo Jara *et al.*, 2022).

The Base Lower Cretaceous (Springhill, Río Jackson, to Beauvoir formations) horizon also corresponds to a positive, moderate- to high-amplitude reflection (dark green horizon in Figure 3a–h), i.e., consistent with a transition from relatively low-density shale–slate-dominated sedimentary rocks of the Springhill, Río Jackson, and Beauvoir formations to relatively high-density volcaniclastic successions of the Tobífera Formation. Underlying reflections display toplap geometries in agreement with reports of an unconformable contact between the Tobífera Formation and Lower Cretaceous units in previous studies (e.g., Gallardo Jara *et al.*, 2022; Muller *et al.*, 2020; Robbiano *et al.*, 1996).

Table 1. Time conversion for the wellbores used to tie drilling results to seismic interpretation in the study area (Figure 3).

Time conversion of exploration wellbore results in Tierra del Fuego					
Lago Mercedes 1 wellbore					
Interval	Thickness from Gallardo Jara *et al.* 2022 (m)	Velocities from Buffoni *et al.* 2018 (m.s-1)	Velocity used	Calculated thickness (s TWT)	Calculated cumulated depth (s TWT)
Cenozoic (deformed)	3250		3500	1.86	1.86
Upper Cretaceous	250	Vs = 2200-2500 ==> Vp = 4200-4800	4500	0.11	1.97
Lower Cretaceous	450	Vs = 2600-2900 ==> Vp = 4900-5300	5050	0.18	2.15
Jurassic-lowermost Cretaceous	50	Vs = 3000-3300 ==> Vp = 5500-5800	5650	0.02	2.16
Paleozoic basement rocks	200				
Rio Chico 1 wellbore					
Interval	Thickness from Gallardo Jara *et al.* 2022 (m)	Velocities from Buffoni *et al.* 2018 (m.s-1)	Velocity used	Calculated thickness (s TWT)	Calculated cumulated depth (s TWT)
Cenozoic (partly deformed)	2250		2500	1.80	1.80
Upper Cretaceous	100	Vs = 2200-2500 ==> Vp = 4200-4800	4500	0.04	1.84
Lower Cretaceous	550	Vs = 2600-2900 ==> Vp = 4900-5300	5050	0.22	2.06
Jurassic-lowermost Cretaceous	50	Vs = 3000-3300 ==> Vp = 5500-5800	5650	0.02	2.08
Paleozoic basement rocks	0				
Cachimba 1 wellbore					
Interval	Thickness from Gallardo Jara *et al.* 2022 (m)	Velocities from Buffoni *et al.* 2018 (m.s-1)	Velocity used	Calculated thickness (s TWT)	Calculated cumulated depth (s TWT)
Cenozoic (partly deformed)	1950		2500	1.56	1.56
Upper Cretaceous	100	Vs = 2200-2500 ==> Vp = 4200-4800	4500	0.04	1.60
Lower Cretaceous	600	Vs = 2600-2900 ==> Vp = 4900-5300	5050	0.24	1.84

Table 1. *Continued*

Time conversion of exploration wellbore results in Tierra del Fuego					
Jurassic-lowermost Cretaceous	50	Vs = 3000-3300 ==> Vp = 5500-5800	5650	0.02	1.86
Paleozoic basement rocks	0				
Carmen 1 wellbore					
Interval	Thickness from Gallardo Jara *et al.* 2022 (m)	Velocities from Buffoni *et al.* 2018 (m.s-1)	Velocity used	Calculated thickness (s TWT)	Calculated cumulated depth (s TWT)
Cenozoic (partly deformed)	1550		2200	1.41	1.41
Upper Cretaceous	100	Vs = 2200-2500 ==> Vp = 4200-4800	4500	0.04	1.45
Lower Cretaceous	500	Vs = 2600-2900 ==> Vp = 4900-5300	5050	0.20	1.65
Jurassic-lowermost Cretaceous	50	Vs = 3000-3300 ==> Vp = 5500-5800	5650	0.02	1.67
Paleozoic basement rocks	0				
Gaviota 1 wellbore					
Interval	Thickness from Gallardo Jara *et al.* 2022 (m)	Velocities from Buffoni *et al.* 2018 (m.s-1)	Velocity used	Calculated thickness (s TWT)	Calculated cumulated depth (s TWT)
Cenozoic (undeformed)	1350		1950	1.38	1.38
Upper Cretaceous	100	Vs = 2200-2500 ==> Vp = 4200-4800	4500	0.04	1.43
Lower Cretaceous	500	Vs = 2600-2900 ==> Vp = 4900-5300	5050	0.20	1.63
Jurassic-lowermost Cretaceous	50	Vs = 3000-3300 ==> Vp = 5500-5800	5650	0.02	1.64
Paleozoic basement rocks	0				
Cisne 1 wellbore					
Interval	Thickness from Gallardo Jara *et al.* 2022 (m)	Velocities from Buffoni *et al.* 2018 (m.s-1)	Velocity used	Calculated thickness (s TWT)	Calculated cumulated depth (s TWT)
Cenozoic (undeformed)	1300		1950	1.33	1.33
Upper Cretaceous	100	Vs = 2200-2500 ==> Vp = 4200-4800	4500	0.04	1.38

Table 1. *Continued*

Time conversion of exploration wellbore results in Tierra del Fuego					
Lower Cretaceous	600	Vs = 2600-2900 ==> Vp = 4900-5300	5050	0.24	1.62
Jurassic-lowermost Cretaceous	100	Vs = 3000-3300 ==> Vp = 5500-5800	5650	0.04	1.65
Paleozoic basement rocks	0				
Maria Emilia 1 wellbore					
Interval	Thickness from Gallardo Jara *et al.* 2022 (m)	Velocities from Buffoni *et al.* 2018 (m.s-1)	Velocity used	Calculated thickness (s TWT)	Calculated cumulated depth (s TWT)
Cenozoic (undeformed)	1000		1800	1.11	1.11
Upper Cretaceous	250	Vs = 2200-2500 ==> Vp = 4200-4800	4500	0.11	1.22
Lower Cretaceous	450	Vs = 2600-2900 ==> Vp = 4900-5300	5050	0.18	1.40
Jurassic-lowermost Cretaceous	1100	Vs = 3000-3300 ==> Vp = 5500-5800	5650	0.39	1.79
Paleozoic basement rocks	50				

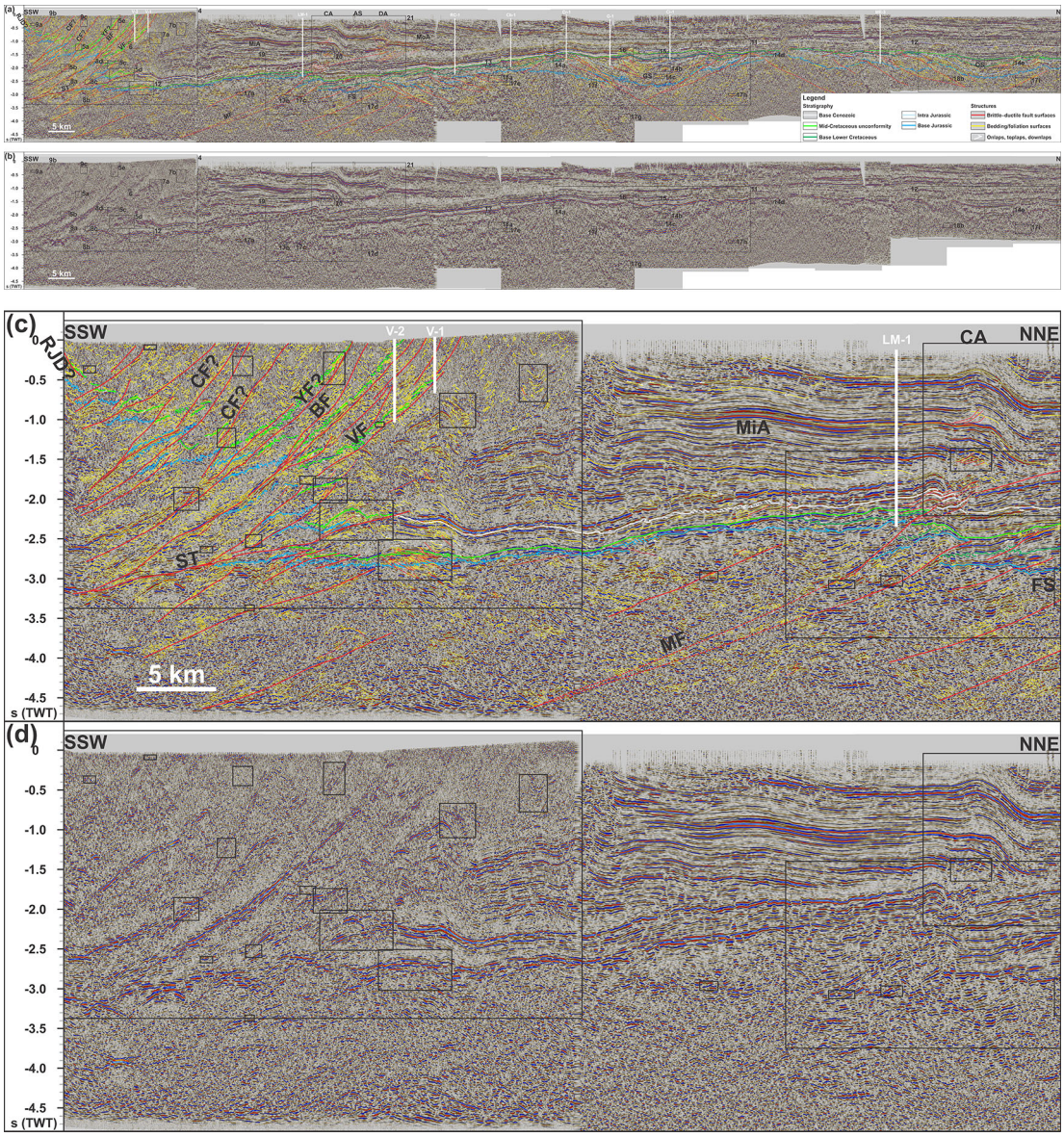

Figure 3. (a) Interpreted and (b) uninterpreted regional seismic transect (PR-1) across the study area. (c–h) Interpreted (up) and uninterpreted (down) zooms in (a) and (b) (c–d: southwestern part of PR-1; e–f: central part of PR-1; g–h: northeastern part of PR-1). Location of PR-1 transect is shown in Figure 1b–c. Abbreviations: AS: Aurelia Syncline; BF: Bahia Bell fault zone; CA: Constancia Anticline; CF: Colo-Colo fault zone; Cb-1: Cachimba 1 wellbore; Cr-1: Carmen 1 wellbore; Cs-1: Cisne 1 wellbore; DA: Despedida Anticline; FS: Fueguino syncline; G-1: Gaviota 1 wellbore; GS: Gaviota syncline; LM-1: Lago Mercedes 1 wellbore; ME-3: María Emilia 3 wellbore; MiA: Miraflores Anticline; MF: Mercedes fault zone; MoA: Moneta Anticline; OS: Oriental/Ostión/Calafate syncline; RC-1: Río Chico 1 wellbore; RJD: Río Jackson detachment; ST: sole thrust; VF: Vicuña fault zone; V-1: Vicuña 1 wellbore; V-2: Vicuña 2 wellbore; YF: Yartou fault zone.

The potential base of the foreland sedimentary deposits corresponds to a major erosional unconformity, which typically appears as a regional, positive, high-amplitude reflection characterized by toplap reflections in underlying Jurassic–Cretaceous rocks (light green horizon in Figure 3a–h). In places, the boundary appears as a disconformity (non-angular unconformity; Horton, 2021). However, the dominant toplap geometries of underlying stratigraphic units clearly suggest a hiatus with overlying units. The positive, high-amplitude character of the unconformity is in agreement with a transition from relatively young, poorly deformed to undeformed, low-density (because buried to shallower depths and for a shorter duration and, thus, less compacted) Upper Cretaceous sedimentary rocks to older, tightly folded, Jurassic–Lower Cretaceous volcaniclastic and Paleozoic igneous and (up to high-grade) metamorphic rocks with a resulting higher

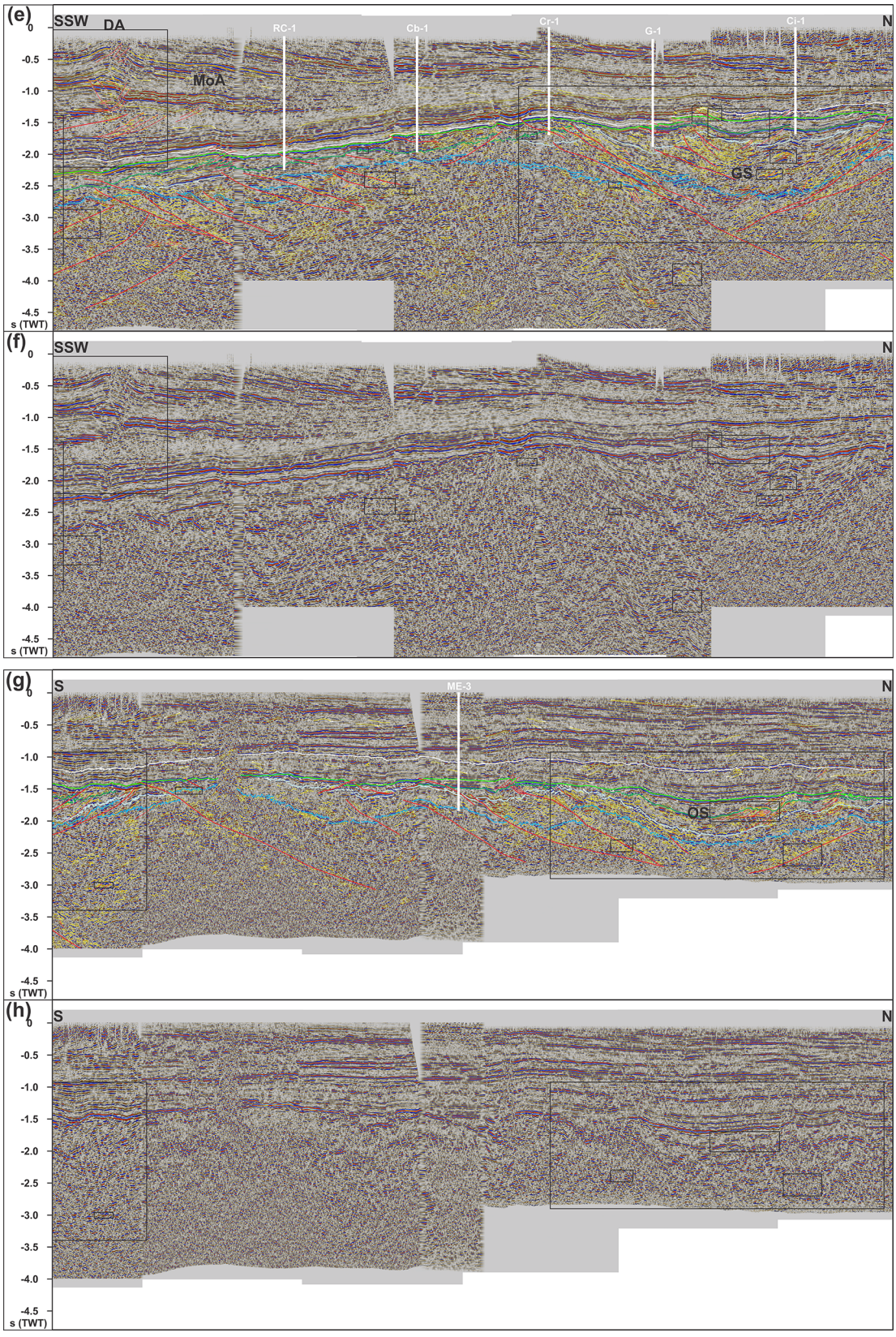

Figure 3. (continued)

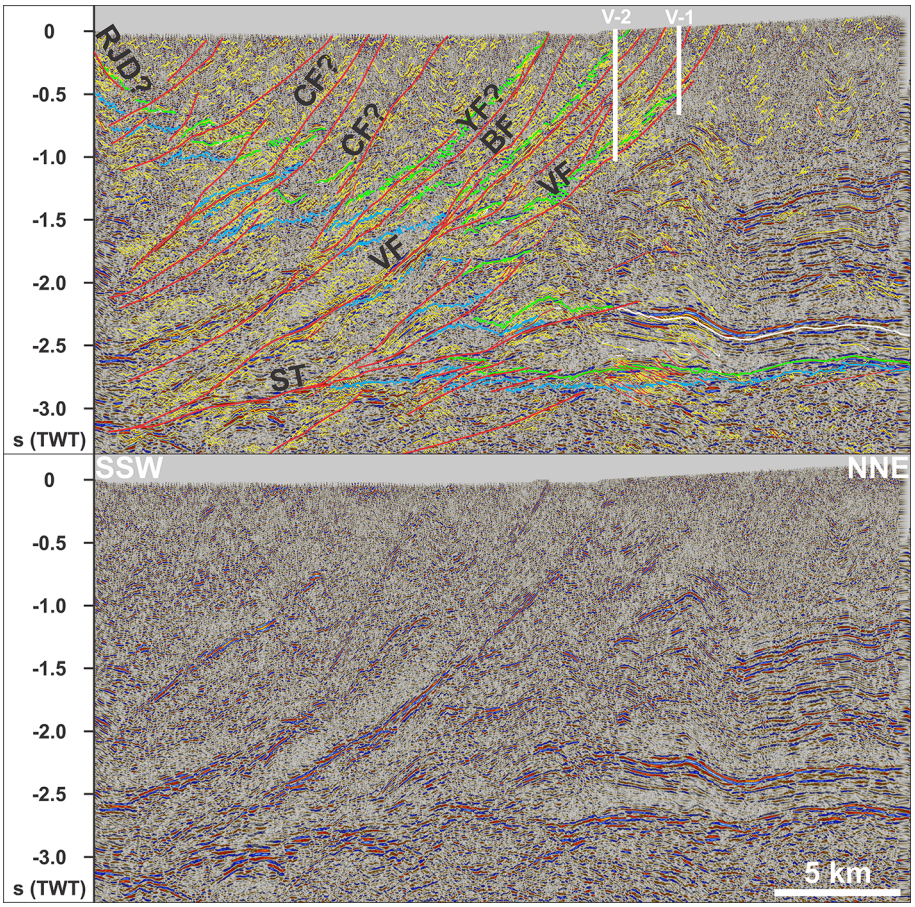

Figure 4. Interpreted (up) and uninterpreted (down) zoom in the Tierra del Fuego fold-and-thrust belt in the southwestern part of seismic transect PR-1 showing the overall imbricate geometry of thrust faults (e.g., Colo-Colo, Yartou, Bahia Bell, and Vicuña fault zones), which flatten at depth into the sole thrust (SF). Notice how the Yartou and Vicuña faults parallel and detach major stratigraphic boundaries (light green Mid-Cretaceous unconformity reflection) observed both in outcrops and in nearby wellbores (V-1 and V-2; Zanella et al., 2014), thus suggesting that these faults initiated as bedding-parallel décollements at depth. Also notice the transition of tightly deformed Paleozoic–Mesozoic strata in the Tierra del Fuego fold-and-thrust belt in the hanging wall of the Vicuña fault zone in the southwest to more mildly deformed Cenozoic strata in the northeast. See location and legend in Figure 3a. Abbreviations: BF: Bahia Bell fault zone; CF: Colo-Colo fault zone; RJD: Río Jackson detachment; ST: Sole thrust; VF: Vicuña fault zone; V-1: Vicuña 1 wellbore; V-2: Vicuña 2 wellbore; YF: Yartou fault zone.

density (associated seismic velocities are shown in Table 1). This unconformity is believed to be of mid (possibly earliest Late) Cretaceous age (i.e., pre-Lutitas Arenosas–Rio Garcia formations; Gallardo Jara *et al.*, 2022). Upper Cretaceous sedimentary rocks crop out in the southwestern part of the study area (southwestern domain) and can be directly correlated with seismic reflections in the subsurface (e.g., Mosqueira González *et al.*, 2021; Torres Carbonell *et al.*, 2020; Figure 3a–d). In contrast, Jurassic–Lower Cretaceous and Paleozoic rocks crop out farther southwest but likely occur in the subsurface in the study area (Mosqueira González *et al.*, 2021; Torres Carbonell *et al.*, 2020; Figure 3a–h).

The Base Cenozoic horizon contrasts with the above-mentioned stratigraphic boundaries, which correlate with dominantly high-amplitude reflections. Exploration wellbores in Tierra del Fuego suggest a more subtle acoustic impedance contrast between Cenozoic and Upper Cretaceous sediments, which shows as a moderate- to low-amplitude (alternating positive and negative) reflection (Figure 3a–h). This is consistent with a deposition of both successions in similar (tectonic and sedimentary) settings, including limited deformation and burial depth and time.

In the southwestern domain, the uncertainty in tracing individual horizons is quite high given the high number of major disruption surfaces with large offsets. The only exceptions are the regional, high-amplitude, truncating reflections separating the northeastern domain from the lower domain and basement rocks from Mesozoic volcanosedimentary rocks

(light green and light blue horizons in Figure 3a–h), which shallow gradually in a step-like manner towards the southwest up to a depth of 0.6 second and are characterized by toplap geometries in underlying reflections (TWT; Figure 3a–d).

Results

Description

The study area consists of three seismic domains: (1) a shallow (≤ 3.0 seconds TWT), wedge-shaped domain of highly disrupted, tightly curving, moderate- to low-amplitude reflections in the southwest, (2) a shallow (≤ 2.5 seconds TWT) domain of northeast-prograding, continuous, high- and low-amplitude reflections in the northeast, and (3) a deep, lower domain of moderate to high-amplitude reflections bounded from the southwestern domain by a major, gently SSW-dipping disruption surface (labelled "ST" in Figure 3a–d) and from the northeastern domain by a prominent, positive, high-amplitude, truncating reflection (light green horizon in Figure 3a–h).

Southwestern domain

The up to 3.0-second-thick (TWT), shallow (≤ 3.0 seconds deep; TWT), c. 30 km wide southwestern seismic domain displays a wedge geometry, which thins down gradually and pinches out to the northeast (Figure 3a–d). Thus, discontinuous, moderate- to low-amplitude, curving up and down reflections of the southwestern domain gradually transition into gently undulating, dominantly northward-prograding, high- to low-amplitude, continuous reflections of the northeastern domain. The transition occurs first at a depth of ca. 2.0–2.8 (TWT) and gradually to shallower levels (Figure 3a–d). Within this wedge-shaped domain, seismic reflections show a relatively higher amplitude at depth ≥ 0.5 second (TWT) in the southwesternmost portion of the southwestern domain and gradually deeper in a step-like fashion northwards (e.g., blue and light green horizons in Figure 3a–d and Figure 4).

The southwestern domain is truncated by major, tens of km wide, 0.5–3.0 seconds (TWT) thick, steeply to moderately SSW-dipping, listric disruption surfaces (Figure 3a–d and Figure 4). Most of these disruption surfaces are characterized by relatively planar, high-amplitude reflections, which contrast with the dominantly highly discontinuous, moderate- to low-amplitude, curving up and down reflections of the southwestern domain (Figure 3a–d and Figure 4). Offset across these major disruption surfaces is typically ≥ 5 km top-northeast (Figure 3a–d and Figure 4). At a depth of 2.5–3.0 seconds (TWT), most major disruption surfaces flatten into and merge with a gently SSW-dipping disruption surface at the boundary with the lower domain (Figure 3a–d and Figure 4). Minor, up to a few km wide, steeply to gently SSW-dipping, listric disruption surfaces also occur and typically display tens to hundreds of meters wide, reverse (top-northeast) offsets (Figure 5a–e). In places, they flatten into major disruption surfaces and/or one another downwards, resulting in fan-shaped clusters (Figure 3a–d, Figure 4, Figure 5a–e).

Moderate- to low-amplitude curving reflections in the southwestern domain show both open to close, in places (in the southwestern domain) chevron-like (i.e., tight, triangular, Λ- or V-shaped), symmetric geometries with wavelengths of a few kilometers and close up to isoclinal, upright to overturned, asymmetric geometries with associated wavelengths of a few hundred meters to a kilometer (Figure 6, Figure 7a–b, Figure 8a–d, and Figure 9a–c). Asymmetric reflections typically consist of a relatively gently–moderately dipping long edge and a steeply (generally oppositely) dipping narrow edge (Figure 7a–b and Figure 8a–d). While asymmetric reflections show both SSW- (i.e., a gently NNE-dipping, long edge in the northeast and a steeply SSW-dipping narrow edge in the southwest) and NNE-verging geometries (i.e., a gently SSW-dipping, long edge in the southwest and a steeply NNE-dipping narrow edge in the northeast), the latter type dominates the northeastern flank of symmetric curving reflections and along major SSW-dipping disruption surfaces (Figure 3a–d, Figure 4, Figure 6, Figure 7a–b, Figure 7a–b, Figure 8a–d, and Figure 10). Asymmetric reflections in the southwestern domain also commonly occur as stacks (Figure 4, Figure 5b–e, and Figure 8c–d). In places, these stacks include dense sets of dominantly Z-shaped asymmetric reflections, especially along major disruption surfaces (Figure 5b–e and Figure 8c–d).

Lower domain

The upper part of the lower domain is characterized by 10–25 km wide, ca. 1.0–1.5 seconds (TWT) thick, undulating, U-shaped seismic packages consisting of alternating low- and high-amplitude reflections (Figure 3a–h). These packages consist dominantly of asymmetric (locally π-shaped), curving reflections and are thickest at the center of the U-shaped troughs. For example, the thin (typically 0.1 second thick; TWT) uppermost package of the lower domain (package between dark green and light green horizons in Figure 3a–h, Figure 11, Figure 12, Figure 13, and Figure 14a–e) thickens up to 0.2–0.3 second (TWT) and the areas where this succession is thickest are bounded on either side by minor, low-angle to subhorizontal disruption surfaces dipping towards the thickened area and showing hundreds of meters top-NNE and top-SSW reverse offsets (Figure 3a–b and e–h, Figure 11, Figure 12, Figure 14e, Figure 15, and Figure 16).

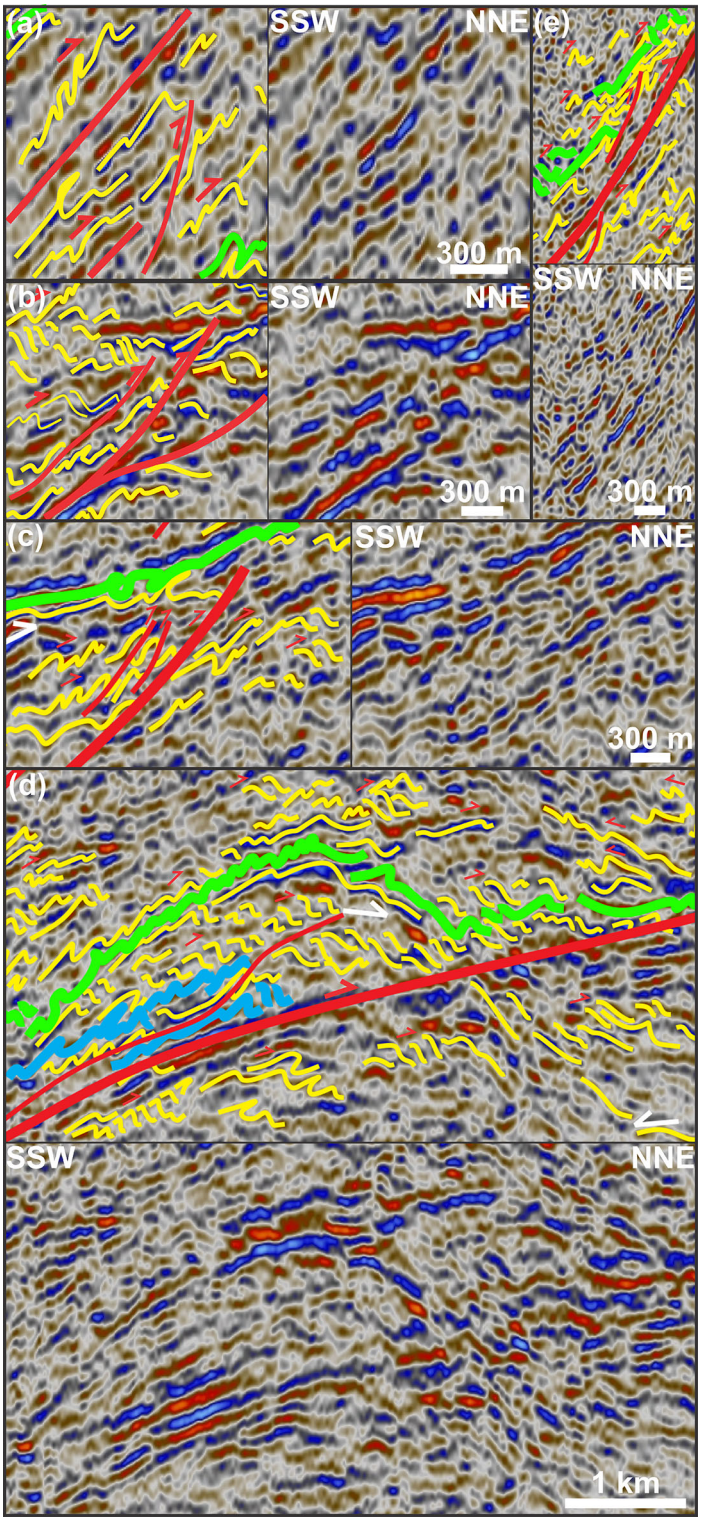

Figure 5. (a) Interpreted (left) and uninterpreted (right) zoom in potentially soft-linked top-NNE thrust faults flanked by NNE-verging, close to isoclinal, inclined to recumbent folds along the Colo-Colo fault zone. (b) Interpreted (left) and uninterpreted (right) zoom in possibly mylonitic thrust fault splays of the Colo-Colo fault zone associated with NNE-verging folds, and tight, Z-shaped, forward-dipping duplexes. (c) Interpreted (left) and uninterpreted (right) zoom in thrust fault splays of the Vicuña fault zone showing NNE-verging, inclined to isoclinal folds, possible early-stage, top-NNE duplexes consisting of Z-shaped horses, and potential toplap reflection terminations (white half arrow) below the Mid-Cretaceous unconformity (light green lines). (d) Interpreted (up) and uninterpreted (down) zoom in the sole thrust (thick red line) showing NNE-verging folds, an antiformal thrust stack, and top-NNE duplexes and décollement–detachment faults with ramp-flat geometries soling into the sole thrust. (e) Interpreted (up) and uninterpreted (down) zoom in a shallow segment possibly of the Yartou fault zone associated with NNE-verging, inclined to overturned folds and minor thrust imbricates, and potential duplexing of the Mid-Cretaceous unconformity reflection (light green lines) along the main, likely mylonitic, fault surface (thick red line). See location and legend in Figure 3a.



Figure 6. Interpreted (left) and uninterpreted (right) zoom in upright symmetrical folds transitioning to tight, NNE-verging asymmetric folds along the Vicuña fault zone in the Tierra del Fuego fold-and-thrust belt. See location and legend in Figure 3a.

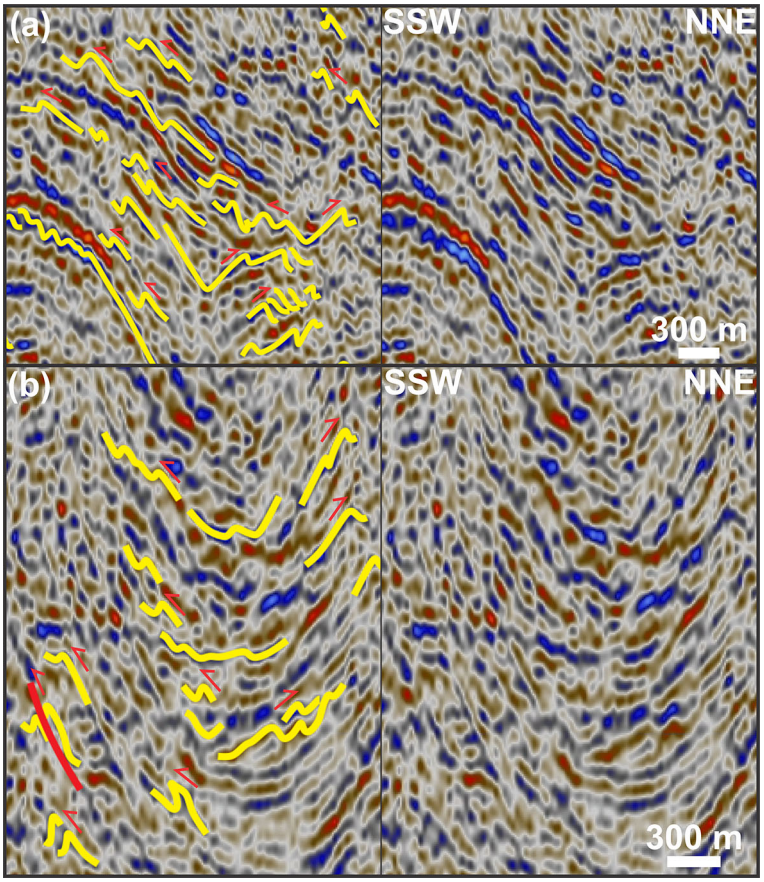

Figure 7. (a) Interpreted (left) and uninterpreted (right) zoom in hundred-meter- to km-scale, SSW-verging asymmetric folds showing opposite vergence to the dominant top-NNE transport direction in the Tierra del Fuego fold-and-thrust belt. The folds are located on the northern limb of a several km wide, open, upright anticline and likely correspond to parasitic folds. (b) Interpreted (left) and uninterpreted (right) zoom in asymmetric parasitic folds showing opposite vergence on opposite limbs of a several km wide open, upright syncline, thus suggesting overall limited tectonic transport. See location and legend in Figure 3a.

Comparably to the southwestern domain, asymmetric reflections in the lower domain also occur as stacks, but also display S-shaped geometries in places, e.g., on the southwestern flanks of U-shaped seismic packages (Figure 3a–b and e–h, Figure 11, Figure 12, Figure 17a–i, and Figure 18a–b).

Similarly to the southwestern domain, the lower domain is crosscut by major disruption surfaces (Figure 3a–h). However, these display both SSW- and NNE-dipping geometries and dip more gently than in the southwestern domain, thus truncating the U-shaped packages at an acute angle (Figure 3a–h). Their upward terminations coincide with gentle, open, km-scale, upward curving geometries of the overlying, continuous reflections in the northeastern domain (Figure 3a–h, Figure 19, Figure 20, and Figure 21). Offset along major disruption surfaces in the lower domain are reverse and generally about a few hundred meters to a few km ($\leq$ 5 km). Their dip direction typically but not exclusively matches that of

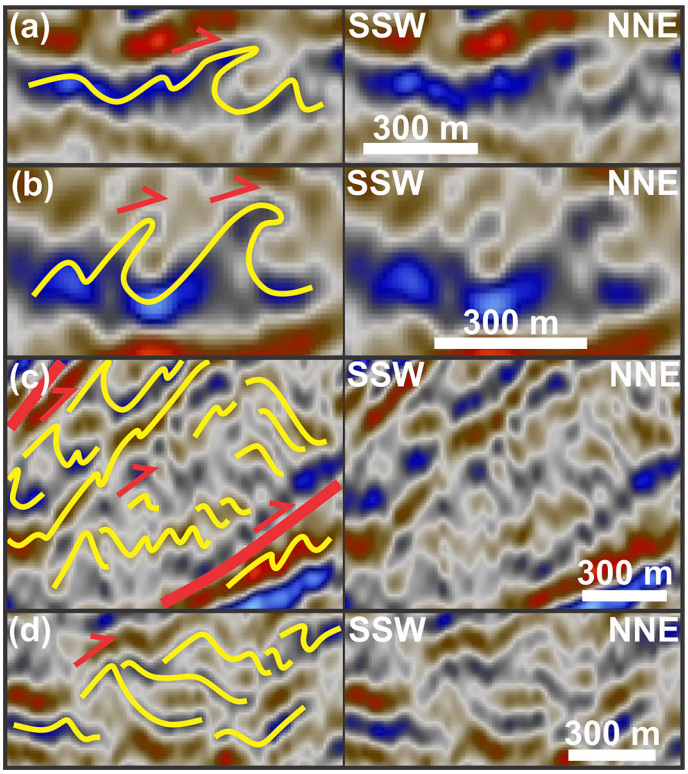

Figure 8. (a) Interpreted (left) and uninterpreted (right) zoom in a hundred-meter-scale, NNE-verging, recumbent, isoclinal fold in the Tierra del Fuego fold-and-thrust belt. (b) Interpreted (left) and uninterpreted (right) zoom in hundred-meter-scale, NNE-verging, overturned to recumbent folds in the Tierra del Fuego fold-and-thrust belt. (c) Interpreted (left) and uninterpreted (right) zoom in hundreds of meters wide, NNE-verging asymmetric folds transitioning to top-NNE duplexes. Notice how the packages consisting of relatively low-amplitude reflections characterizing duplex horses are overlain and underlain by more mildly deformed units characterized by relatively continuous, high-amplitude reflections deformed into inclined to overturned asymmetric folds. This illustrates strain partitioning and decoupling between intensely deformed, weak volcanosedimentary units and more mildly deformed, competent units, i.e., initiation of bedding-parallel décollements–detachments. (d) Interpreted (left) and uninterpreted (right) zoom in NNE-verging asymmetric folds transitioning into Z-shaped, top-NNE duplex horses. See location and legend in Figure 3a.

bedding surfaces in the U-shaped packages, generally switching dip direction across the center of U-shaped packages (Figure 3a–h, Figure 11, and Figure 12). A similar switch is observed for asymmetric reflections both within and below the U-shaped troughs, which display opposite vergence on either flank of U-shaped troughs (Figure 3a–b and e–h, Figure 11, and Figure 12). Notably, they display dominantly S-shaped and SSW-leaning geometries (narrow and steep south-southwestern limb and long more gently dipping north-northeastern limb) on the NNE-dipping southern flank of the troughs and Z-shaped and NNE-leaning geometries on the northern, SSW-dipping flank of the troughs (Figure 3a–b and e–h, Figure 11, and Figure 12).

Upwards, the U-shaped troughs are bounded from prograding continuous reflections of the northeastern domain by a gently undulating, overall gently SSW-dipping, continuous, high-amplitude reflection, which truncates gently southwest- and northeast-dipping underlying reflections, resulting in toplap reflection geometries (light green horizon in Figure 3a–h, and Figure 15). In places, this horizon is offset in a reverse fashion by low-angle to sub-horizontal disruption surfaces, which typically flatten and die out within a few km downwards and within a few hundred meters upwards. Towards the southwestern domain, this high-amplitude reflection curves more tightly. In the southwestern domain, it is offset in a reverse fashion by several km along multiple, gently- to steeply-SSW-dipping disruption surfaces and can be tentatively traced up to a depth of 0.5 second (TWT; Figure 3a–d and Figure 4).

Northeastern domain

The northeastern domain consists of several elongated, wedge-shaped packages of continuous seismic reflections and thins from ca. 2.5 seconds (TWT) thickness in the southwest to ca. 1.5 seconds (TWT) in the northeast (Figure 3a–h).

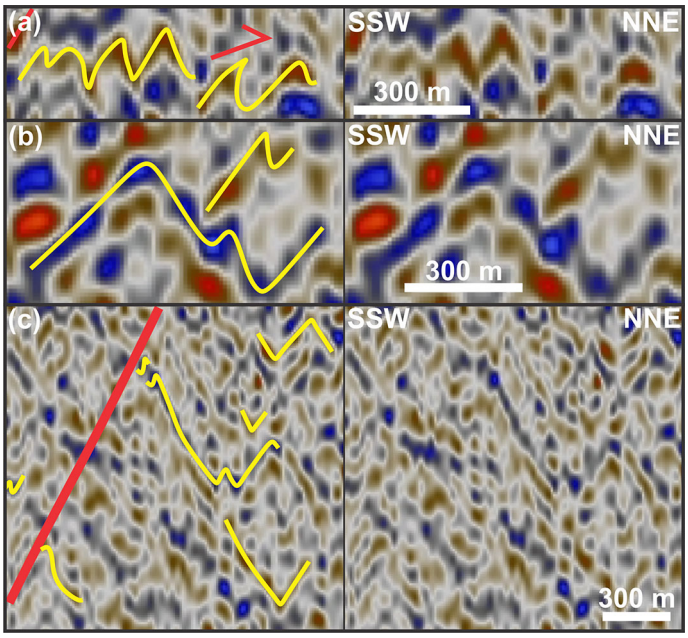

Figure 9. (a) Interpreted (left) and uninterpreted (right) zoom in close to tight, upright shallow chevron folds transitioning to NNE-verging asymmetric folds in Upper Cretaceous rocks in the Tierra del Fuego fold-and-thrust belt. (b) Interpreted (left) and uninterpreted (right) zoom in hundreds of meters wide, upright, open chevron folds with a potential, SSW-verging, parasitic fold. (c) Interpreted (left) and uninterpreted (right) zoom in shallow, hundred-meter-scale, upright, open chevron folds in Upper Cretaceous rocks in the Tierra del Fuego fold-and-thrust belt. See location and legend in Figure 3a.

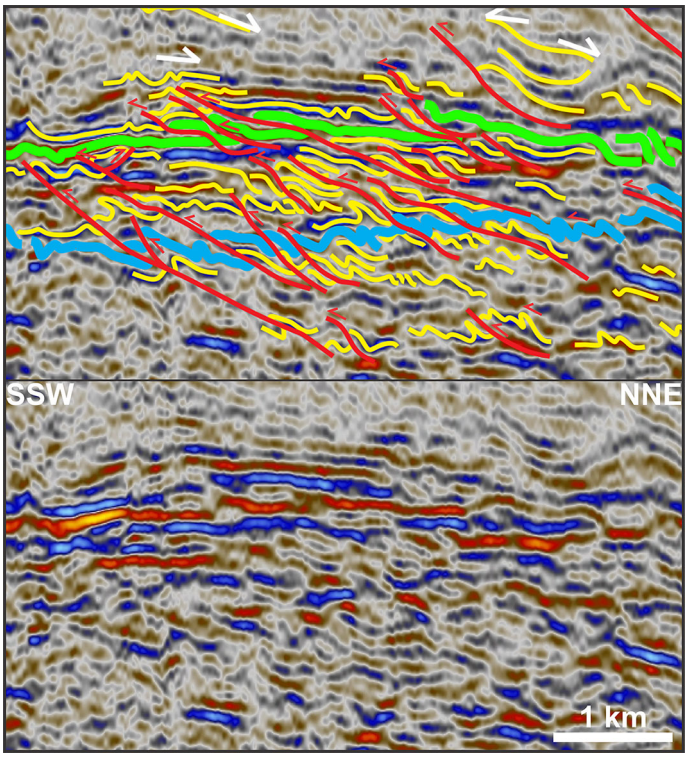

Figure 10. Interpreted (up) and uninterpreted (down) zoom in hundred-meter-scale offsets of major stratigraphic boundaries (blue and light green lines) by a cluster of minor, top-SSW, low-angle thrusts showing ramp–flat, imbricate, and splaying geometries with potential floor, roof, and link thrusts within an early-stage, backward-dipping duplex structure in the footwall of the sold thrust. The thrusts are associated with inclined to overturned, open to isoclinal folds. Notice the dominant SSW-verging character of the folds and thrusts, i.e., opposite the dominant tectonic transport direction in the Tierra del Fuego fold-and-thrust belt, which suggests limited tectonic transport. See location and legend in Figure 3a.

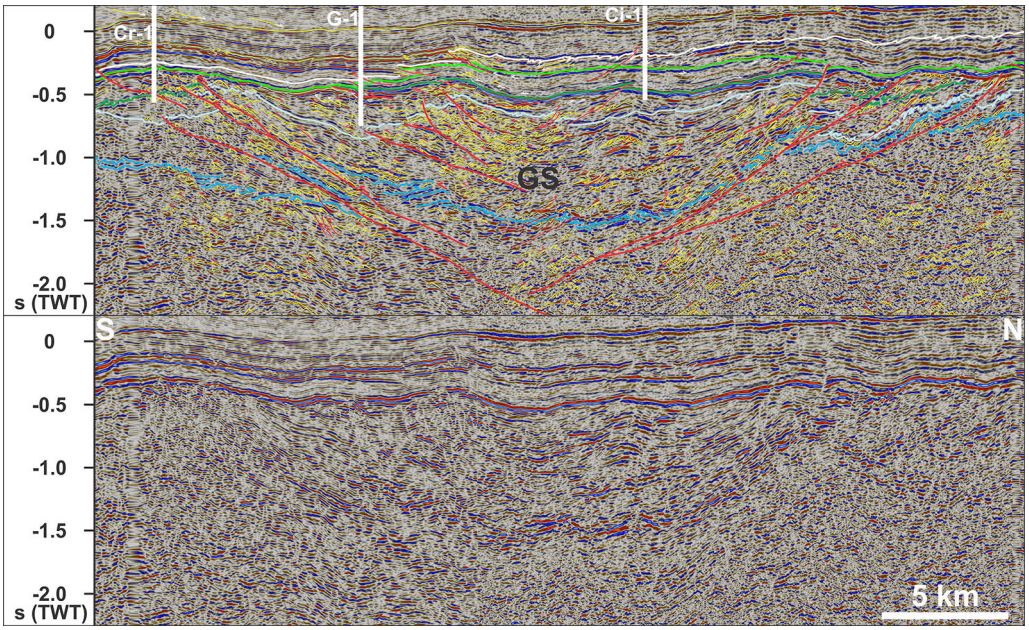

Figure 11. Interpreted (up) and uninterpreted (down) zoom in the U-shaped, tens of km wide, upright, open Gaviota syncline. The syncline consists of Jurassic–Lower Cretaceous volcanosedimentary rocks deformed into hundreds of meters asymmetric folds and thrusts showing opposite vergence on either flank of the syncline (i.e., NNE-verging in the northern limb and SSW-verging in the southern limb of the syncline), thus indicating limited tectonic transport and displacement. Overlying Upper Cretaceous–Cenozoic sedimentary rocks are significantly less intensely deformed, which suggests a syn- to post-tectonic deposition. In contrast, the thickening of Lower Cretaceous succession towards the center of the Gaviota syncline signals the onset of contraction. Notice the southward thinning of the Upper Cretaceous succession in this area suggesting sediment input (uplift?) from the north. See location and legend in Figure 3a. Abbreviations: Ci-1: Cisne 1 wellbore; Cr-1: Carmen 1 wellbore; GS: Gaviota syncline; G-1: Gaviota 1 wellbore.

Seismic reflections in the northeastern domain typically display prograding geometries, which result in gradual thinning of the seismic units and downlap reflection geometries in the direction of progradation and onlap and toplap reflection geometries in the opposite direction (Figure 3a–h and Figure 15). The thin (≤ 0.5 second thick; TWT) seismic succession at the bottom of the northeastern domain progrades northwards in the south and southwards in the north, thinning to ≤ 0.1 second (TWT) in the center of the study area (Figure 3a–h). This succession is locally offset and abruptly thickens from ca. 0.1 to 0.5 second (TWT), e.g., above sets of gently to moderately SSW-dipping to subhorizontal disruption surfaces, some of which offset the lower domain by up to a few km top-northeast in the southwest near the location of the Lago Mercedes 1 wellbore (Figure 3a–h and Figure 19).

Internal reflection packages in the overlying, up to 2.0 seconds (TWT) thick succession, which makes up most of the northeastern domain, display dominantly NNE-prograding geometries (with minor local shifts in the north), thinning to a thickness of ca. 1.0 second (TWT) in the north. Disruption surfaces are generally absent in this thick succession, and only locally occur in conjunction with broad, open, km-scale upward curving of seismic reflections in the southwest, showing minor reverse offsets (≤ a few hundred meters; Figure 3a–f, Figure 20, and Figure 21). The broad, open, upward-curving geometries generally extend into the lower domain, but in places are restricted to the upper part of the northeastern domain and coincide at depth with low-angle, dominantly SSW-dipping disruptions (Figure 3a–f and Figure 21).

Interpretation

Southwestern domain (Tierra del Fuego fold-and-thrust belt)

The highly disrupted, dominantly low-amplitude and asymmetric curving character of seismic reflections and the large number of major moderately- to steeply-SSW-dipping disruption surfaces in the southwestern domain suggest intensely deformed and ruptured bedding surfaces (Figure 3a–d and Figure 4). This is consistent with previous field studies in the area, which reported hundred-meter- to km-scale NNE-verging folds and top-NNE thrusts (e.g., Mosqueira González *et al.*, 2021; Torres Carbonell *et al.*, 2020; Zanella *et al.*, 2014). The extent of the southwestern domain coincides with that

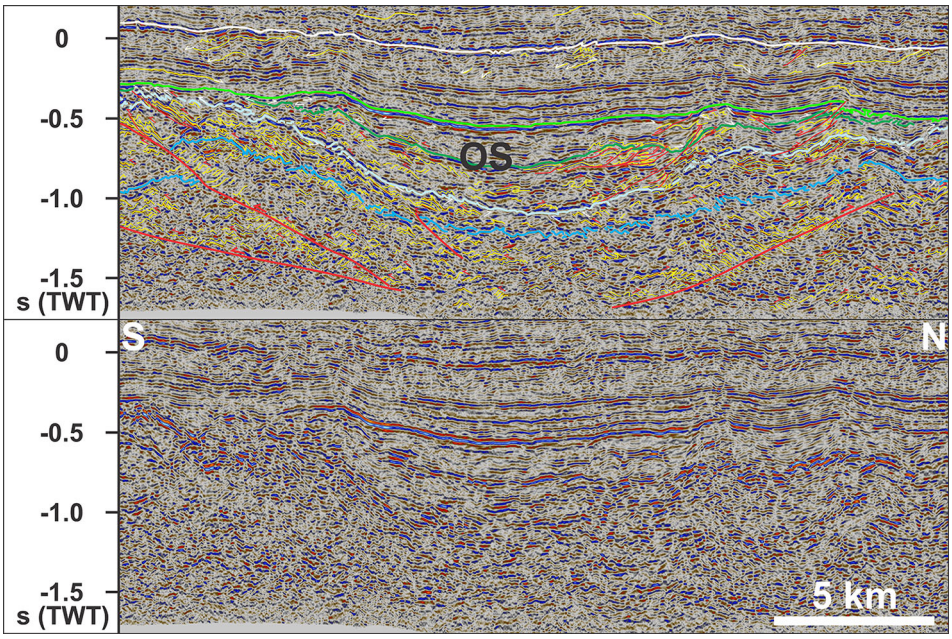

Figure 12. Interpreted (up) and uninterpreted (down) zoom in the Oriental syncline, showing comparable structures as in the Gaviota syncline, e.g., opposite vergence of asymmetric folds and thrust faults on either limb of the syncline, and thickening of the Lower Cretaceous succession (between dark and light green horizons) in the syncline hinge. The northern half of the syncline displays bedding-parallel décollements and thrusts with duplex and antiformal stack geometries in Jurassic–Lower Cretaceous successions (between blue and dark green horizons). Notice the fewer thrust faults and relatively smaller (reverse) offsets than in the Gaviota syncline. See location and legend in Figure 3a. Abbreviations: OS: Oriental syncline.

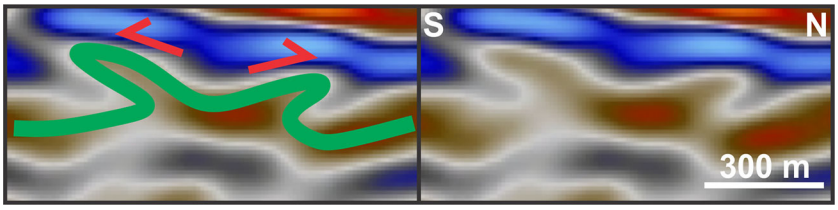

Figure 13. Interpreted (left) and uninterpreted (right) zoom in π-shaped reflections reflecting the occurrence of double-verging folds, i.e., limited tectonic transport. See location and legend in Figure 3a.

of the Tierra del Fuego fold-and-thrust belt in surface outcrops. It is therefore interpreted as the subsurface expression of this orogen.

More specifically, the comparable size and geometry of NNE-verging folds in outcrops in the Sierra de Beauvoir, Sierra de Apen, and Lago Blanco (Figure 1b–c) to that of asymmetric, dominantly 'NNE-leaning' and Z-shaped reflections in the southwestern domain suggest that the latter correspond to tightly folded sedimentary rocks and that their asymmetry indicates the direction of tectonic transport (Figure 3a–d, Figure 4, Figure 5a–e, Figure 7a–b, and Figure 8a–d). The occurrence of asymmetric folds of opposite vergence on the opposite limbs of symmetric, (up to several) km-wide curving reflections suggest that the former initiated as parasitic folds on the limbs of (initially) broader, more gentle, typically open to close, in places chevron-like symmetric folds (Figure 3a–d, Figure 4, Figure 6, Figure 7a–b, Figure 9a–c, and Figure 10). The numerous stacks of NNE-leaning and Z-shaped asymmetric folds, especially adjacent to major disruption surfaces, suggest the occurrence of dense networks of folds and faults defining shear fabrics probably arranged in contractional duplexes, e.g., antiformal (thrust) stacks, forward-dipping duplexes, imbricate fans, including link thrusts, bedding-parallel décollements, and roof and floor thrusts and detachments (Boyer & Elliott, 1982; Koehl, 2021; McClay, 1992; McClay and Insley, 1986).

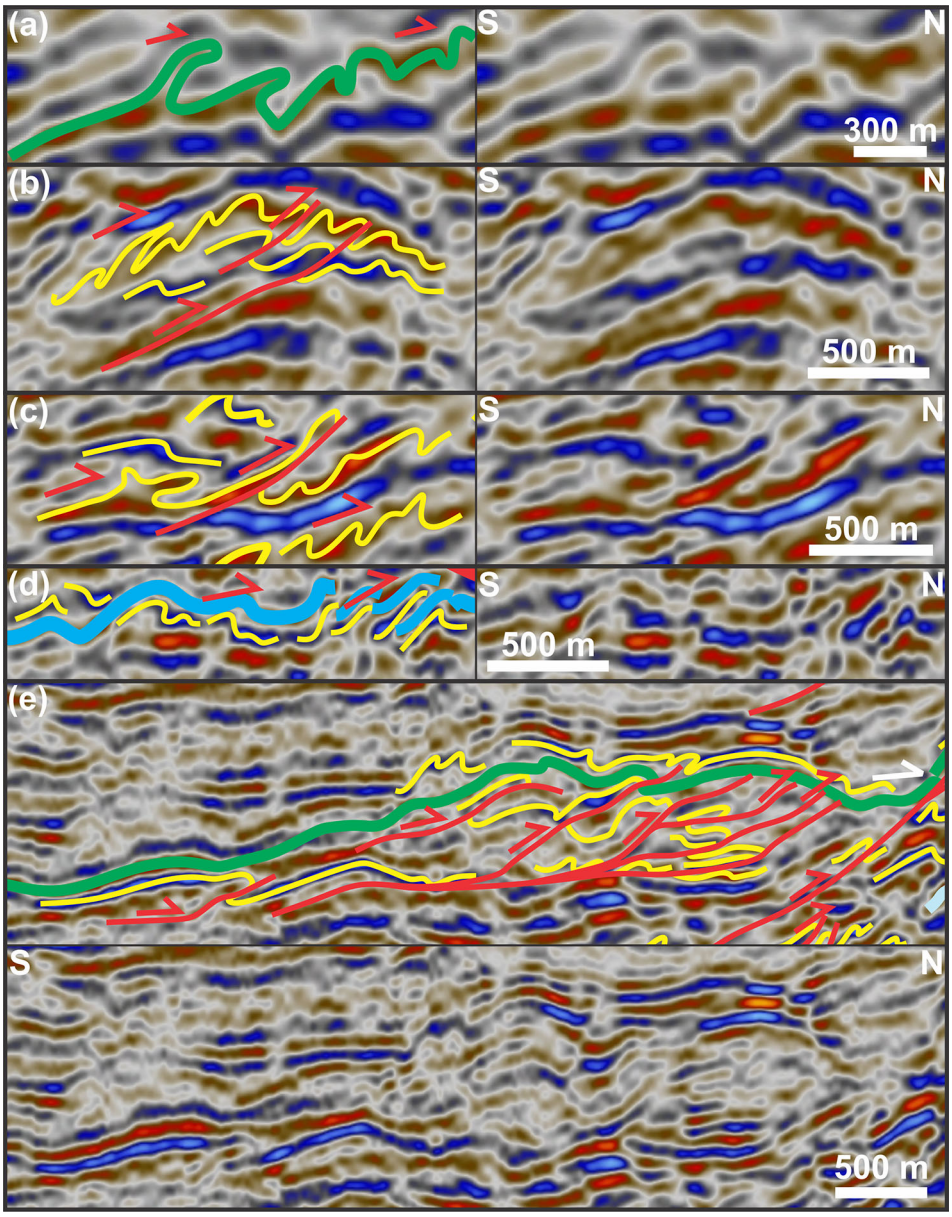

Figure 14. (a) Interpreted (left) and uninterpreted (right) zoom in NNE-verging, overturned to recumbent, isoclinal folds. (b) Interpreted (left) and uninterpreted (right) zoom in NNE-verging asymmetric folds and minor, top-NNE thrusts in Jurassic volcanosedimentary rocks of the Gaviota syncline. The thrusts flatten downwards into bedding surfaces and, thus, possibly initiated as (partial) décollements. (c) Interpreted (left) and uninterpreted (right) zoom in dominantly NNE-verging asymmetric folds and top-NNE thrust in Jurassic rock units in the Gaviota syncline. Notice the occurrence of a double-verging, π-shaped fold in the south. (d) Interpreted (left) and uninterpreted (right) zoom in NNE-verging folds transitioning into top-NNE imbricate thrusts and/or (backward-dipping) duplexes. (e) Interpreted (up) and uninterpreted (down) zoom in imbricate thrusts soling into a bedding-parallel décollement and showing an early-stage, antiformal stack geometry. See location and legend in Figure 3a.

The tight deformation (e.g., NNE-verging folds and duplexes; Figure 4, Figure 5a–e, and Figure 8a–d) and up to 5–10 km top-NNE reverse offsets (e.g., Mid-Cretaceous unconformity; light green horizon in Figure 3a–d and Figure 4) along the tens of km wide, up to 3.0 seconds (TWT) thick (i.e., several km thick), moderately to steeply SSW-dipping disruption surfaces in the southwestern domain (i.e., in the Tierra del Fuego fold-and-thrust belt) suggest that they correspond top-NNE thrust faults (Figure 3a–d and Figure 4). This is supported by the occurrence of dominantly top-NNE brittle–ductile thrusts and shear zones of the Tierra del Fuego fold-and-thrust belt in outcrops in the study area and is consistent with the

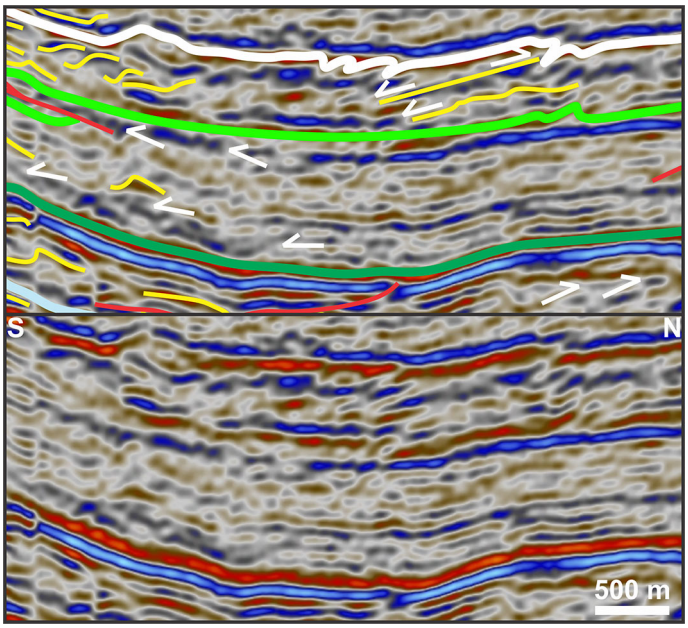

Figure 15. Interpreted (up) and uninterpreted (down) zoom in onlap, toplap, and downlap reflection geometries (white half arrows) in the Lower and Upper Cretaceous successions in the Gaviota syncline, suggesting respectively deposition during the formation of the Gaviota syncline in the mid-Early Cretaceous (onset of contraction), continued folding and uplift in the mid-Cretaceous resulting in regional erosion of Lower Cretaceous rock units (cf. Mid-Cretaceous unconformity; light green horizon), and a northern provenance for southward-prograding Upper Cretaceous succession. See location and legend in Figure 3a.

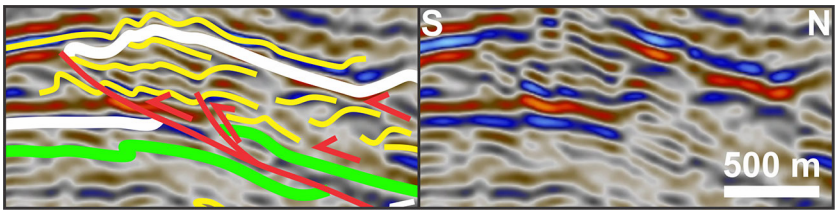

Figure 16. Interpreted (left) and uninterpreted (right) zoom in top-SSW, bedding-parallel décollement and minor thrusts and related SSW-verging asymmetric folds in Cretaceous–lower Cenozoic sedimentary rocks in the Gaviota syncline.

dominance of NNE-verging folds in the southwestern domain both in outcrop and the subsurface (Mosqueira González *et al.*, 2021; Torres Carbonell *et al.*, 2020; Zanella *et al.*, 2014; Figure 3a–d, Figure 4, Figure 5a–e, and Figure 8a–d).

Furthermore, offset seismic horizons are generally curving upwards above and downwards below major disruption surfaces (e.g., light green horizon in Figure 4 and Figure 5b–c and e). This together with the imbricate (i.e., partly overlapping), fan-shaped arrangement (i.e., flattening at depth and merging with a gently SSW-dipping disruption surface) suggests that the disruption surfaces correspond to top-NNE imbricate thrusts with related ramp anticlines in the hanging wall and footwall synclines (Figure 3a–d, Figure 4, and Figure 5b–c and e; McClay, 1992). This is consistent with previous studies of seismic reflection data in the area (e.g., Álvarez-Marrón *et al.*, 1993; Gallardo Jara *et al.*, 2022). Five discrete clusters of SSW-dipping thrust surfaces are recognized in the southwestern domain (Figure 3a–d and Figure 4). The upper four clusters of moderately- to steeply-dipping surfaces correlate from north to south with the Vicuña, Bahia Bell, Yartou, and Colo-Colo fault zones and the lower, gently-dipping thrust surfaces coincide with the sole thrust at the base of the imbricate thrust fan (Álvarez-Marrón *et al.*, 1993; Gallardo Jara *et al.*, 2022; Zanella *et al.*, 2014). Similarly to Álvarez-Marrón *et al.* (1993), the present interpretation separates the steeply-dipping Vicuña fault zone from the low-angle sole thrust, the former merging into the latter at depth (Figure 3a–d and Figure 4).

Thin, up to a few km wide fault-bounded slivers of Lower Cretaceous sedimentary rocks of the Río Jackson and Beauvoir–Vicuña formations crop out and were penetrated by the Vicuña 1 and Vicuña 2 wellbores along the Vicuña fault

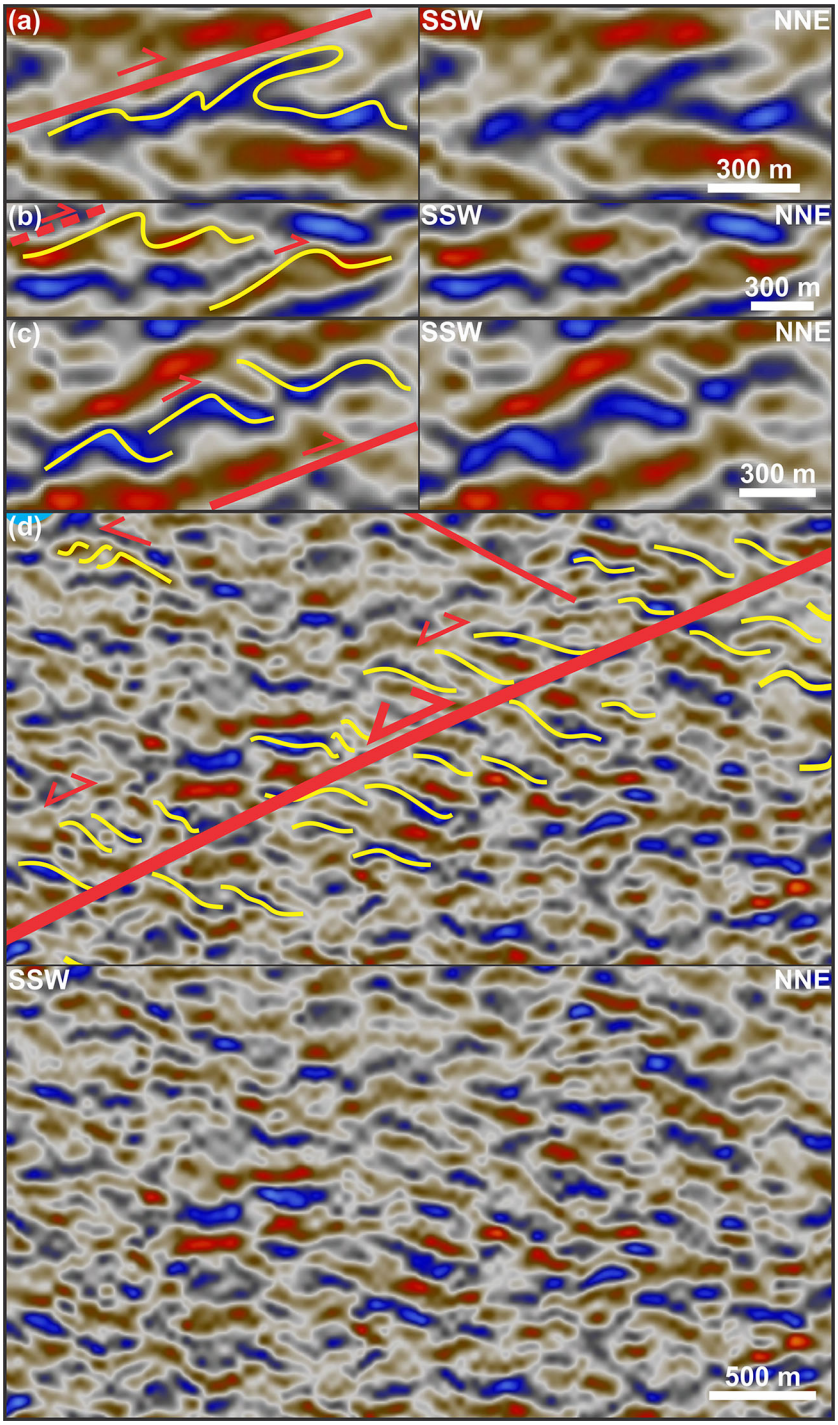

Figure 17. (a) Interpreted (left) and uninterpreted (right) zoom in a hundred-meter-scale, NNE-verging, recumbent, isoclinal fold in (Paleozoic?) basement rocks. (b) Interpreted (left) and uninterpreted (right) zoom in hundred-meter-scale, inclined, open to close, NNE-verging asymmetric folds in basement rocks within the Mercedes fault zone. (c) Interpreted (left) and uninterpreted (right) zoom in NNE-verging asymmetric folds at the transition to an early-stage duplex geometry within the Mercedes fault zone. (d) Interpreted (up) and uninterpreted (down) zoom in potentially inverted, forward-dipping duplexes consisting of Z-shaped horses in the Fueguino syncline in the footwall of the Mercedes fault zone. (e) Interpreted (left) and uninterpreted (right) zoom in hundred-meter-scale, NNE-verging folds showing overturned close to recumbent isoclinal geometries in (Paleozoic?) basement rocks. (f) Interpreted (left) and uninterpreted (right) zoom in a hundred-meter-scale, SSW-verging overturned isoclinal fold in basement rocks in the southern limb of the Gaviota syncline. (g) Interpreted (left) and uninterpreted (right) zoom in open, upright, symmetric folds and SSW-verging, inclined to overturned folds in basement rocks on the southern limb of the Gaviota syncline. (h) Interpreted (left) and uninterpreted (right) zoom in NNE-verging, inclined, open to close folds and top-NNE thrusts and associated forward-dipping duplexes in (Paleozoic?) basement rocks. (i) Interpreted (left) and uninterpreted (right) zoom in potentially inverted, top-NNE duplexes consisting of Z-shaped horses along a low-angle thrust fault in basement rocks on the northern limb of the Oriental syncline. See location and legend in Figure 3a.

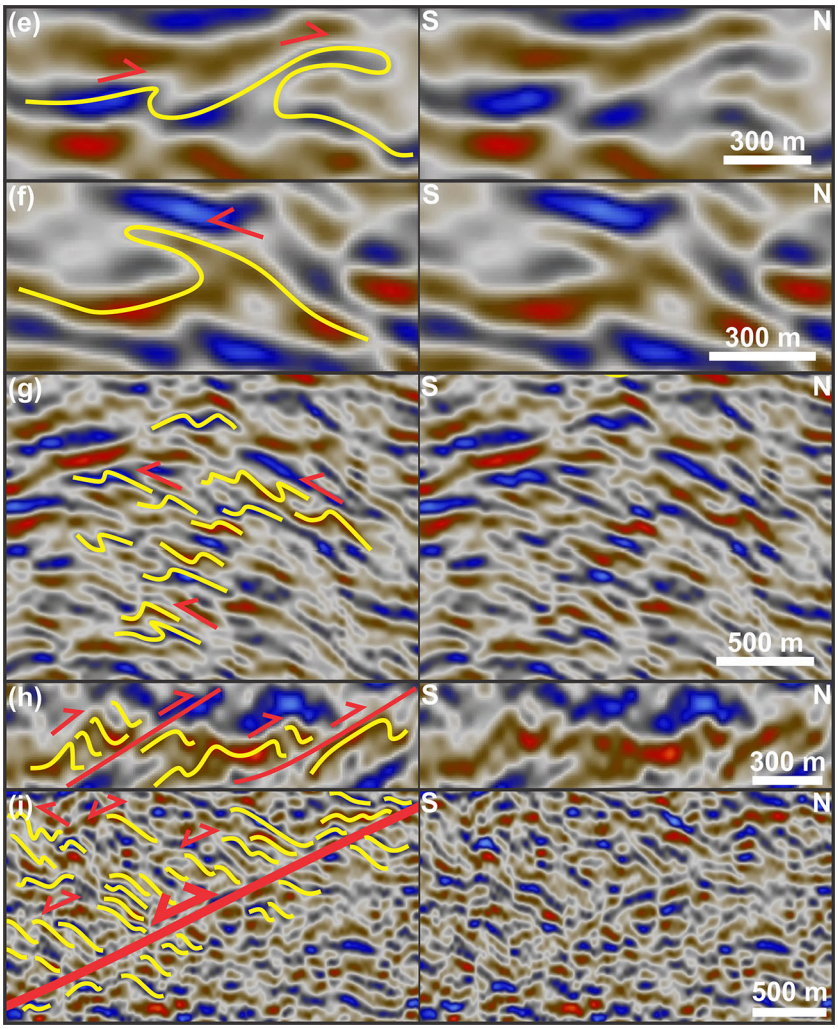

Figure 17. (continued)

zone at Lago Blanco (Zanella *et al.*, 2014). In the subsurface, these units appear intensely deformed into thrust-parallel imbricates dragged along major fault surfaces (light green horizon along the Vicuña and Yartou fault zones in Figure 3a–d and Figure 4). These suggest that weak (shale–slate-rich) Lower Cretaceous rocks of the Río Jackson and Beauvoir formations (and possibly Jurassic–earliest Cretaceous, interbedded volcanics and clastic rocks of the Tobífera Formation?) acted as a décollement that initially localized the formation of the Vicuña and Yartou fault zones, which later evolved into major detachments (Figure 3a–d, Figure 4, and Figure 5d–e). This is consistent with previous tectonic models for the study area (Álvarez-Marrón *et al.*, 1993; Zanella *et al.*, 2014).

In the southwesternmost part of the data, a moderately-NNE-dipping disruption surface parallels and occurs just below the Mid-Cretaceous unconformity (Figure 3a–d and Figure 4). It is suggested that this disruption surface corresponds to the northern subsurface continuation of the Río Jackson detachment (back thrust), which crops out a few km south of the seismic section shown in Figure 3a–b and occurs between Jurassic–earliest Cretaceous rocks of the Tobífera and Lemaire–Lapataia formations and Lower Cretaceous strata of the Río Jackson Formation (Klepeis, 1994a; Torres Carbonell *et al.*, 2020). This provides some constraints on the approximate depth of this stratigraphic boundary in the southwestern end of the data, which deepens northwards in a step-like manner across major thrust faults within the Tierra del Fuego fold-and-thrust belt, except along the Vicuña and Yartou fault zones (Figure 3a–d and Figure 4). This suggests the presence of a wedge of pre-Jurassic (likely Paleozoic igneous and metamorphic) basement rocks characterized by moderate-amplitude reflections at depth ≥ 0.5 second (TWT) in the southwestern part of the Tierra del Fuego fold-and-thrust belt (Figure 3a–d and Figure 4). However, the absence of wellbores and numerous thrust faults in this area make regional stratigraphic correlations in the southwestern domain relatively uncertain.

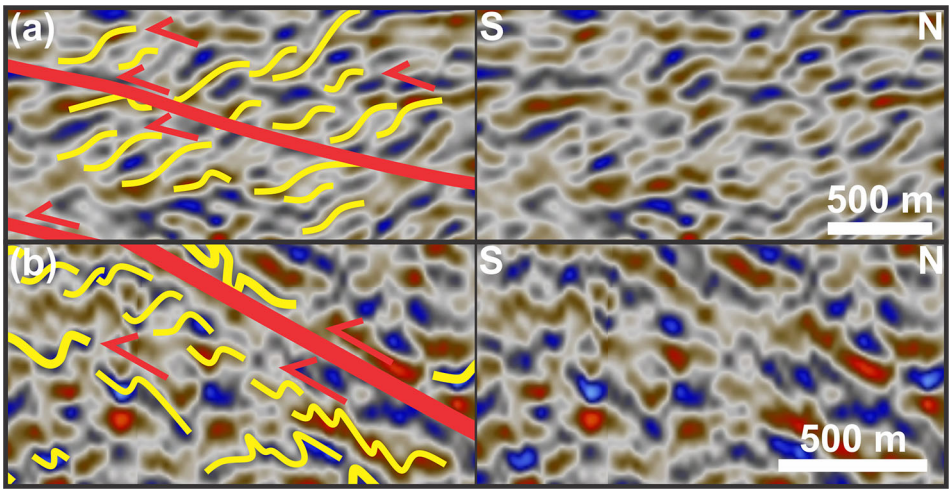

Figure 18. (a) Interpreted (left) and uninterpreted (right) zoom in (inverted?) top-SSW, S-shaped duplexes in basement rocks on the southern limb of the Gaviota syncline. (b) Interpreted (left) and uninterpreted (right) zoom in SSW-verging asymmetric folds transitioning into top-SSW, S-shaped, forward-dipping duplexes in the footwall of a major thrust fault in basement rocks on the southern limb of the Gaviota syncline. See location and legend in Figure 3a.

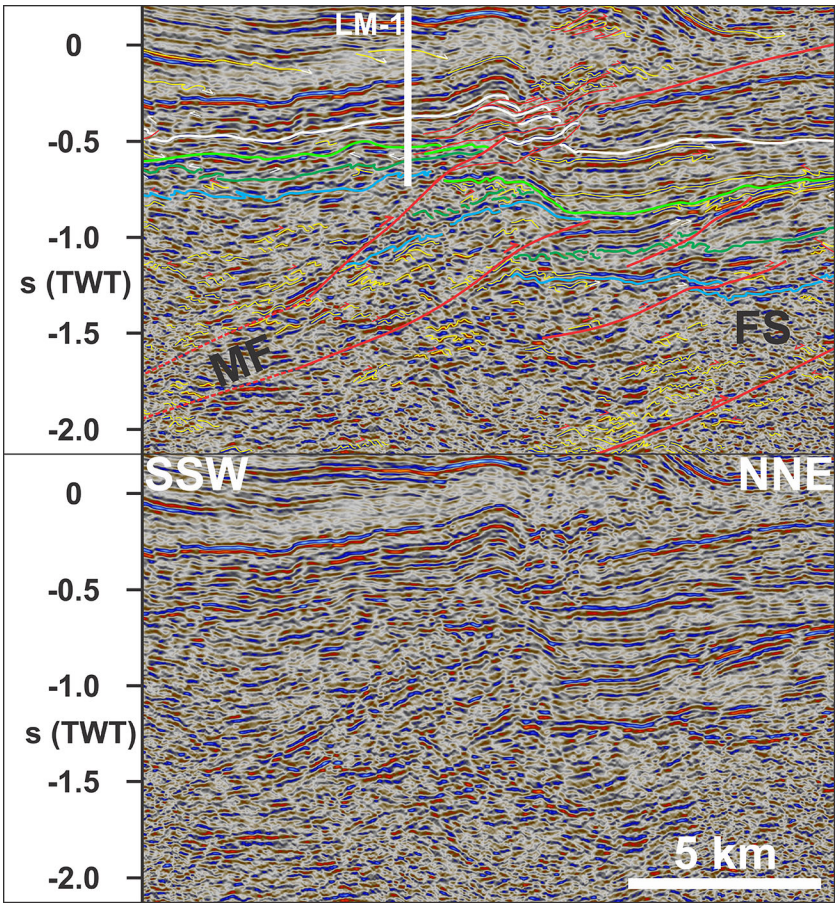

Figure 19. Interpreted (up) and uninterpreted (down) zoom in the Mercedes fault zone showing several km top-NNE offset of major pre-Cenozoic stratigraphic boundaries (i.e., blue and dark and light green horizons) consistent with NNE-verging folds and top-NNE duplexes along major thrust fault surfaces. Upwards, the Mercedes fault zone splays into multiple, soft-linked segments showing hundred-meter- to km-scale offsets associated with a several km-wide, upright, open anticline in Upper Cretaceous–Cenozoic strata. See location and legend in Figure 3a. Abbreviations: FS: Fueguino syncline; LM-1: Lago Mercedes 1 wellbore; MF: Mercedes fault zone.

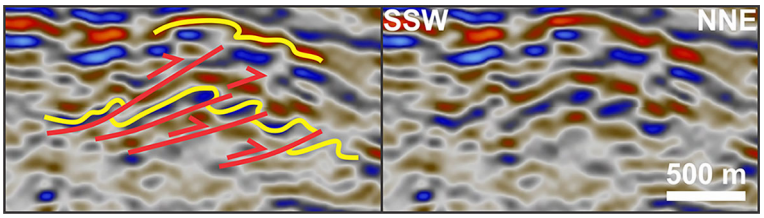

Figure 20. Interpreted (left) and uninterpreted (right) zoom in minor, top-NNE, imbricate thrusts within Cenozoic sedimentary strata above the Mercedes fault zone. See location and legend in Figure 3a.

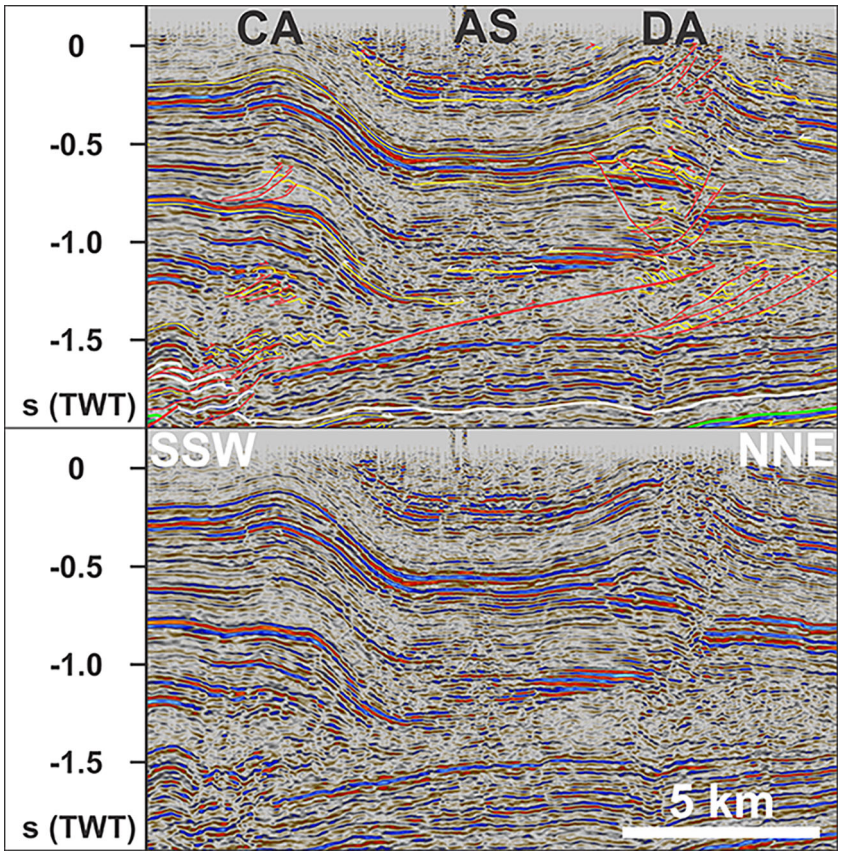

Figure 21. Interpreted (up) and uninterpreted (down) zoom in several km wide, upright, open folds about the Mercedes fault zone, i.e., in the proximal foreland of the Tierra del Fuego fold-and-thrust belt. Notice the monoclinal geometry of the Constancia Anticline and the probable formation of the Despedida Anticline as detachment fold, i.e., formed in the hanging wall of a shallow, gently SSW-dipping, soft-linked segment of the Mercedes fault zone. See location and legend in Figure 3a. Abbreviations: AS: Aurelia Syncline; CA: Constancia Anticline; DA: Despedida Anticline.

While the apparent top-NNE offsets indicate brittle (cataclastic) deformation (e.g., Mosqueira González *et al.*, 2021), the high-amplitude, locally asymmetrically folded geometry of the reflections characterizing the thrust faults suggests the occurrence of relatively dense rocks along the faults (Figure 4). A probable candidate is mylonite, which typically develops along major thrust fault surfaces and has a higher density due to the formation of high-grade metamorphic minerals during deformation (e.g., Arbaret & Burg, 2003; Bell & Etheridge, 1973; Bell & Hammond, 1984; Colombu *et al.*, 2015; Lapworth, 1885; Platt, 1983; Sibson, 1977; Sibson, 1980; White *et al.*, 1980). Thus, mylonitic thrust surfaces generally appear as dominantly planar (locally folded), high-amplitude seismic reflections in seismic reflection data (e.g., Christensen, 1965; Christensen, 1966; Fazlikhani *et al.*, 2017; Fountain *et al.*, 1984; Hurich *et al.*, 1985; Koehl *et al.*, 2022; Phillips *et al.*, 2016; Reeve *et al.*, 2013), i.e., comparable to disruption surfaces in the Tierra del Fuego fold-and-thrust belt in the south, which are hence interpreted as brittle–ductile thrust systems (Figure 3a–d and Figure 4). This is

supported by outcrops of mylonites in the Tierra del Fuego fold-and-thrust belt in the study area (Esteban *et al.*, 2011; González Guillot *et al.*, 2010; Menichetti *et al.*, 2008; Suárez *et al.*, 2000; Torres Carbonell *et al.*, 2020) and farther west (Muller *et al.*, 2020), and in the Darwin Cordillera in the south (Betka *et al.*, 2022; Nelson *et al.*, 1980).

Lower domain (Paleozoic basement rocks)

The transition from dominantly low-amplitude, highly disrupted reflections of the wedge-shaped southwestern domain (i.e., Tierra del Fuego fold-and-thrust belt) to moderate–high-amplitude reflections of the lower domain suggests a change in both rock type and deformation style across the gently SSW-dipping disruption surface (i.e., sole thrust; Figure 3a–d). A notable abrupt change is the gentler dip of major disruption surfaces within the lower domain (Figure 3a–d). Since these are also typically associated with km- to several-km-scale top-NNE reverse offsets (e.g., blue and light green horizons in Figure 3a–d and Figure 4) and NNE-verging asymmetric- and Z-shaped reflections, which are comparable to those along disruption surfaces in the overlying southwestern domain (i.e., Tierra del Fuego fold-and-thrust belt), they are interpreted as major brittle–ductile thrust faults. The abrupt change from moderate–steep to more gentle dips of thrust faults in the lower domain indicates a major rheological boundary. It is therefore proposed that the lower domain consists mostly of tightly deformed Paleozoic basement rocks of the Tierra del Fuego igneous and metamorphic complex (Figure 3a–d and Figure 4).

The presence of a major rheological boundary between the southwestern and lower domains is supported by the location and attitude of the sole thrust, i.e., subparallel to and partly localized along the interpreted boundary between Paleozoic basement and Mesozoic volcanosedimentary rocks (i.e., blue horizon in Figure 3a–d and Figure 4). It is also supported by the (thrust-related) thickening of pre-Cordilleran (i.e., pre-contraction), Jurassic–Lower Cretaceous volcanosedimentary units in the Tierra del Fuego fold-and-thrust belt (up to 0.4–0.5 second TWT) compared to equivalent strata just north of the fold-and-thrust belt (ca. 0.1–0.2 second TWT and c. 500 m thick in the Lago Mercedes 1 wellbore; Gallardo Jara *et al.*, 2022; Table 1), which suggests partial strain partitioning by these units. This is consistent with previous seismic interpretation in the area (e.g., Álvarez-Marrón *et al.*, 1993; Gallardo Jara *et al.*, 2022).

North of the Tierra del Fuego fold-and-thrust belt, most major low-angle thrust faults there die out below the Mid-Cretaceous unconformity, thus suggesting that these mostly formed prior to the mid-Cretaceous and/or strain partitioning (and, thus, a possible major rheological boundary) between the lower domain and northeastern domain (Figure 3a–h). A notable exception is the thrust fault system below the Lago Mercedes 1 wellbore, which offsets the Mid-Cretaceous unconformity and Base Cenozoic horizon by up to c. 2 km top-NNE and coincides with a broad, c. 5 km wide, asymmetric upright anticline to monocline in the overlying northeastern domain (Figure 3a–d and Figure 19). This fault system correlates with the Mercedes fault zone (Gallardo Jara *et al.*, 2022).

A major rheological boundary between the lower and northeastern domains is further supported by the occurrence of multiple gently dipping to subhorizontal, a few km wide disruption surfaces displaying hundred-meter- to km-scale reverse offsets of Mesozoic volcanosedimentary units and the Mid-Cretaceous unconformity and Base Cenozoic horizons (Figure 3a–h, Figure 11, Figure 12, and Figure 16). Their subhorizontal, downward-flattening geometry, i.e., subparallel to stratigraphic boundaries, suggests that they correspond to minor décollements–detachments.

North of the sole thrust of the Tierra del Fuego fold-and-thrust belt, major thrust faults and associated asymmetric folds and duplexes in the lower domain show alternating top-NNE and top-SSW kinematics, including both S- and Z-shaped duplex horses (Figure 3a–h, Figure 4, Figure 11, Figure 12, Figure 14a–e, Figure 17a–i, and Figure 18a–b). Notably, they display opposite kinematics on opposite flanks of the U-shaped troughs of Jurassic–Lower Cretaceous units (Figure 3a–b and e–h, Figure 11, Figure 12, Figure 14a–e, and Figure 16). For example, structures along the northern flank of the Gaviota and Oriental (also called Ostión and Calafate) troughs include NNE-verging asymmetric folds and top-NNE thrust faults and Z-shaped duplexes, whereas the southern flanks show SSW-verging folds and top-SSW thrusts and S-shaped duplexes (Figure 3a–b and e–h, Figure 11, Figure 12, and Figure 18a–b). In addition, the local π-shaped geometry of asymmetric reflections in U-shaped seismic packages suggest double-verging folds (Figure 13). Like between the southwestern and lower domains, the subparallelism of major thrust faults and stratigraphic boundaries suggests that these localize strain partitioning, which is in agreement with the rheological difference between competent igneous and metamorphic basement rocks and weaker volcanosedimentary rocks.

The U-shaped geometry and the occurrence of folds and thrust faults with opposite kinematics on either flank of the Gaviota and Oriental troughs, together with evidence of oppositely-verging parasitic folds on the limbs of several-km-wide symmetric folds in the Tierra del Fuego fold-and-thrust belt in the southwest suggest that the two troughs correspond to tens of km wide, upright synclines, hereby named the Gaviota and Oriental synclines. The erosional truncation

(e.g., toplap reflection geometries) of gently north-and south-dipping Jurassic–Lower Cretaceous strata indicate that these folds formed in the mid-Cretaceous (Figure 3a–b and e–h and Figure 15).

Overall, Paleozoic–Mesozoic rocks in the lower domain show a northwards decrease in the intensity of contractional deformation, i.e., in agreement with previous works in the area. This is exemplified by the transition from large, several km wide, top-NNE offsets and tight (e.g., isoclinal recumbent) folding of Mesozoic–Cenozoic successions along the sole thrust and multiple imbricate thrust faults in the Tierra del Fuego fold-and-thrust belt (Figure 3a–d and Figure 4) to localized km-scale offset at the Mercedes fault zone (Figure 19) and hundred-meter- to km-scale offsets along sparser, oppositely-dipping thrust faults and gentle open (in places, π-shaped double-verging) folding of Mesozoic–Cenozoic strata in the north (Figure 3a–b and e–h and Figure 13).

Northeastern domain (Magallanes foreland basin)

Overall, the largely continuous character of seismic reflections in the northeastern domain suggests it consists of relatively undeformed sedimentary strata (Figure 3a–h). This is supported by the low number of disruption surfaces (apart from a few subhorizontal décollement–detachments in the lower part) in this domain and by local gentle, open folding in the southwestern part (Figure 3a–h, Figure 20, and Figure 21). There, broad, gentle, open anticlines north of the Tierra del Fuego fold-and-thrust belt coincide from south to north with the Miraflores Anticline, which dies out to the southeast (Álvarez-Marrón *et al.*, 1993), and the Constancia Anticline, Aurelia Syncline, Despedida Anticline, and Moneta Anticline (Figure 1c, Figure 3a–f, Figure 20, and Figure 21; Torres Carbonell *et al.*, 2013). While most folds affect the entire rock column, some only affect the uppermost successions and coincide at depth with low-angle, dominantly SSW-dipping disruption surfaces (e.g., Despedida Anticline; Figure 3a–f, Figure 20, and Figure 21). These are interpreted as detachment folds, in agreement with previous studies in the area (e.g., Torres Carbonell *et al.*, 2013).

The localization of deformation in the southwest and significant southward thickening of the northeastern domain and of dominantly northward-prograding individual successions suggest that this domain consists of Upper Cretaceous–Cenozoic sedimentary deposits related to uplift and erosion in the Tierra del Fuego fold-and-thrust belt in the southwest, i.e., corresponding to the Magallanes foreland basin. More specifically, the northward- and southward-prograding character of seismic reflections and associated thinning of the basal succession towards the center of the northeastern domain and the correlation of this seismic succession with Upper Cretaceous sedimentary rock units in nearby wellbores suggest initial sediment input from the north and south in the Late Cretaceous (Figure 3a–h and Figure 11). In addition, local thickening in conjunction with the absence of or limited deformation of this unit in the footwall of major thrust faults (e.g., Mercedes fault zone) indicates a syn-thrusting deposition (Figure 19). This succession is therefore suggested to reflect the onset of significant uplift and erosion in the Tierra del Fuego fold-and-thrust belt (i.e., early-foreland sediments), which is consistent with previous interpretation (e.g., Gallardo Jara *et al.*, 2022).

The up to 2.5 seconds thick overlying succession of northward-prograding and northward-thinning reflections and units indicates sediment input almost exclusively from the Tierra del Fuego fold-and-thrust belt (Figure 3a–h). Hence, it is interpreted as the main Cenozoic foreland succession of the Magallanes basin. This is consistent with the gradual northward thinning of Cenozoic sedimentary rock units in nearby exploration wells from > 3000 m thick in the south (Lago Mercedes 1 wellbore) to c. 1000 m in the north (e.g., María Emilia 3 wellbore; Gallardo Jara *et al.*, 2022; Figure 3a–h and Table 1).

Discussion

Outcrop–subsurface correlations and implications for Orogenic Bridge Theory

The present work correlates hundreds of meters wide to km-scale asymmetric (dominantly NNE-verging) folds and duplexes in outcrops with seismic reflections of comparable shape and size (Figure 3a–f and Figure 4). The range of geometrical variations of the interpreted hundred-meter-wide fold structures, e.g., isoclinal, overturned to recumbent, asymmetric parasitic folds on the limbs of several km-wide symmetric (chevron-like) folds, is comparable to that of structures in fold-and-thrust belts worldwide (e.g., Butler *et al.*, 2018; Calvert *et al.*, 2021; Dentith *et al.*, 2018; Freeman *et al.*, 1988; Hedin *et al.*, 2016; Klemperer *et al.*, 1991; Koehl, 2021; Koehl, 2025; Koehl *et al.*, 2022; Koehl *et al.*, 2023a; Koehl & Stokmo, 2025; Morley *et al.*, 2017; Stanca *et al.*, 2022; Stewart & Salem, 2023). The dominant top-NNE contractional kinematics derived from their geometry is consistent with offsets along major thrust faults in the area, both in outcrops and in seismic data (Figure 3a–f and Figure 4; Álvarez-Marrón *et al.*, 1993; Gallardo Jara *et al.*, 2022; Mosqueira González *et al.*, 2021; Torres Carbonell *et al.*, 2020).

Despite preliminary modelling work (e.g., Ji & Long, 2006) and identification of a few individual structures locally (e.g., antiformal stack in Morley *et al.*, 2017 their Figure 8), hundred-meter-scale folds remain challenging to confidently

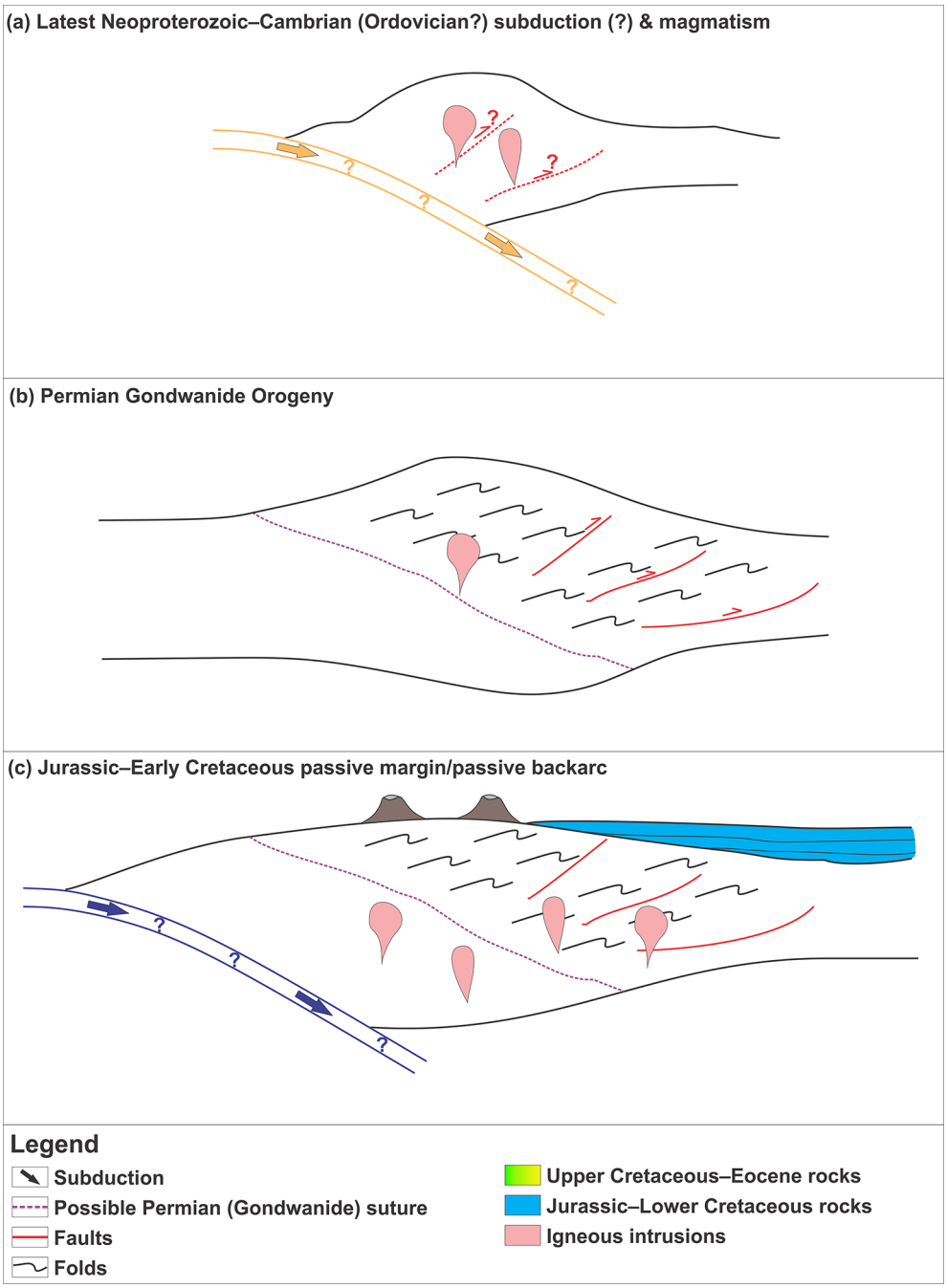

Figure 22. Simplified tectonic evolution of the Tierra del Fuego region in southern Patagonia, including (a) potential subduction and (related?) magmatism leading to the formation of rocks of the Tierra del Fuego igneous and metamorphic complex, (b) Permian orogenesis and magmatism during the Gondwanide Orogeny, which deformed and metamorphosed Paleozoic basement rocks, (c) Jurassic–Early Cretaceous magmatism and volcanism in a passive (backarc?) setting, (d) mid-Early Cretaceous to Eocene contraction and magmatism resulting in the formation of the Tierra del Fuego fold-and-thrust belt (TdF FTB), broad, open, upright synclines of Jurassic–Lower Cretaceous volcanosedimentary rocks, and the Magallanes foreland basin (MFB), (e) possible mild inversion of thrust faults during extensional collapse and/or rifting of the Central Scotia Sea, and (f) Oligocene to present-day transtension with lateral movements along the Magallanes–Fagnano fault zone. Abbreviations: DCMC: Darwin Cordillera metamorphic complex; FB: Fuegian batholith; MFB: Magallanes foreland basin; MFFZ: Magallanes–Fagnano fault zone; TdF FTB: Tierra del Fuego fold-and-thrust-belt.

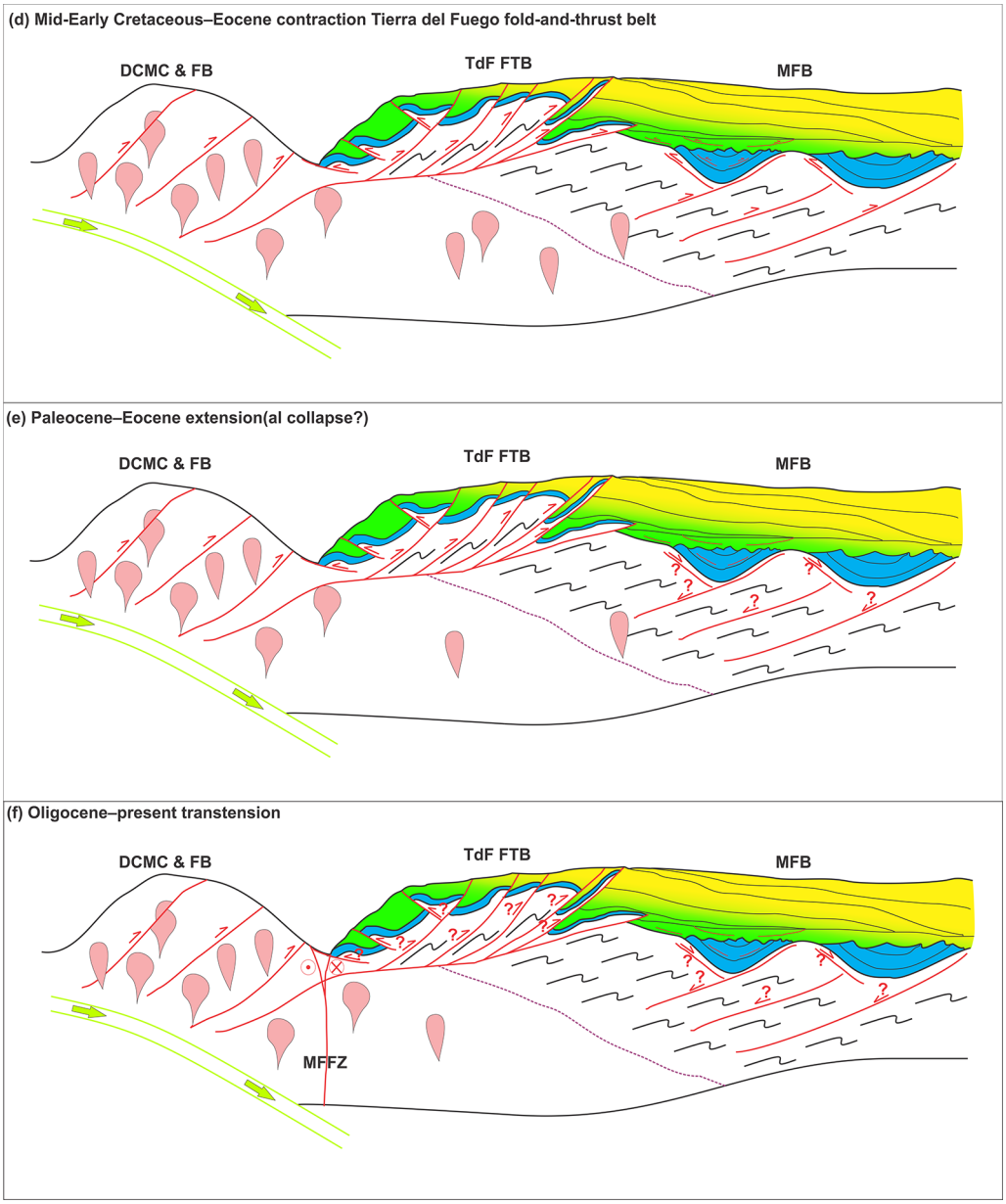

Figure 22. (continued)

identify in the subsurface. Thus far, most seismic interpretation and modelling studies have focused on relatively large (several km to tens of km wide) folds and thrust structures, generally in well-bedded (i.e., unmetamorphosed and/or not intensely deformed) sedimentary rocks (e.g., Butler *et al.*, 2018; Calvert *et al.*, 2021; Dentith *et al.*, 2018; Freeman *et al.*, 1988; Gabrielsen *et al.*, 2022; Ghanadian *et al.*, 2017; Klemperer *et al.*, 1991; Ma *et al.*, 2019; Sobornov, 1992; Sobornov *et al.*, 2015; Stewart & Salem, 2023; Wrona *et al.*, 2020). Hundreds of meters wide folds have only recently started to be consistently described and interpreted in detail and used as kinematic indicators for major thrust systems and shear zones in orogens and fold-and-thrust belts in subsurface seismic data. A key example was described in central Svalbard, where tightly folded and sheared uppermost Devonian–Mississippian coal seams in outcrops were tied to their continuation in nearshore seismic data (Koehl, 2021). Coal has a relatively low density, thus making it likely to produce negative high-amplitude reflections in seismic data (e.g., Koehl *et al.*, 2018; Qi *et al.*, 2025; Tonstad, 2018; Yao & *Han*, 2008). Further support came from subsequent studies of regional 2D (e.g., Koehl, 2021; Koehl, 2025; Koehl & Allaart, 2021; Koehl *et al.*, 2022) and high-resolution 3D seismic data in Svalbard and the Barents Sea (Koehl *et al.*, 2023a; Koehl &

Stokmo, 2025). The seismic facies of these structures in now being systematized and further tested worldwide (e.g., present study; Koehl *et al.*, 2024; Koehl, 2026a).

In contrast, the seismic facies of mylonitic faults and shear zones has been known for some time and is now well understood, from early theoretical studies (e.g., Christensen, 1965; Christensen, 1966) and ensuing applied studies of specific examples (e.g., Brewer *et al.*, 1980; Brocher & Christensen, 1990; Christensen & Szymanski, 1988; Fountain *et al.*, 1984; Hajnal *et al.*, 1996; Hurich *et al.*, 1985; McDonough & Fountain, 1988; Wang *et al.*, 1989) to a renewed recent interest (e.g., Bird *et al.*, 2016; Collenaga *et al.*, 2019; Deng *et al.*, 2022; Fazlikhani *et al.*, 2017; Fossen *et al.*, 2024; Hedin *et al.*, 2016; Lenhart *et al.*, 2019; Osagiede *et al.*, 2020; Phillips *et al.* 2016; Phillips & McCaffrey, 2019; Reeve *et al.*, 2013). Studies of mylonitic shear zones are expected to further help the mapping of hundred-meter-scale folds in subsurface seismic data since the latter typically occur along or adjacent to major mylonitic thrust faults and shear zones (e.g., Figure 3a–d, Figure 4, Figure 5a–e, and Figure 8a–d; Bell, 1978; Bell & Hammond, 1984; Fletcher & Bartley, 1994 their Figures 5 and 9; Platt, 1983; Sibson, 1977; Xypolias *et al.*, 2013 their Figures 2d and 3a–b).

The present study further gives weight to previous results and interpretations supporting the concept of orogenic bridges (e.g., Koehl, 2025; Koehl *et al.*, 2024; Koehl, 2026a). Orogenic Bridge Theory suggests that orogens striking perpendicular to incipient rifts hinder rifting and breakup and localize the formation of major transform faults (Koehl & Foulger, 2025). This notion is based on a global correlation of all major (≥ a few tens of km offset) transform faults with rift-orthogonal orogens on adjacent rifted margins and associated delayed breakup due to the unsuitable orientation of preexisting crustal fabrics (Koehl & Foulger, 2025). In the North Atlantic region, regional subsurface datasets have shown the existence of continental crustal domains offshore extending well beyond the previously postulated continent–ocean transition, e.g., in the Fram Strait (Dumais *et al.*, 2020; Koehl, 2025), Greenland–Iceland–Faroe Ridge (Geoffroy *et al.*, 2021; Foulger *et al.*, 2020; Koehl *et al.*, 2024; Koehl, 2026a), and Davis Strait (Dafoe *et al.*, 2022; Dalhoff *et al.*, 2006; Longley *et al.*, 2024; Peace *et al.*, 2018). Seismic reflection data at these extended offshore continental domains show indications of fold and thrust structures of comparable size (hundred-meter-scale) and geometries (asymmetric, recumbent, isoclinal, and duplexes) to those observed in the Tierra del Fuego fold-and-thrust belt and Paleozoic basement rocks under the Magallanes foreland basin (Figure 3a–h, Figure 4, Figure 5a–e, Figure 6, Figure 7a–b, Figure 8a–d, Figure 9a–c, Figure 10, Figure 11, Figure 12, Figure 13, Figure 14a–e, Figure 15, Figure 16, Figure 17a–i, Figure 18a–b, and Figure 19). The present study reduces the uncertainty around the interpretation of hundred-meter-scale orogenic structures in the subsurface, thus further supporting Orogenic Bridge Theory.

Permian Gondwanide deformation in southern Patagonia

In the Tierra del Fuego fold-and-thrust belt in the southwest, the transition from Jurassic–Lower Cretaceous volcano-sedimentary rocks to Paleozoic igneous and metamorphic basement rocks is subtle, corresponding to a mild increase in seismic amplitude at depth in the southwest as both rock units are truncated by comparable deformation structures (Figure 3a–d). In contrast, this transition is more pronounced in the northeast below the Magallanes foreland basin. There, the Jurassic–Lower Cretaceous rock units are considerably less deformed than in the Tierra del Fuego fold-and-thrust belt, whereas basement rocks are as tightly deformed as in the south and truncated by comparable folds and thrusts (Figure 3a–b and e–h, Figure 4, Figure 11, and Figure 12).

It is possible that the more intense deformation in Paleozoic basement rocks than in overlying Jurassic–Lower Cretaceous units may reflect strain partitioning of Late Cretaceous–Cenozoic contraction. However, Jurassic–Lower Cretaceous volcanosedimentary rock units are less competent than underlying Paleozoic metamorphic–igneous rocks and would thus preferentially localize deformation, ending up being more deformed.

Hence, Paleozoic basement rocks of the Tierra del Fuego igneous and metamorphic complex were likely involved in more than one episode of contraction and at least part of the deformation in basement rocks was inherited from (a) pre-Jurassic tectonic episode(s) (Figure 22a–b). A probable scenario is an involvement in the Permian Gondwanide Orogeny (Falco *et al.*, 2024; López-Gamundí, 2006; Pankhurst *et al.*, 2006; Figure 22b). This is supported by Permian ages for high-grade metamorphism and magmatism in rocks of the Tierra del Fuego igneous and metamorphic complex below the Magallanes foreland basin in the north, e.g., in the Punta Baja 1, Cormorán 1, María Emilia 3, and Catalina 1 wellbores, in the northern part of the study area (Castillo *et al.*, 2017; Halpern, 1973; Hervé *et al.*, 2010a; Figure 1b and Figure 3a–h).

This is consistent with records of Permian contraction and related metamorphism and magmatism in nearby onshore–offshore areas in South America such as the Falkland Islands (Adie, 1952; Curtis & Hyam, 1998; Ramos *et al.*, 2017), Deseado Massif (Navarette *et al.*, 2023), North Patagonian Massif (along called Somoncura/Somún Cura Massif; Caminos *et al.*, 1988; Castillo *et al.*, 2017; Falco *et al.*, 2022; Grillo Vidal *et al.*, 2024; Uliana & Biddle, 1987), Sierra

de la Ventana (Ballivián Justiniano *et al.*, 2023; Limarino *et al.*, 1999; Trouw & de Wit, 1998; von Gosen *et al.*, 1990), and San Rafael Massif (Kleiman & Japas, 2009; Figure 1a).

The present interpretation is further supported by folded Paleozoic sedimentary rocks unconformably overlain by Mesozoic strata in the Malvinas Basin, Falkland Plateau, and Maurice Ewing Bank (McCarthy *et al.*, 2017; Ramos *et al.*, 2019; Stanca *et al.*, 2022). Moreover, early Paleozoic basement rocks (granite and gneiss) in Maurice Ewing Bank yielded comparable (early Cambrian) ages to those of the Tierra del Fuego igneous and metamorphic complex and were affected by a thermal event in the Permian at ca. 287 ± 7 Ma (Beckinsale *et al.*, 1977; Tarney, 1977), i.e., coeval with high-grade metamorphism in Tierra del Fuego (Halpern, 1973; Hervé *et al.*, 2010a). It is therefore probable that the Permian fold-and-thrust belt in early Paleozoic basement rocks in Tierra del Fuego, which was reworked during mid-Cretaceous–Cenozoic contraction, represents the continuation of the Gondwanide fold-and-thrust belt in the Falkland Island–Maurice Ewing Bank continental salient (Figure 3a–h; Figure 22b). This suggests that these crustal blocks (i.e., Patagonia and Falkland Islands–Maurice Ewing Bank) retained a somewhat similar relative position since at least the Permian, but probably much earlier as suggested by early Cambrian and Mesoproterozoic ages for basement rocks in the Falkland Islands and Maurice Ewing Bank (e.g., Beckinsale *et al.*, 1977; Chemale Jr *et al.*, 2018; Jacobs, 1999) and Cambrian ages for the Tierra del Fuego igneous and metamorphic complex in the study area (e.g., Hervé *et al.*, 2010b; Pankhurst *et al.*, 2003; Söllner *et al.*, 2000; Figure 22a–b), the latter of which suggest a potential involvement in the Pampean–Famatinian orogenies (Cristofolini *et al.*, 2014; Pankhurst *et al.*, 1998; Ramos *et al.*, 2014; Ramos *et al.*, 2015; Rapela *et al.*, 1998; Schwartz *et al.*, 2008; Steenken *et al.*, 2011; Verdecchia *et al.*, 2011; von Gosen *et al.*, 2002).

A broad, continuous, Permian Gondwanide fold-and-thrust belt extending from northern to southern Patagonia and to Maurice Ewing Bank in the east can be reconstructed smoothly prior to rifting and fitted with its counterparts in South Africa (Cape Fold Belt; Johnston, 2000; Paton *et al.*, 2022), Antarctica (Graham Land and Ellsworth Mountains; Curtis, 2001; Elliott *et al.*, 2019), Indonesia (folded Silurian–Devonian Omung Group; Brown *et al.*, 1979; Davies, 1980; Harahap, 2012; Hill & Raza, 1999; Page, 1976; Pigram & Davies, 1987), and New Zealand and northeastern Australia (e.g., Median Batholith and Tuhua Orogen; Allibone *et al.*, 2009; Campbell *et al.*, 2020; Gibson, 1992; McCoy-West *et al.*, 2014; Mortimer *et al.*, 1999; Robertson *et al.*, 2019; Suggate, 1965), thus providing a new anchor for Precambrian–Paleozoic plate reconstructions. Notably, it is now necessary to consider Patagonia (Sierra de la Ventana to Fuegan Andes) and the Falkland Islands salient (Malvinas Basin to Maurice Ewing Bank) as a single continental block with limited relative movement between each segment since the Permian (but probably since Cambrian times).

Jurassic–Lower Cretaceous tectonic quiescence

The Gaviota and Oriental synclines and related depocenters consist of Jurassic–Lower Cretaceous volcanosedimentary rocks folded into 10–25 km wide open synclines (Figure 3a–b and e–h, Figure 11, and Figure 12). These successions are up to ca. 1.0–1.5 second thick (TWT), i.e., > 1.5 km thick as suggested by results from the María Emilia 3 wellbore where Jurassic–Lower Cretaceous successions are 1.0 second thick (TWT) and parallel low-angle thrusts. Both these and the truncated Jurassic–Lower Cretaceous successions are consistently truncated upwards at an angle by the Mid-Cretaceous unconformity on the limbs of the broad open synclines (toplap reflection geometries; Figure 3a–b and e–h, Figure 11, Figure 12, and Figure 15). This together with the absence of steeply-dipping disruptions showing normal offsets in pre-mid-Cretaceous rocks (lower domain), even if restoring the successions prior to broad open folding, precludes a formation as normal-fault-bounded, rift-related grabens as previously suggested (e.g., Gallardo Jara *et al.*, 2022; Miller *et al.*, 2022; Robbiano *et al.*, 1996). Instead, the Gaviota and Oriental synclines and related open folds are interpreted to reflect the onset of contraction and widespread deformation in the (mid-Early–) mid-Cretaceous. These broad synclines were then eroded and unconformably covered by Upper Cretaceous deposits reflecting gradual strain localization southwards in the Tierra del Fuego fold-and-thrust belt (Figure 3a–b and e–h, Figure 11, and Figure 12).

Previously interpreted Jurassic (half-) grabens in the study area, e.g., Dorado, Delfin–Neptuno, Fueguino, Olivos, Vania, and Dungeness grabens, all display a rounded base with an overall U-shaped basin geometry comparable to that of the Gaviota and Oriental synclines (Gallardo Jara *et al.*, 2022 their Figures 8b, 10, 11, and 14; Miller *et al.*, 2022 their Figures 3–4). This is also the case of Jurassic–Lower Cretaceous basins in nearby areas, e.g., folded (sheared) contact (décollement) between late Paleozoic basement rocks of the Cordillera Darwin metamorphic complex and overlying Jurassic–earliest Cretaceous rocks of the Tobífera Formation (e.g., Betka *et al.*, 2022), and sedimentary basins in the offshore Malvinas Basin in the east (e.g., Lovecchio *et al.*, 2019 their Figures 6–8; Ramos *et al.*, 2019 their Figure 6; Robbiano *et al.*, 1996 their Figures 4–9) and both onshore (e.g., Huemul Group; Giacosa & Heredia, 1999; Giacosa *et al.*, 2010; Navarette *et al.*, 2023) and offshore northern Patagonia (e.g., Lovecchio *et al.*, 2024 their Figure 11; Rojas Vera *et al.*, 2024 their Figures 8–9). The lack of clear disruption and offset along the presumed normal faults, combined with excessive vertical exaggeration of seismic transects and/or, in some instances, relatively low data quality suggest that these basins could instead be synclines formed during (Permian and/or) Cretaceous–Cenozoic contraction. Notably,

excessive vertical exaggeration of regional seismic transects, although convenient for dissemination purposes, distorts gently-dipping thrust faults and fold limbs into steeper geometries, thus potentially biasing their interpretation into normal faults instead of thrusts and folds. Working with vertically exaggerated seismic sections typically biases towards increased interpretation of steep faults (i.e., biasing interpretation of fault kinematics towards normal and/or strike-slip) and increased vertical connectivity between fault segments (i.e., interpretation of hard-linked faults instead of soft-linked/disconnected fault segments; e.g., Bond, 2015; Butler, 2023; Stewart, 2011).

Thus, the present results suggest that Jurassic–lowermost (/Lower?) Cretaceous sedimentary rocks were deposited in a passive margin or passive backarc setting rather than in an active rift (Figure 22c). This is consistent with regional seismic transects showing unfaulted Jurassic successions, e.g., in the Malvinas Basin (McCarthy *et al.*, 2017 their Figure 2; Ramos *et al.*, 2019 their Figure 4).

Onset of contraction in Tierra del Fuego in the Cretaceous

Jurassic–Lower Cretaceous rocks in the Gaviota and Oriental synclines show two phases of folding. First, they were deformed into broad, 10–25 km wide open folds prior to being eroded in the mid-Cretaceous. This episode includes tight deformation of the lower succession (Jurassic–earliest Cretaceous Tobífera Formation), which was deformed into hundred-meter- to km-scale asymmetric folds (Figure 3a–h, Figure 11, Figure 12, and Figure 22d). A second phase of post-erosion (i.e., post-mid-Cretaceous) deformation involved gentle, 1–5 km wide, open folds generally associated with minor hundred-meter- to km-scale offsets of Upper Cretaceous–lower Cenozoic sedimentary rocks, including detachment folds and low-angle décollements–detachments in Paleocene–Oligocene sedimentary units (Gallardo Jara *et al.*, 2022; Figure 3a–h, Figure 15, Figure 16, Figure 20, and Figure 21).

Modest thickening (ca. 0.1–0.2 second TWT; c. 100 m thickening in the Cisne 1 wellbore; Gallardo Jara *et al.*, 2022; Table 1) of Lower Cretaceous sedimentary successions towards the center of the Gaviota and Oriental synclines and the bounding of the areas of thickened deposits by low-angle to subhorizontal thrusts (Figure 3a–h, Figure 15, Figure 16, Figure 11, and Figure 12) indicate post-deposition tectonic thickening due to strain partitioning during thin-skinned deformation, which is common in the area (e.g., detachment folding in overlying lower Cenozoic units; Figure 3a–f, Figure 20, and Figure 21; Torres Carbonell *et al.*, 2013). However, although brittle thrusts appear to accommodate most of the thickening, the toplap and onlap geometries of reflections in Lower Cretaceous units, with both the eroded (toplap) and onlapping reflections dominantly dipping towards the center of the Gaviota and Oriental synclines, suggest that folding initiated in the Early Cretaceous, i.e., during the deposition of Lower Cretaceous sedimentary rocks of the Lower Cretaceous Río Jackson and Beauvoir formations and during or prior to erosion in the mid-Cretaceous, and was ubiquitously distributed in the entire study area (Figure 3a–h, Figure 11, Figure 12, Figure 15, Figure 16, and Figure 22d).

This is consistent with the 130–91 Ma K–Ar ages for brittle–ductile shear zones in southern Tierra del Fuego (Suárez *et al.*, 2000) and with ca. 126–112 Ma K–Ar illite ages farther northwest, which were previously interpreted as mixed ages but may in fact reflect the onset of contraction (Süssenberger *et al.*, 2018). It is also in line with other geochronological studies in the southern Andes and the study area reporting Late Cretaceous ages (Klepeis *et al.*, 2010; Kohn *et al.*, 1995; Muller *et al.*, 2020; Torres Carbonell *et al.*, 2020), e.g., ca. 86 Ma ^{40}Ar–^{39}Ar age for high-grade metamorphism in the Darwin Cordillera metamorphic complex (Kohn *et al.*, 1995) and ca. 86–74 Ma U–Pb crystallization ages for post-tectonic granites and pegmatites crosscutting early thrusts (Klepeis *et al.*, 2010), and with the 98.3 ± 1.2 Ma K–Ar age for deformation (Süssenberger *et al.*, 2018) and the 101.0 ± 1.0 Ma age for volcanic ash in the upper part of the transition between the Lower Cretaceous Zapata Formation and the Upper Cretaceous Punta Barrosa Formation (Río Garcia and Lutitas Arenosas formations time equivalent; Gallardo Jara *et al.*, 2022) west of the study area (Fosdick *et al.*, 2011). A mid-Early Cretaceous onset of contraction is also potentially supported by tight folding of Lower Cretaceous sedimentary strata of the Canal Bertrand Formation but not of overlying Upper Cretaceous sedimentary units in the west (McAtamney *et al.*, 2011). However, these structural differences could be related to strain partitioning between shale-dominated Lower Cretaceous and sand-rich Upper Cretaceous rocks.

The northwards and southward-prograding character of the Upper Cretaceous sedimentary succession, which is supported by thicker successions in the Lago Mercedes 1 and María Emilia 3 wellbores (Gallardo Jara *et al.*, 2022) and its thickening in the footwall of the sole thrust and Mercedes fault zone (Figure 3a–d, Figure 4, and Figure 19) indicate that significant uplift and erosion had already started both in the south (Tierra del Fuego fold-and-thrust belt) and north. This further supports the initiation of contraction in the Early Cretaceous.

It is probable that the coeval, mid-Early Cretaceous to Cenozoic, global eustatic sea-level fall, which initiated at ca. 125–120 Ma (van der Meer *et al.*, 2022 and references therein; Figure 2), also contributed to expose Jurassic–Lower Cretaceous sedimentary rocks to erosion between the two phases of contractional deformation, thus resulting in the

observed, regional, mid-Cretaceous erosional truncation of the broad mid-Early to mid-Cretaceous synclines (light green horizon in Figure 3a–h, Figure 11, and Figure 12). The mid-Early–mid-Cretaceous synclines were then covered by Upper Cretaceous–Cenozoic sediments and further (mildly) folded and thrust in the (Late Cretaceous?–) Paleogene (Figure 22d).

Cenozoic transtension

The only potential evidence of Cenozoic extension in the interpreted data is the geometry of S-and Z-shaped duplexes below the Magallanes foreland basin. In places, the counterclockwise curvature of some duplex horse reflections into major low-angle thrust fault may suggest partial reworking and mild extensional inversion of mid Cretaceous–early Cenozoic thrusts (Figure 17d and i, Figure 18a, and Figure 22e). The timing of thrust inversion is, however, uncertain and could have been partly coeval with late contraction in the Tierra del Fuego fold-and-thrust belt, which ended in the Oligocene–early Miocene (Torres Carbonell *et al.*, 2016). Thrust inversion could reflect extensional collapse and/or rifting of the Central Scotia Sea in the (latest?) Paleocene–(early?) Eocene (e.g., Dalziel & Brown, 1989; Eagles, 2010; Ghiglione *et al.*, 2008; Klepeis, 1994b; Figure 22e) and/or have occurred much later, e.g., in conjunction with seafloor spreading and related transtension at the West and/or East Scotia ridges, i.e., ≤ 30 Ma (Barker, 2001; Klepeis, 1994b; Riley *et al.*, 2019; Rossello, 2005; Torres Carbonell *et al.*, 2008; Figure 22f).

There is, however, no trace of primary extensional structures in the subsurface in the study area (Figure 3a–h, Figure 11, and Figure 12), which contrasts with the occurrence of small brittle faults with meter-scale normal offsets and related pull-apart basins along the Magallanes–Fagnano fault zone just south of the study area (e.g., Esteban *et al.*, 2014; Klepeis, 1994b; Lodolo *et al.*, 2003; Menichetti *et al.*, 2008; Restelli *et al.*, 2025) and farther east on the Mitre Peninsula (e.g., Ghiglione *et al.*, 2008; Figure 1b). This suggests a limited extensional component to Cenozoic transtension and/or that extension is confined to a narrow zone along the Magallanes–Fagnano fault zone and related fault segments (Figure 22e–f). However, minor, meter-scale normal faults also truncate lower–middle Paleocene deposits of the Chorrillo Chico Formation away from the Magallanes–Fagnano fault zone in Otway Sound in the northwest (Figure 1b; e.g., Pinto *et al.*, 2022 their Figure 6). There, the lower–middle Paleocene sedimentary units show growth strata, thus indicating a syn-tectonic deposition and relatively widespread and distributed (late-orogenic, collapse-related?) extension in the early Cenozoic. It is thus more probable that the extensional component has been of limited intensity (i.e., "transcurrent" tectonic setting in the Neogene in Figure 2).

Conclusions

1) Hundred-meter- to km-scale asymmetric folds are correlated from onshore outcrops to their subsurface equivalents in seismic reflection data, confirming the seismic facies of these structures suggested by previous studies in the North Atlantic region and opening new avenues for detailed mapping and exploration of the subsurface in fold-and-thrust belts and orogens and for emerging concepts, e.g., orogenic bridges.

2) Paleozoic basement rocks below the Magallanes foreland basin and the Tierra del Fuego fold-and-thrust belt were involved in an episode of pre-Jurassic contraction, likely during the Permian Gondwanide Orogeny, thus suggesting that Patagonia and the Falkland–Maurice Ewing Bank block should be treated as a single crustal block for plate reconstructions at least since the Permian and probably since the early Cambrian.

3) NW–SE- to NNW–SSE-striking U-shaped troughs previously interpreted as rift-related (half-) grabens correspond instead to deeply eroded synclines of Jurassic–Lower Cretaceous volcanosedimentary rocks, which were folded during an early phase of contraction in the mid-Early to mid-Cretaceous.

4) Contraction then gradually localized in the Tierra del Fuego fold-and-thrust belt in the south and only minor contraction occurred in the Magallanes foreland basin in the Late Cretaceous–Paleogene.

5) There is no trace of primary extensional structures in the subsurface in the study area, thus suggesting a limited extensional component to Cenozoic transtension.

Ethics and consent

Ethical approval and consent were not required.

Data availability

Underlying data

The seismic reflection profiles are private industry data and were provided by the Chilean National Hydrocarbon Company (ENAP; https://www.enap.cl/). To access the data, any prospective user may contact the Chilean National Hydrocarbon Company (https://www.enap.cl/consultas).

Extended data

Zenodo: High-resolution versions of the figures for "Onshore surface–subsurface correlation of orogenic structures and the continuation of the late Paleozoic Gondwanides in the Tierra del Fuego fold-and-thrust belt, southern Patagonia" https://doi.org/10.5281/zenodo.20640160 (Koehl, 2026b).

The project contains the following extended data:

- 00_ReadMe.txt
- Figure_1a.jpg
- Figure_1b.jpg
- Figure_1c.jpg
- Figure_2.jpg
- Figure_3a.jpg
- Figure_3b.jpg
- Figure_3c–d.jpg
- Figure_3e–f.jpg
- Figure_3g–h.jpg
- Figure_4.jpg
- Figure_5a–e.jpg
- Figure_6.jpg
- Figure_7a–b.jpg
- Figure_8a–d.jpg
- Figure_9a–c.jpg
- Figure_10.jpg
- Figure_11.jpg
- Figure_12.jpg
- Figure_13.jpg
- Figure_14a–e.jpg
- Figure_15.jpg

- Figure_16.jpg
- Figure_17a–d.jpg
- Figure_17e–i.jpg
- Figure_18a–b.jpg
- Figure_19.jpg
- Figure_20.jpg
- Figure_21.jpg
- Figure_22a–c.jpg
- Figure_22d–f.jpg
- Table_1.pdf
- Table_1.xls

The data is available under the terms of the Creative Commons Zero "No rights reserved" waiver (CC0 1.0 Public domain dedication).

Acknowledgements

The authors thank the Chilean National Hydrocarbon Company (ENAP) for access and permission to publish seismic reflection data in Patagonia.

References

Adie RJ: **The position of the Falkland Islands in a reconstruction of Gondwanaland.** *Geol. Mag.* 1952; **89**: 401–410.
Publisher Full Text

Allibone AH, Jongens R, Scott JM, *et al.*: **Plutonic rocks of the Median Batholith in eastern and central Fiordland, New Zealand: field relations, geochemistry, correlation, and nomenclature.** *N. Z. J. Geol. Geophys.* 2009; **52**(2): 101–148.
Publisher Full Text

Aguirre G: **Perfil Sismico Regional 1**. *ENAP – Magallanes*. 2003; **12**: 00001/0002.

Álvarez P, Elgueta S, Mpodozis C, *et al.*: **Proyecto Tranquilo–Otway.** *Empresa Nacional de Petróleo (ENAP), unpublished technical report.* 2006; 290.

Álvarez-Marrón J, McClay KR, Harambour S, *et al.*: **Geometry and evolution of the frontal part of the Magallanes foreland thrust and fold belt (Vicuna-Area), Tierra del Fuego, Southern Chile.** *AAPG Bull.* 1993; **77**: 1904–1921.
Publisher Full Text

Angulo A, Vargas CA: **Global distribution of the hydrocarbon Golden Zone.** *Mar. Pet. Geol.* 2022; **144**: 105832.
Publisher Full Text

Aramendía I, Cuitiño JI, Ghiglione MC, *et al.*: **Timing and stratigraphic evolution of a Miocene foreland unroofing sequence in the Austral-Magallanes Basin during Southern Patagonian Andes uplift.** *J. Geol. Soc.* 2022; **180**(1): jgs2022–jgs2038.
Publisher Full Text

Arbaret L, Burg J-P: **Complex flow in lowest crustal, anastomosing mylonites: Strain gradients in akohistan gabbro, northern Pakistan.** *J. Geophys. Res.* 2003; **108**(B10).
Publisher Full Text

Ballivián Justiniano CA, Oriolo S, Basei MAS, *et al.*: **The Gondwanide deformation along the southwestern border of the Río de la Plata Craton: Geochemical and geochronological constraints on ductile shear zones from the Ventania System basement, Argentina.** *J. S. Am. Earth Sci.* 2023; **124**: 104275.
Publisher Full Text

Barbeau DL Jr, Olivero E, Swanson-Hysell N, *et al.*: **Detrital-zircon geochronology of the eastern Magallanes foreland basin: Implications for Eocene kinematics of the northern Scotia Arc and Drake Passage.** *EPSL.* 2009; **284**: 489–503.
Publisher Full Text

Barker PF: **Scotia Sea regional tectonic evolution: Implications for mantle flow and palaeocirculation.** *Earth Sci. Rev.* 2001; **55**: 1–39.
Publisher Full Text

Beckinsale RD, Tarney J, Darbyshire DFP, *et al.*: **Re–Sr and K–Ar Age Determinations on Samples of the Falkland Plateau Basement at Site 330, DSDP.** *Init Repts DSDP.* 1977; **36**: 923–927.
Publisher Full Text

Bell TH: **Progressive deformation and reorientation of fold axes in a ductile mylonite zone: the Woodroffe Thrust.** *Tectonophy.* 1978; **44**: 285–320.
Publisher Full Text

Bell TH, Etheridge MA: **Microstructure of mylonites and their descriptive terminology.** *Lithos.* 1973; **6**(4): 337–348.
Publisher Full Text

Bell TH, Hammond RL: **On the Internal Geometry of Mylonite Zones.** *J. Geol.* 1984; **92**(6): 667–686.
Publisher Full Text

Bernhardt A, Jobe ZR, Grove M, *et al.*: **Palaeogeography and diachronous infill of an ancient deep-marine foreland basin, Upper Cretaceous**

Cerro Toro Formation, Magallanes Basin. *Basin Res.* 2012; **24**: 269–294.
Publisher Full Text

Betka P, Mosher S, Klepeis K: **Progressive Development of a Distributed Ductile Shear Zone beneath the Patagonian Retroarc Fold-Thrust Belt, Chile.** *Lithosphere.* 2022; **2022**(1): 3820115.
Publisher Full Text

Bird PC, Cartwright JA, Davies TL: **Basement reactivation in the development of rift basins: an example of reactivated Caledonide structures in the West Orkney Basin.** *J. Geol. Soc.* 2016; **172**: 77–85.
Publisher Full Text

Blisniuk PM, Stern LA, Chamberlain CP, *et al.*: **Links between mountain uplift, climate, and surface processes in the Southern Patagonian Andes.** *The Andes.* Oncken O, Chong G, Franz G, *et al.*, editors. Berlin, Heidelberg, Germany: Frontiers in Earth Sciences, Springer; 2006; 429–440.
Publisher Full Text

Bond CE: **Uncertainty in structural interpretation: Lessons to be learnt.** *J. Struct. Geol.* 2015; **74**: 185–200.
Publisher Full Text

Boyer SE, Elliott D: **Thrust systems.** *AAPG Bull.* 1982; **66**: 1196–1230.
Publisher Full Text

Brewer JA, Smithson SB, Oliver JE, *et al.*: **The Laramide Orogeny: evidence from Cocorp Deep Crustal Seismic Profiles in the Wind River Mountains, Wyoming.** *Tectonophy.* 1980; **62**: 165–189.
Publisher Full Text

Brocher TM, Christensen NI: **Seismic anisotropy due to preferred mineral orientation observed in shallow crustal rocks in southern Alaska.** *Andean Geol.* 1990; **18**: 737–740.
Publisher Full Text

Brown CM, Pigram CJ, Skwarko SK: **Mesozoic stratigraphy and geological history of Papua New Guinea.** *Palaeogeogr. Palaeoclimatol. Palaeoecol.* 1979; **29**: 301–322.
Publisher Full Text

Buffoni C, Schimmel M, Sabbione NC, *et al.*: **Rayleigh waves from correlation of seismic noise in Great Island of Tierra del Fuego, Argentina: Constraints on upper crustal structure.** *Geod Geodyn.* 2018; **9**: 2–12.
Publisher Full Text

Butler RWH: **Training the creation, visualization and interpretation of fault maps for the subsurface– using tectonic geomorphology.** *Geological Mapping of Our World and Others.* Butler RWH, Torvela T, Williams L, editors. London: Geological Society; 2023; **541**: 181–205. Special Publications.
Publisher Full Text

Butler RWH, Bond CE, Cooper MA, *et al.*: **Interpreting structural geometry in fold-thrust belts: Why style matters.** *J. Struct. Geol.* 2018; **114**: 251–273.
Publisher Full Text

Calderón M, Fildani A, Hervé F, *et al.*: **Late Jurassic bimodal magmatism in the northern sea-floor remnant of the Rocas Verdes basin, southern Patagonian Andes.** *J. Geol. Soc. Lond.* 2007; **164**: 1011–1022.
Publisher Full Text

Calvert AJ, Doublier MP, Sellars SE: **Seismic reflections from a lithospheric suture zone below the Archaean Yilgarn Craton.** *Nat. Commun.* 2021; **12**: 7245.
PubMed Abstract | Publisher Full Text | Free Full Text

Caminos R, Llambias EJ, Rapela CW, *et al.*: **Late Paleozoic-Early Triassic magmatic activity of Argentina and the significance of new Rb–Sr ages from northern Patagonia.** *J. S. Am. Earth Sci.* 1988; **1**(2): 137–145.
Publisher Full Text

Campbell MJ, Rosenbaum G, Allen CM, *et al.*: **Continental crustal growth processes revealed by detrital zircon petrochronology: insights from Zealandia.** *JGR Solid Earth.* 2020; **125**(8): e2019JB019075.
Publisher Full Text

Castillo P, Fanning CM, Pankhurst RJ, *et al.*: **Zircon O- and Hf-isotope constraints on the genesis and tectonic significance of Permian magmatism in Patagonia.** *J. Geol. Soc.* 2017; **174**: 803–816.
Publisher Full Text

Chemale F Jr, Ramos VA, Naipauer M, *et al.*: **Age of basement rocks from the Maurice Ewing Bank and the Falkland/Malvinas Plateau.** *Precambrian Res.* 2018; **314**: 28–40.
Publisher Full Text

Christensen NI: **Compressional wave velocities in metamorphic rocks at pressures to 10 kilobars.** *J. Geophys. Res.* 1965; **70**(24): 6147–6164.
Publisher Full Text

Christensen NI: **Shear wave velocities in metamorphic rocks at pressures to 10 kilobars.** *J. Geophys. Res.* 1966; **71**(14): 3549–3556.
Publisher Full Text

Christensen NI, Szymanski DL: **Origin of reflections from the Brevard Fault Zone.** *J. Geophys. Res.* 1988; **93**(B2): 1087–1102.
Publisher Full Text

Collenaga L, Siuda K, Jackson CA-L, *et al.*: **Normal fault growth influenced by basement fabrics: The importance of preferential nucleation from pre-existing structures.** *Basin Res.* 2019; **31**: 659–687.
Publisher Full Text

Colombu S, Cruciani G, Fancello D, *et al.*: **Petrophysical properties of a granite-protomylonite-ultramylonite sequence: insight from the Monte Grighini shear zone, central Sardinia, Italy.** *Eur. J. Mineral.* 2015; **27**: 471–486.
Publisher Full Text

Cristofolini EA, Otamendi JE, Walker BA Jr, *et al.*: **A Middle Paleozoic shear zone in the Sierra de Valle Fertil, Argentina: Records of a continent-arc collision in the Famatinian margin of Gondwana.** *J. S. Am. Earth Sci.* 2014; **56**: 170–185.
Publisher Full Text

Cuitiño JI, Pimentel MM, Ventura Santos R, *et al.*: **High resolution isotopic ages for the early Miocene "Patagoniense" transgression in Southwest Patagonia: Stratigraphic implications.** *J. S. Am. Earth Sci.* 2012; **38**: 110–122.
Publisher Full Text

Curtis ML: **Tectonic history of the Ellsworth Mountains, West Antarctica: Reconciling a Gondwana enigma.** *GSA Bull.* 2001; **113**(7): 939–958.
Publisher Full Text

Curtis ML, Hyam DM: **Late Palaeozoic to Mesozoic structural evolution of the Falkland Islands: a displaced segment of the Cape Fold Belt.** *J. Geol. Soc. Lond.* 1998; **155**: 115–129.
Publisher Full Text

Dafoe LT, DesRoches KJ, Williams GL: **A structural and stratigraphic framework for the western Davis Strait region.** *Geological synthesis of Baffin Island (Nunavut) and the Labrador–Baffin Seaway.* Dafoe LT, Bingham-Koslowski N, editors. Geological Survey of Canada Bulletin; 2022; **608**: 181–218.
Publisher Full Text

Dalhoff F, Larsen LM, Ineson JR, *et al.*: **Continental crust in the Davis Strait: new evidence from Seabed sampling.** *Geol Surv Den Greenl.* 2006; **10**(10): 33–36.
Publisher Full Text

Dalziel IWD, Brown RL: **Tectonic denudation of the Cordillera Darwin metamorphic core complex, Tierra del Fuego, implications for cordilleran orogenesis.** *Geology.* 1989; **17**: 699–703.
Publisher Full Text

Daniels BG, Auchter NC, Hubbard SM, *et al.*: **Timing of deep-water slope evolution constrained by large-*n* detrital and volcanic ash zircon geochronology, Cretaceous Magallanes.** *GSA Bull.* 2018; **130**(3–4): 438–454.
Publisher Full Text

Daniels BG, Hubbard SM, Romans BW, *et al.*: **Revised chronostratigraphic framework for the Cretaceous Magallanes-Austral Basin, Última Esperanza Province, Chile.** *J. S. Am. Earth Sci.* 2019; **94**: 102209.
Publisher Full Text

Davies HL: **Folded thrust fault and associated metamorphics in the Suckling-Dayman Massif, Papua New Guinea.** *Am. J. Sci.* 1980; **280A**: 171–191.
Reference Source

Deng H, McClay K, Belgarde C: **Low-Angle Normal Faults on the NW Shelf of Australia: Implications for Late Paleozoic Rifting.** *Tectonics.* 2022; **41**: e2021TC007088.
Publisher Full Text

Dentith M, Yuan H, Murdie RE, *et al.*: **Improved Interpretation of Deep Seismic Reflection Data in Areas of Complex Geology Through Integration With Passive Seismic Data Sets.** *JGR Solid Earth.* 2018; **123**: 10810–10830.
Publisher Full Text

Domeier M, Torsvik TH: **Plate tectonics in the late Paleozoic.** *Geosci. Front.* 2014; **5**(3): 303–350.
Publisher Full Text

Dumais MA, Gernigon L, Johansen SE, *et al.*: **New interpretation of the spreading evolution of the Knipovich Ridge derived from aeromagnetic data.** *Geophys. J. Int.* 2020; **224**(2): 1422–1428.
Publisher Full Text

Eagles G: **Newangles on South Atlantic opening.** *Geophys. J. Int.* 2007; **168**: 353–361.
Publisher Full Text

Eagles G: **South Georgia and Gondwana's Pacific margin: lost in translation?.** *J. S. Am. Earth Sci.* 2010; **30**: 65–70.
Publisher Full Text

Earle S: *Physical Geology.* British Columbia, Canada: Victoria;2nd ed 2019.
Reference Source

Elliott DH, Fanning CM, Mukasa SB, *et al.*: **Hf- and O-isotope data from detrital and granitoid zircons reveal characteristics of the Permian–**

Triassic magmatic belt along the Antarctic sector of Gondwana. *Geosphere.* 2019; **15**(2): 576–604.
Publisher Full Text

ENAP: **Dataciones radiométricas Cuenca Gaviota.** *Empresa Nacional de Petróleo (ENAP), unpublished technical report.* 1991; **5**.

Esteban FD, Tassone A, Lodolo E, *et al.*: **Basement geometry and sediment thickness of Lago Fagnano (Tierra del Fuego).** *Andean Geol.* 2014; **41**(2): 293–313.
Publisher Full Text

Esteban F, Tassone A, Menichetti M, *et al.*: **Magnetic fabric and microstructures across the Andes of Tierra del Fuego, Argentina.** *Andean Geol.* 2011; **38**(1): 64–81.

Falco JI, Hauser N, Scivetti N, *et al.*: **The origin of Patagonia: insights from Permian to Middle Triassic magmatism of the North Patagonian Massif.** *Geol. Mag.* 2022; **159**: 1490–1512.
Publisher Full Text

Falco JI, Suárez RJ, Hauser N, *et al.*: **The Permian to late Triassic magmatic evolution of SW Pangea: Reconciling evidence from Patagonia and the Antarctic Peninsula.** *J. S. Am. Earth Sci.* 2024; **150**: 105201.
Publisher Full Text

Fazlikhani H, Fossen H, Gawthorpe RL, *et al.*: **Basement structure and its influence on the structural configuration of the northern North Sea rift.** *Tectonics.* 2017; **36**(6): 1151–1177.
Publisher Full Text

Fildani A, Cope TD, Graham SA: **Initiation of the Magallanes foreland basin: timing of the southernmost Patagonian Andes orogeny revised by detrital zircon provenance analysis.** *Geology.* 2003; **31**: 1081–1084.
Publisher Full Text

Fletcher JM: **Bartley JM: Constrictional strain in a non-coaxial shear zone: implications for fold and rock fabric development, central Mojave metamorphic core complex, California.** *J. Struct. Geol.* 1994; **16**(4): 555–570.
Publisher Full Text

Fosdick JC, Bostelmann JE, Leonard J: **Timing and rates of foreland sedimentation—New detrital zircon U/Pb geochronology of the Cerro Dorotea, Rio Turbio, and Rio Guillermo formations, Magallanes basin.** *XIV Congreso Geologico Chileno, La Serena, Chile, 4–8th October.* 2015; **4**: 86.

Fosdick JC, Graham SA, Hilley GE: **Influence of attenuated lithosphere and sediment loading on flexure of the deep-water Magallanes retroarc foreland basin, Southern Andes.** *Tectonics.* 2014; **33**: 2505–2525.
Publisher Full Text

Fosdick JC, Romans BW, Fildani A, *et al.*: **Kinematic evolution of the Patagonian retroarc fold-and-thrust belt and Magallanes foreland basin, Chile and Argentina, 51°30°S.** *GSA Bull.* 2011; **123**: 1679–1698.
Publisher Full Text

Fossen H, Polonio I, Bauck MS, *et al.*: **The North Sea rift basement records extensional collapse of the Caledonian orogen.** *Commun. Earth Environ.* 2024; **5**: 206.
Publisher Full Text

Foulger GR, Doré T, Emeleus CH, *et al.*: **The Iceland microcontinent and a continental Greenland-Iceland-Faroe Ridge.** *Earth-Sci. Rev.* 2020; **206**: 102926.
Publisher Full Text

Fountain DM, Hurich CA, Smithson SB: **Seismic reflectivity of mylonite zones in the crust.** *Geology.* 1984; **12**(4): 195–198.
Publisher Full Text

Freeman B, Klemperer SL, Hobbs RW: **The deep structure of northern England and the Iapetus Suture zone from BIRPS deep seismic reflection profiles.** *J. Geol. Soc. Lond.* 1988; **145**: 727–740.
Publisher Full Text

Gabrielsen RH, Roberts D, Gjelsvik T, *et al.*: **Double-folding and thrust-front geometries associated with the Timanian and Caledonian orogenies in the Varanger Peninsula, Finnmark, North Norway.** *J. Geol. Soc.* 2022; **179**(6): jgs2021–jgs2153.
Publisher Full Text

Gallardo RE: **Seismic sequence stratigraphy of a foreland unit in the Magallanes- Austral Basin, Dorado Riquelme Block, Chile: Implications for deep-marine reservoirs.** *Lat Am J Sed Basin Anal.* 2014; **21**(1): 49–64.

Gallardo Jara RE, Ghiglione MC, Rojas Galliani L: **Tectonic evolution of the southern Austral-Magallanes Basin in Tierra del Fuego.** *Lat Am J Sed Basin Anal.* 2019; **16**: 57–74.

Gallardo Jara RE, Ghiglione MC, Rojas Galliani L, *et al.*: **From rift to foreland basin: A case example from the Magallanes- Austral basin, southernmost Andes.** *Basin Res.* 2022; **35**(3): 865–897.
Publisher Full Text

Gao L, Guo X, Pei J, *et al.*: **The Initial Opening of the Drake Passage Occurred During ca. 62–59 Ma.** *Geophys. Res. Lett.* 2025; **52**: e2024GL111455.
Publisher Full Text

Geoffroy L, Gernigon L, Foulger GR, *et al.*: **Linear magnetic anomalies and the limits of oceanic crust in oceans.** *In the footsteps of Warren B. Hamilton: New Ideas in Earth Science.* Foulger GR, Hamilton LC, Jurdy DM, *et al.*, editors. Geological Society of America Special Paper; 2021; 553.
Publisher Full Text

George SW, Davis SN, Fernandez RA, *et al.*: **Chronology of deposition and unconformity development across the Cretaceous—Paleogene boundary, Magallanes-Austral Basin, Patagonian Andes.** *J. S. Am. Earth Sci.* 2019; **95**: 102237.

Ghanadian M, Faghih A, Abdollahie Fard I, *et al.*: **On the role of incompetent strata in the structural evolution of the Zagros Fold-Thrust Belt, Dezful Embayment, Iran.** *Mar. Pet. Geol.* 2017; **81**: 320–333.
Publisher Full Text

Ghiglione MC, Naipauer M, Sue C, *et al.*: **UePb zircon ages from the northern Austral basin and their correlation with the Early Cretaceous exhumation and volcanism of Patagonia.** *Cretac. Res.* 2015; **55**: 116–128.
Publisher Full Text

Ghiglione MC, Yagupsky D, Ghidella M: **Continental Stretching Preceding the Opening of Drake passage: Evidence from Tierra del Fuego.** *Geology.* 2008; **36**: 643–646.
Publisher Full Text

Giacosa R, Heredia N: **La cuenca de antepaís terciaria asociada a la faja plegada y corrida de los Andes Patagónicos entre los 41° y 42° S, SO de Argentina.** *Acta Geol. Hisp.* 1999; **32**(1–2): 103–111.

Giacosa R, Zubia M, Sánchez M, *et al.*: **Meso-Cenozoic tectonics of the southern Patagonian foreland: Structural evolution and implications for AueAg veins in the eastern Deseado Region (Santa Cruz, Argentina).** *J. S. Am. Earth Sci.* 2010; **30**: 134–150.
Publisher Full Text

Gibson GM: **Medium-high-pressure metamorphic rocks of the Tuhua Orogen, western New Zealand, as lower crustal analogues of the Lachlan Fold Belt, SE Australia.** *Tectonophy.* 1992; **214**(1–4): 145–157.
Publisher Full Text

Gombosi DJ, Barbeau DL Jr, Garver JI: **New thermochronometric constraints on the rapid Paleogene exhumation of the Cordillera Darwin complex and related thrust sheets in the Fueguian Andes.** *Terra Nova.* 2009; **21**: 507–515.
Publisher Full Text

González Guillot M, Acevedo R, Escayola M: **El Gabro Rancho Lata: Magmatismo mesozoico off-axis de la cuenca marginal Rocas Verdes en los Andes Fueguinos de Argentina.** *Revista Mexicana de Ciencias Geológicas.* 2010; **27**(3): 431–448.

González Guillot M, Urraza I, Acevedo RD, *et al.*: **Magmatismo básico Jurásico–Cretácico en los Andes Fueguinos y su relación con la cuenca marginal Rocas Verdes.** *Rev. Asoc. Geol. Argent.* 2016; **73**(1): 1–22.

Grillo Vidal C, Lopez de Luchi MG, Martinez Dopico C, *et al.*: **Timing of the deformation in the Gondwanide orogeny: a structural and geochemical shift from syn- to post-tectonic magmatism recorded in the Permian Mamil Choique Granitoids, Patagonia.** *Lithos.* 2024; **482-483**: 107717.
Publisher Full Text

Gutiérrez NM, Le Roux JP, Vásquez A, *et al.*: **Tectonic events reflected by palaeocurrents, zircon geochronology, and palaeobotany in the Sierra Baguales of Chilean Patagonia.** *Tectonophy.* 2017; **695**: 76–99.
Publisher Full Text

Hajnal Z, Lucas S, White D, *et al.*: **Seismic reflection images of high-angle faults and linked detachments in the Trans-Hudson Orogen.** *Tectonics.* 1996; **15**(2): 427–439.
Publisher Full Text

Halpern M: **Regional geochronology of Chile south of 50° latitude.** *GSA Bull.* 1973; **84**: 2407–2422.
Publisher Full Text

Halpern M, Rex DC: **Time of Folding of the Yaghan Formation and Age of the Tekenika Beds, Southern Chile, South America.** *GSA Bull.* 1972; **83**: 1881–1886.
Publisher Full Text

Hansma J, Tohver E, Schrank C, *et al.*: **The timing of the Cape Orogeny: New $^{40}Ar/^{39}Ar$ age constraints on deformation and cooling of the Cape Fold Belt, South Africa.** *Gondwana Res.* 2016; **32**: 122–137.
Publisher Full Text

Harahap BH: **Tectonostratigraphy of the southern part of Papua and Arafura Sea, Eastern Indonesia.** *Indones J Geosci.* 2012; **7**(3): 167–187.
Publisher Full Text

Hedin P, Almqvist B, Berthet T, *et al.*: **3D reflection seismic imaging at the 2.5 km deep COSC-1 scientific borehole, central Scandinavian Caledonides.** *Tectonophy.* 2016; **689**: 40–55.
Publisher Full Text

Hervé F, Godoy E, Mpodozis C: **Monitoring magmatism of the Patagonian Batholith trough the U-Pb SHRIMP dating of detrital zircons in sedimentary units of the Magallanes basin.** *International Symposium on the Geology and Geophysics of the Southernmost Andes, the*

Scotia Arc and Antartic Peninsula (GEOSUR). Carcione J, Donda F, Lodolo E, editors. Bollettino di Geofisica teorica ed applicata; 2004; **45**: 113–117.

Hervé F, Calderón M, Fanning CM, *et al.*: **SHRIMP chronology of the Magallanes basin basement, Tierra del Fuego: Cambrian plutonism and Permian high-grade metamorphism.** *Andean Geol.* 2010a; **37**(2): 253–275.
Publisher Full Text

Hervé F, Fanning CM, Pankhurst RJ, *et al.*: **Detrital zircon SHRIMP U-Pb age study of the Cordillera Darwin Metamorphic Complex of Tierra del Fuego: sedimentary sources and implications for the evolution of the Pacific margin of Gondwana.** *J. Geol. Soc. Lond.* 2010b; **167**: 555–568.
Publisher Full Text

Hill K, Raza A: **Arc-continent collision in Papua Guinea: constraints from fission track thermochronology.** *Tectonics.* 1999; **18**(6): 950–966.
Publisher Full Text

Horton BK: **Unconformity development in retroarc foreland basins: implications for the geodynamics of Andean-type margins.** *J. Geol. Soc.* 2021; **179**: jgs2020–jgs2263.
Publisher Full Text

Hurich CA, Smithson SB, Fountain DM, *et al.*: **Seismic evidence of mylonite reflectivity and deep structure in the Kettle dome metamorphic core complex, Washington.** *Geology.* 1985; **13**(8): 577–580.
Publisher Full Text

Jacobs J: **Neoproterozoic/Lower Palaeozoic events in central Dronning Maud Land (East Antarctica).** *Gondwana Res.* 1999; **2**(3): 473–480.
Publisher Full Text

Ji S, Long C: **Seismic reflection response of folded structures and implications for the in terpretation of deep seismic reflection profiles.** *J. Struct. Geol.* 2006; **28**(8): 1380–1387.
Publisher Full Text

Johnston ST: **The Cape Fold Belt and syntaxis.** *J. Afr. Earth Sci.* 2000; **31**(1): 51–63.
Publisher Full Text

Kleiman LE, Japas MS: **The Choiyoi volcanic province at 34°S–36°S (San Rafael, Mendoza, Argentina): Implications for the Late Palaeozoic evolution of the southwestern margin of Gondwana.** *Tectonophy.* 2009; **473**: 283–299.
Publisher Full Text

Klemperer SL, Ryan PD, Snyder DB: **A deep seismic reflection transect across the Irish Caledonides.** *J. Geol. Soc.* 1991; **148**: 149–164.
Publisher Full Text

Klepeis KA: **Relationship between uplift of the metamorphic core of the southernmost Andes and shortening in the Magallanes foreland fold and thrust belt, Tierra del Fuego, Chile.** *Tectonics.* 1994a; **13**(4): 882–904.
Publisher Full Text

Klepeis KA: **The Magallanes and Deseado fault zones: Major segments of the South American-Scotia transform plate boundary in southernmost South America, Tierra del Fuego.** *J. Geophys. Res.* 1994b; **99**(B11): 22001–22014.
Publisher Full Text

Klepeis K, Betka P, Clarke G, *et al.*: **Continental underthrusting and obduction during the Cretaceous closure of the Rocas Verdes rift basin, Cordillera Darwin, Patagonian Andes.** *Tectonics.* 2010; **29**: 1–24.
Publisher Full Text

Koehl J-BP: **Eurekan strain partitioning and decoupling in central Spitsbergen.** *Solid Earth.* 2021; **12**: 1025–1049.
Publisher Full Text

Koehl J-BP: **The myth of the De Geer Zone: a change of paradigm for the opening of the Fram Strait.** *Open Res Europe.* 2025; **4**(1): 1.
PubMed Abstract | **Publisher Full Text** | **Free Full Text**

Koehl J-BP: **Inverted rift-orthogonal thrust systems in the Greenland–Iceland–Faroe Ridge: implications for the nature of the crust and plate tectonics.** *Open Res Europe.* 2026a.

Koehl J-BP: **High-resolution versions of the figures for "Onshore surface–subsurface correlation of orogenic structures and the continuation of the late Paleozoic Gondwanides in the Tierra del Fuego fold-and-thrust belt, southern Patagonia".** *Zenodo.* 2026b; V1.0.
Publisher Full Text

Koehl J-BP, Allaart L: **The Billefjorden Fault Zone in northern Spitsbergen: A major terrane boundary?.** *Polar Res.* 2021; **40**: 7668.
Publisher Full Text

Koehl J-BP, Allaart L, Noormets R: **Devonian–Carboniferous extension and Eurekan inversion along an inherited WNW–ESE-striking fault system in Billefjorden.** *Open Res Europe.* 2023b; **3**: 124.
Publisher Full Text

Koehl J-BP, Bergh SG, Henningsen T, *et al.*: **Middle to Late Devonian—Carboniferous collapse basins on the Finnmark Platform and in the southwesternmost Nordkapp basin, SW Barents Sea.** *Solid Earth.* 2018; **9**: 341–372.
Publisher Full Text

Koehl J-BP, Foulger GR: **Orogenic bridge theory: towards a predicting tool for past and future plate tectonics.** *Open Res Europe.* 2025; **4**: 76.
Publisher Full Text

Koehl J-BP, Jolley DW, Peace AL, *et al.*: **Impact of sub-basalt thrust systems on the Faroe continental shelf for the late Paleoproterozoic–Cenozoic tectonic evolution of the margin.** *Open Res Europe.* 2024; **4**: 181.
PubMed Abstract | **Publisher Full Text** | **Free Full Text**

Koehl J-BP, Magee C, Anell IM: **Timanian thrust systems and their implications for the late Neoproterozoic–Phanerozoic tectonic history of the northern Barents Sea and Svalbard.** *Solid Earth.* 2022; **13**: 85–115.
Publisher Full Text

Koehl J-BP, Polonio I, Rojo L: **Timanian Fold-and-thrust Belt and Caledonian Overprint in the Selis Ridge Imaged by New 3D Seismic Attributes and Spectral Decomposition *Tektonika*.** 2023a; **1**(1): 76–100.
Publisher Full Text

Koehl J-BP, Stokmo EMB: **Caledonian reactivation and reworking of Timanian thrust systems and implications for latest Mesoproterozoic–mid Paleozoic tectonics and magmatism in northern Norway and the southern Barents Sea.** *Open Res Europe.* 2025; **4**: 30.
PubMed Abstract | **Publisher Full Text** | **Free Full Text**

Kohn MJ, Spear FS, Harrison TM, *et al.*: **^{40}Ar/^{39}Ar Geochronology and P–T–T Paths from the Cordillera Darwin Metamorphic Complex, Tierra del Fuego, Chile.** *J. Metamorph. Geol.* 1995; **13**: 251–270.
Publisher Full Text

Lapworth C: **On the Stratigraphy and Metamorphism of the Rocks of the Durness—Eriboll District.** *Proc. Geol. Assoc.* 1885; **8**(8): 438–442.
Publisher Full Text

Le Roux J: **A review of Tertiary climate changes in southern South America and the Antarctic Peninsula. Part 1: Oceanic conditions.** *Sediment. Geol.* 2012; **247-248**: 1–20.
Publisher Full Text

Lefeuvre N, Truche L, Donzé FV, *et al.*: **Native H2 Exploration in the Western Pyrenean Foothills.** *Geochem. Geophys. Geosyst.* 2021; **22**: 1–20.
Publisher Full Text

Lenhart A, Jackson CAL, Bell RE, *et al.*: **Structural architecture and composition of crystalline basement offshore West Norway.** *Lithosphere.* 2019; **11**(2): 273–293.
Publisher Full Text

Limarino CO, Massabie A, Rossello E, *et al.*: **El Paleozoico de Ventania, Patagonia e Islas Malvinas.** *Instituto de Geologia y Recursos Minerales Geologia Argentina Anales.* 1999; **29**(13): 319–347.
Reference Source

Lodolo E, Menichetti M, Bartole R, *et al.*: **Magallanes—Fagnano continental transform fault (Tierra del Fuego, southernmost South America).** *Tectonics.* 2003; **22**: 1076.
Publisher Full Text

Longley L, Phethean JJJ, Schiffer C: **The Davis Strait proto-microcontinent: The role of plate tectonic reorganization in continental cleaving.** *Gondwana Res.* 2024; **133**: 14–29.
Publisher Full Text

López-Gamundí O: **Permian plate margin volcanism and tuffs in adjacent basins of west Gondwana: Age constraints and common characteristics.** *J. S. Am. Earth Sci.* 2006; **22**: 227–238.
Publisher Full Text

Lovecchio JP, Naipauer M, Cayo LE, *et al.*: **Rifting evolution of the Malvinas basin, offshore Argentina: new constrains from zircon U–Pb geochronology and seismic characterization.** *J. S. Am. Earth Sci.* 2019; **95**: 102253.
Publisher Full Text

Lovecchio JP, Abdelmalak MM, Planke S, *et al.*: **Mesozoic rifting in SW Gondwana and break-up of the Southern South Atlantic Ocean.** *The Impacts of Igneous Systems on Sedimentary Basins and their Energy Resources.* Kilhams B, Holford S, Gardiner D, *et al.*, editors. Geological Society, London, Special Publications; 2024; **547**: 75–107.
Publisher Full Text

Lozano JG, Bran DM, Peroni JI, *et al.*: **The central Fuegian fold and thrust belt in Tierra del Fuego: Strike-slip tectonics superimposed onto compressional deformation.** *Geol. J.* 2020; **55**: 6079–6097.
Publisher Full Text

Ma D, Koyi HA, Yuan J, *et al.*: **The role of deep-seated half-grabens in the evolution of Huoerguosi-Manasi-Tugulu fold-and-thrust belt, northern Tian Shan, China.** *J Geodyn.* 2019; **131**: 101647.
Publisher Full Text

Malkowski MA, Sharman GR, Graham SA, *et al.*: **Characterisation and diachronous initiation of coarse clastic deposition in the Magallanes–Austral foreland basin, Patagonian Andes.** 2015; **29**(S1): 298–326.
Publisher Full Text

Martinioni DR, Olivero EB, Medina FA, *et al.*: **Cretaceous stratigraphy of Sierra de Beauvoir, Fuegian Andes, Argentina.** *Rev. Asoc. Geol. Argent.* 2013; **70**(1): 70–95.

Mcatamney J, Klepeis K, Mehrtens C, *et al.*: **Along-strike variability of back-arc basin collapse and the initiation of sedimentation in the Magallanes foreland basin, southernmost Andes (53-54.5°S).** *Tectonics.* 2011; **30**(5): 1–26.
Publisher Full Text

McCarthy D, Aldiss D, Arsenikos S, *et al.*: **Comment on "Geophysical evidence for a large impact structure on the Falkland (Malvinas) Plateau".** *Terra Nova.* 2017; **29**: 411–415.
Publisher Full Text

McClay KR: **Glossary of thrust tectonics terms.** *Thrust tectonics.* McClay KR, editor. London, UK: Chapman and Hall; 1992; 419–433.
Publisher Full Text

McClay KR, Insley MW: **Duplex structures in the Lewis thrust sheet, Crowsnest Pass, Rocky Mountains, Alberta, Canada.** *J. Struct. Geol.* 1986; **1986**(8): 911–922.

McCoy-West AJ, Mortimer N, Ireland TR: **U–Pb geochronology of Permian plutonic rocks, Longwood Range, New Zealand: implications for Median Batholith–Brook Street Terrane relations.** *N. Z. J. Geol. Geophys.* 2014; **57**(1): 65–85.
Publisher Full Text

McDonough DT, Fountain DM: **Reflection characteristics of a mylonite zone based on compressional wave velocities of rock samples.** *Geophys. J.* 1988; **93**: 547–558.
Publisher Full Text

Menichetti M, Lodolo E, Tassone A: **Structural geology of the Fuegian Andes and Magallanes fold-and-thrust belt – Tierra del Fuego Island.** *Geol. Acta.* 2008; **6**(1): 19–42.

Millar L, Pankhurst RJ, Fanning CM: **Basement chronology of the Antarctic Peninsula: recurrent magmatism and anatexis in the Palaeozoic Gondwana Margin.** *J. Geol. Soc. Lond.* 2002; **159**: 145–157.
Publisher Full Text

Miller CA, Barton M, Hanson R, *et al.*: **An Early Cretaceous volcanic arc-marginal basin transition zone, Peninsula Hardy, southernmost Chile.** *J. Volcanol. Geotherm. Res.* 1994; **63**: 33–58.
Publisher Full Text

Miller M, Rivero M, Jait D, *et al.* **El relleno de cuenca Austral-Magallanes revelado a través de cuatro transectas regionales.** *XI Congreso de Exploracion y Desarrollo de Hidrocarburos, Estratigrafia y analisis de cuencas, 8–11th November 2022, Mendoza, Argentina.* 2022; **11**: 339–373.

Moretti I, Brouilly E, Loiseau K, *et al.*: **Hydrogen Emanations in Intracratonic Areas: New Guide Lines for Early Exploration Basin Screening.** *Geosciences.* 2021; **11**(145): 1–28.
Publisher Full Text

Morley CK, von Hagke C, Hansberry RL, *et al.*: **Review of major shale-dominated detachment and thrust characteristics in the diagenetic zone: Part I, meso- and macro-scopic scale.** *Earth-Sci. Rev.* 2017; **173**: 168–228.
Publisher Full Text

Mortimer N, Tulloch AJ, Spark RN, *et al.*: **Overview of the Median Batholith, New Zealand: a new interpretation of the geology of the Median Tectonic Zone and adjacent rocks.** *J. Afr. Earth Sci.* 1999; **29**(1): 257–268.
Publisher Full Text

Mosqueira González V, Torres Carbonell PJ, Turienzo MM: **Structural overprinting and style of deformation at sierra Beauvoir and sierra de Apen: A geometric and kinematic model for the evolution of the internal thrust-fold belt, Fuegian Andes, Argentina.** *J. S. Am. Earth Sci.* 2021; **112**: 103575.
Publisher Full Text

Muller V, Calderén M, Fosdick JC, *et al.*: **The closure of the Rocas Verdes Basin and early tectono-metamorphic evolution of the Magallanes Fold-and-Thrust Belt, southern Patagonian Andes (52–54°S).** *Tectonophy.* 2020; **798**: 228686.
Publisher Full Text

Navarette C, Bastías-Silva J, Gianni G, *et al.*: **Late Paleozoic–Jurassic tectonic evolution of the eastern Deseado Massif in central–southern Patagonia.** *J. Geodyn.* 2023; **158**: 101997.
Publisher Full Text

Nelson EP, Dalziel IWD, Milnes AG: **Structural geology of the Cordillera Darwin-collisional-style orogenesis in the southernmost Chilean Andes.** *Eclogae Geol. Helv.* 1980; **73**: 727–751.

Osagiede EE, Rotevatn A, Gawthorpe R, *et al.*: **Pre-existing intrabasement shear zones influence growth and geometry of non-colinear normal faults, western Utsira High–Heimdal terrace, North Sea.** *J. Struct. Geol.* 2020; **130**: 103908.
Publisher Full Text

Osselin F, Soulaine C, Fauguerolles C, *et al.*: **Orange hydrogen is the new green.** *Nat. Geosci.* 2022; **15**: 765–769.
Publisher Full Text

Otero RA, Torres T, Le Roux JP, *et al.*: **A Late Eocene age proposal for the Loreto Formation (Brunswick Peninsula, southernmost Chile), based on fossil cartilaginous fishes, paleobotany and radiometric evidence.** *Andean Geol.* 2012; **39**(1): 180–200.
Publisher Full Text

Page RW: **Geochronology of igneous and metamorphic rocks in the New Guinea Highlands.** *BMR J Australian Geol Geophys.* 1976; **162**(10): 1–125.

Pankhurst RJ, Rapela CW, Fanning CM, *et al.*: **Gondwanide continental collision and the origin of Patagonia.** *Earth-Sci. Rev.* 2006; **76**(3–4): 235–257.
Publisher Full Text

Pankhurst RJ, Rapela CW, Laske WP, *et al.*: **Chronological study of the pre-Permian basement rocks of southern Patagonia.** *J. S. Am. Earth Sci.* 2003; **16**: 27–44.
Publisher Full Text

Pankhurst RJ, Rapela CW, Saavedra J, *et al.*: **The Famatinian magmatic arc in the central Sierras Pampeanas: an Early to Mid-Ordovician continental arc on the Gondwana margin.** In: *The Proto-Andean Margin of Gondwana.* Pankhurst RJ, Rapela CW, editors. Geological Society, London, Special Publications; 1998; **142**: 343–367.
Publisher Full Text

Pankhurst RJ, Riley TR, Fanning CM, *et al.*: **Episodic silicic volcanism in Patagonia and the Antarctic Peninsula: Chronology of magmatism associated with the break-up of Gondwana.** *J. Petrol.* 2000; **41**: 605–625.
Publisher Full Text

Paton DA, Mortimer EJ, Markwick PJ, *et al.*: **Coeval development of extensional and contractional features along transform margins: insights from the Diaz Marginal Ridge.** *Tectonic development, thermal history and hydrocarbon habitat models of transform margins: their differences from rifted margins.* Nemcok M, Doran H, Doré AG, *et al.*, editors. Geological Society, London, Special Publications; 2022; **524**: 307–325.
Publisher Full Text

Peace AL, McCaffrey K, Imber J, *et al.*: **The role of pre-existing structures during rifting, continental breakup and transform system development, offshore West Greenland.** *Basin Res.* 2018; **30**(3): 373–394.
Publisher Full Text

Phillips T, Jackson CAL, Bell RE, *et al.*: **Reactivation of intrabasement structures during rifting: a case study from offshore Southern Norway.** *J. Struct. Geol.* 2016; **91**: 54–73.
Publisher Full Text

Phillips TB, McCaffrey KJW: **Terrane boundary reactivation, barriers to lateral fault propagation and reactivated fabrics: Rifting across the Median Batholith Zone, Great South Basin, New Zealand.** *Tectonics.* 2019; **38**(11): 4027–4053.
Publisher Full Text

Pigram CJ, Davies HL: **Terranes and the accretion history of the New Guinea orogen.** *BMR J Australian Geol Geophys.* 1987; **10**(3): 193–211.
Reference Source

Pinto J, González D, Agurto C, *et al.*: **Revisión de la estratigrafía y potencial petrolífero de la antefosa Paleógena de la cuenca de antepaís Magallanes, Chile.** *XI Congreso de Exploracion y Desarrollo de Hidrocarburos, Estratigrafia y analisis de cuencas, 8–11th November 2022, Mendoza, Argentina.* 2022; **11**: 281–309.

Platt JP: **Progressive refolding in ductile shear zones.** *J. Struct. Geol.* 1983; **5**(6): 619–622.
Publisher Full Text

Poblete F, Roperch P, Hervé F, *et al.*: **The curved Magallanes fold and thrust belt: tectonic insights from a paleomagnetic and anisotropy of magnetic susceptibility study.** *Tectonics.* 2014; **33**: 2526–2551.
Publisher Full Text

Qi Y, Wu K, Li Q, *et al.*: **Seismic prediction technology for thin reservoirs of tight gas in coal measure strata: a case study of Block L in the eastern margin of the Ordos Basin.** *Front. Earth Sci.* 2025; **12**: 1487487.
Publisher Full Text

Quattrocchio ME, Martínez MA, Carpinelli Pavisich A, *et al.*: **Early Cretaceous palynostratigraphy, palynofacies and palaeoenvironments of well sections in northeastern Tierra del Fuego, Argentina.** *Cretac Res.* 2006; **27**: 584–602.
Publisher Full Text

Ramos VA: **Patagonia: A Paleozoic continent adrift?.** *J. S. Am. Earth Sci.* 2008; **26**: 235–251.
Publisher Full Text

Ramos VA, Chemale F Jr, Lovecchio JP, *et al.*: **The Malvinas (Falkland) Plateau derived from Africa? Constraints for its tectonic evolution.** *Sci Rev from the end of the world.* 2019; **1**(1): 6–18.
Publisher Full Text

Ramos VA, Cingolani C, Chemale F Jr, *et al.*: **The Malvinas (Falkland) Islands revisited: The tectonic evolution of southern Gondwana based on U-Pb and Lu-Hf detrital zircon isotopes in the Paleozoic cover.** *J. S. Am. Earth Sci.* 2017; **76**: 320–345.
Publisher Full Text

Ramos VA, Escayola M, Leal P, *et al.*: **The late stages of the Pampean Orogeny, Cordoba (Argentina): Evidence of postcollisional Early Cambrian slab break-off magmatism.** *J. S. Am. Earth Sci.* 2015; **64**(2): 351–364.
Publisher Full Text

Ramos VA, Martino RD, Ottamendi JE, *et al.*: **Evolución geotectónica de las Sierras Pampeanas orientales.** *Relatorio Del XIX Congreso Geológico Argentino, 2–6th June 2014, Córdoba, Argentina.* 2014; **19**: 965–977.
Reference Source

Rapela CW, Pankhurst RJ, Casquet C, *et al.*: **Early evolution of the Proto-Andean margin of South America.** *Geology.* 1998; **26**(8): 707–710.
Publisher Full Text

Reeve MT, Bell RE, Jackson CAL: **Origin and significance of intra-basement seismic reflections offshore Western Norway.** *J. Geol. Soc. Lond.* 2013; **171**: 1–4.
Publisher Full Text

Restelli FB, Bran DM, Almaraz F, *et al.*: **Neotectonics of the Magallanes-Fagnano fault system in Fuegian Patagonia based on high-resolution seismic profiles and geomorphic markers.** *Int. J. Earth Sci.* 2025; **114**: 117–136.
Publisher Full Text

Riccardi AC: **Berriasian invertebrate fauna from the Springhill Formation of Southern Patagonia.** *N. Jb. Geol. Paläont. (Abh.).* 1977; **155**: 216–252.
Publisher Full Text

Riley TR, Carter A, Leat PT, *et al.*: **Geochronology and geochemistry of the Northern Scotia Sea: a revised interpretation of the North and West Scotia ridge junction.** *EPSL.* 2019; **518**: 136–147.
Publisher Full Text

Riley TR, Burton-Johnson A, Flowerdew MJ, *et al.*: **Palaeozoic – Early Mesozoic geological history of the Antarctic Peninsula and correlations with Patagonia: Kinematic reconstructions of the proto-Pacific margin of Gondwana.** *Earth-Sci. Rev.* 2022; **236**: 104265.
Publisher Full Text

Rivera HA, Le Roux JP, Farias M, *et al.*: **Tectonic controls on the Maastrichtian–Danian transgression in the Magallanes–Austral foreland basin (Chile): implications for the growth of the southern Patagonian Andes.** *Sediment. Geol.* 2020; **403**: 105645–105623.
Publisher Full Text

Rivera Rosado HA: *Insights into the Tectonostratigraphic Evolution of the Southern Magallanes Basin, Southern Chile, during the Cenozoic.* Santiago, Chile: University of Chile; 2017; 1–149. Master's Thesis.

Rivera Rosado HA: *Tracing the Cenozoic Southern Patagonian Andes growth (51°15"–53°39" S) from the integrated study of orogen-foreland basin pair.* Santiago, Chile: University of Chile; 2022; 1–321. Ph.D. Thesis.

Robbiano JA, Arbe H, Gangui A: **Cuenca Austral Marina.** *Geologia y Recursos Naturales de la Plataforma Continental. XIII Congreso Geológico Argentino y III Congreso de Exploración de Hidrocarburos, 13–18th October 1996, Buenos Aires, Argentina.* Ramos VA, Turic MA, editors. 1996; **17**: 323–342.

Robertson AHF, Campbell HJ, Johnston MR, *et al.*: **Introduction to Paleozoic–Mesozoic geology of South Island, New Zealand: subduction-related processes adjacent to SE Gondwana.** *Paleozoic–Mesozoic Geology of South Island, New Zealand: Subduction-related Processes Adjacent to SE Gondwana.* Robertson AHF, editor. Geological Society, London Memoirs; 2019; **49**: 1–14.
Publisher Full Text

Rojas L, Mpodozis C: **Geologia estructural de la faja plegada y corrida de Tierra del Fuego, Andes Patagonicos Chilenos.** *XI Congreso Geológico Chileno, 7–11th August 2006, Antofagasta, Chile. Actas.* 2024; 325–328.

Rojas Vera EA, Lovecchio JP, Enrique Späth FG, *et al.*: **Jurassic depocenters development, between Colorado basin, Chelforó sub-basin and Neuquén basin**. *JSAE*. 2024; **149**: 105218.
Publisher Full Text

Romans BW, Fildani A, Graham SA: **Importance of predecessor basin history on the sedimentary fill of a retroarc foreland basin: provenance analysis of the Cretaceous Magallanes basin, Chile (50-52°S).** *Basin Res.* 2010; **22**: 640–658.
Publisher Full Text

Rossello EA: **Kinematics of the Andean sinistral wrenching along the Fagnano- Magallanes fault zone (Argentina-Chile Fueguian foothills).** *VI International Symposium on Andean Geodynamics (ISAG), Barcelona, Spain.* 2005; 623–626.

Sáez Moreno E: *Andlisis sismoestratigrdfico del Cenozoico en sector norte de isla grande de Tierra del Fuego, Cuenca de Magallanes: integracion de datos de subsuelo y afloramientos.* Santiago, Chile: University of Chile; 2017; 1–156. Bachelor's Thesis.

Sánchez A, Pavlishina P, Godoy E, *et al.*: **On the presence of Upper Paleocene rocks in the foreland succession at Cabo Nariz, Tierra del Fuego, Chile; geology and new palynological and U–Pb data.** *Andean Geol.* 2010; **37**(2): 413–432.

Scotchman IC, Gilchrist G, Kuznir NJ, *et al.*: **The breakup of the South Atlantic Ocean: formation of failed spreading axes and blocks of thinned continental crust in the Santos Basin, Brazil and its consequences for petroleum system development.** *Petroleum geology: from mature basins to new frontiers - proceedings of the 7th petroleum geology conference.* Vining BA, Pickering SC, editors. London: Geological Society; 2010; **7**: 855–866.
Publisher Full Text

Schwartz JJ, Gromet LP, Miró R: **Timing and Duration of the Calc-Alkaline Arc of the Pampean Orogeny: Implications for the Late Neoproterozoic to Cambrian Evolution of Western Gondwana.** *J. Geol.* 2008; **116**: 39–61.
Publisher Full Text

Schwartz TM, Fosdick JC, Graham SA: **Using detrital zircon U–Pb ages to calculate Late Cretaceous sedimentation rates in the Magallanes–Austral basin, Patagonia.** *Basin Res.* 2016; **29**: 725–746.
Publisher Full Text

Schwarz E, Veiga GD, Spalletti LA, *et al.*: **The transgressive infill of an inherited-valley system: The Springhill Formation (lower Cretaceous) in southern Austral Basin, Argentina.** *Mar. Pet. Geol.* 2010; **28**: 1218–1241.
Publisher Full Text

Sibson RH: **Fault rocks and fault mechanisms.** *J. Geol. Soc.* 1977; **133**(3): 191–213.
Publisher Full Text

Sibson RH: **Transient discontinuities in ductile shear zones.** *J. Struct. Geol.* 1980; **2**(1–2): 165–171.
Publisher Full Text

Sobornov KO: **Blind duplex structure of the North Urals thrust belt front.** *J. Geodyn.* 1992; **15**(1–2): 1–11.
Publisher Full Text

Sobornov KO, Afanasenkov AP, Danilov VN, *et al.*: **Fold Belts: Shall We Expect a Shift in Petroleum Exploration Priorities?.** *SPE Russian Petroleum Technology Conference, 26–28th October, Moscow, Russia.* 2015; **176609**: 1–12.
Publisher Full Text

Söllner F, Miller H, Hervé M: **An Early Cambrian granodiorite age from the pre-Andean basement of Tierra del Fuego (Chile): the missing link between South America and Antarctica?.** *J. S. Am. Earth Sci.* 2000; **13**: 163–177.
Publisher Full Text

Stanca RM, McCarthy DJ, Paton DA, *et al.*: **The tectono-stratigraphic architecture of the Falkland Plateau basin; implications for the evolution of the Falkland Islands Microplate.** *Gondwana Res.* 2022; **105**: 320–342.
Publisher Full Text

Steenken A, López e Luchi MG, Martínez Dopico C, *et al.*: **The Neoproterozoic-early Paleozoic metamorphic and magmatic evolution of the Eastern Sierras Pampeanas: an overview.** *Int. J. Earth Sci.* 2011; **100**: 465–488.
Publisher Full Text

Stewart SA: **Vertical exaggeration of reflection seismic data in geoscience publications 2006–2010.** *Mar. Pet. Geol.* 2011; **28**: 959–965.
Publisher Full Text

Stewart SA, Salem AS: **Proterozoic fold and thrust belt imaged on reflection seismic in Arabian plate basement.** *Tectonophy.* 2023; **856**: 229847.
Publisher Full Text

Suggate RP: **The tempo of events in New Zealand geological history.** *N. Z. J. Geol. Geophys.* 1965; **8**(6): 1139–1148.
Publisher Full Text

Suárez M: **A Late Mesozoic island arc in the southern Andes, Chile.** *Geol. Mag.* 1979; **116**(3): 181–190.
Publisher Full Text

Suárez M, de la Cruz R, Bell CM: **Timing and origin of deformation along the Patagonian fold and thrust belt.** *Geol. Mag.* 2000; **137**(4): 345–353.
Publisher Full Text

Süssenberger A, Schmidt ST, Wemmer K, *et al.*: **Timing and thermal evolution of fold-and-thrust belt formation in the Ultima Esperanza District, 51°S Chile: Constraints from K–Ar dating and illite characterization.** *GSA Bull.* 2018; **130**(5–6): 975–998.
Publisher Full Text

Tarney J: **Petrology, mineralogy, and geochemistry of the Falkland Plateau basement rocks, Site 330.** *Init Repts DSDP.* 1977; **36**: 893–921.
Publisher Full Text

Tonstad SA: *The Late Paleozoic development of the Ottar basin from seismic 3D interpretation.* Tromsø, Norway: University of Tromsø; 2018; 1–135. Master's Thesis.

Torres Carbonell PJ, Cao SJ, González Guillot M, *et al.*: **The Fuegian thrust-fold belt: From arc-continent collision to thrust-related deformation**

in the southernmost Andes. *J. S. Am. Earth Sci.* 2020; **102**: 102678.
Publisher Full Text

Torres Carbonell PJ, Dimieri LV, Olivero EB: **Evaluation of strain and structural style variations along the strike of the Fuegian thrust-fold belt front, Argentina.** *Andean Geol.* 2013; **40**(3): 438–457.
Publisher Full Text

Torres Carbonell PJ, Olivero EB, Dimieri LV: **Control en la magnitud de desplazamiento de rumbo del Sistema Transformante Fagnano, Tierra del Fuego, Argentina.** *Rev. Geol. Chile.* 2008; **35**(1): 63–77.

Torres Carbonell PJ, Rodríguez Arias L, Atencio MR: **GeometryandkinematicsoftheFuegianthrust-fold belt, southernmost Andes.** *Tectonics.* 2016; **36**: 33–50.
Publisher Full Text

Trouw RAJ, de Wit MJ: **Relation between the Gondwanide Orogen and contemporaneous intracratonic deformation.** *J. Afr. Earth Sci.* 1998; **28**(1): 203–213.

Uliana MA, Biddle KT: **Permian to Late Cenozoic evolution of Northern Patagonia: main tectonic events, magmatic activity, and depositional trends.** *Gondwana Six: Structure, Tectonics, and Geophysics.* McKenzie GD, editor. Washington D.C., USA: Geophysical Monograph Series, AGU; 1987; **40**: 271–286.
Publisher Full Text

Van der Meer DG, Scotese CR, Mills BJW, *et al.*: **Long-term Phanerozoic global mean sea level: Insights from strontium isotope variations and estimates of continental glaciation.** *Gondwana Res.* 2022; **111**: 103–121.
Publisher Full Text

Velásquez Arauna AI: *Condiciones depositacionales de la Formacién Palomares, XII Region de Magallanes.* Santiago, Chile: University of Chile; 2016; 1–155. P. 155. Bachelor's Thesis.

Verdecchia SO, Casquet C, Baldo EG, *et al.*: **Mid- to Late Cambrian docking of the Rı´o de la Plata craton to southwestern Gondwana: age constraints from U–Pb SHRIMP detrital zircon ages from Sierras de Ambato and Velasco (Sierras Pampeanas, Argentina).** *J. Geol. Soc. Lond.* 2011; **168**: 1061–1071.
Publisher Full Text

Von Gosen W, Buggisch W, Dimieri LV: **Structural and metamorphic evolution of the Sierras Australes (Buenos Aires Province/Argentina).** *Geol. Rundsch.* 1990; **79**(3): 797–821.
Publisher Full Text

Von Gosen W, Loske W, Prozzi C: **New isotopic dating of intrusive rocks in the Sierra de San Luis (Argentina): implications for the geodynamic history of the Eastern Sierras Pampeanas.** *J. S. Am. Earth Sci.* 2002; **15**: 237–250.
Publisher Full Text

Wang L, Jin Z, Chen X, *et al.*: **The Origin and Occurrence of Natural Hydrogen.** *Energies.* 2023; **16**: 2400.
Publisher Full Text

Walker JD, Geissman JW: **Geologic Time Scale. GSA.** 2022; 6.
Publisher Full Text

Wang C-Y, Okaya DA, Ruppert C, *et al.*: **Seismic Reflectivity of the Whipple Mountain Shear Zone in Southern California.** *J. Geophys. Res.* 1989; **94**(B3): 2989–3005.
Publisher Full Text

White SH, Burrows SE, Carreras J, *et al.*: **On mylonites in ductile shear zones.** *J. Struct. Geol.* 1980; **2**(1–2): 175–187.
Publisher Full Text

Wrobel-Daveau JC, Nicoll G, Tetley MT, *et al.*: **Plate tectonic modelling and the energy transition.** *Earth-Sci. Rev.* 2022; **234**: 104227.
Publisher Full Text

Wrona T, Fossen H, Lecomte I, *et al.*: **Seismic expression of shear zones: Insights from 2-D point-spread-function based convolution modelling.** *J. Struct. Geol.* 2020; **140**: 104121.
Publisher Full Text

Xypolias P, Chatzaras V, Beane R, *et al.*: **Heterogeneous constrictional deformation in a ductile shear zone resulting from the transposition of a lineation-parallel fold.** *J. Struct. Geol.* 2013; **52**: 44–59.
Publisher Full Text

Yao Q, Han D-H: **Acoustic properties of coal from lab measurement.** *SEG Annual Meeting, 9–14th November, Las Vegas, Nevada, USA 2008* 2008; 1815–1819.

Zanella A, Cobbold PR, Rojas L: **Beef veins and thrust detachments in Early Cretaceous source rocks, foothills of Magallanes-Austral Basin, southern Chile and Argentina: Structural evidence for fluid overpressure during hydrocarbon maturation.** *Mar. Pet. Geol.* 2014; **55**: 250–261.
Publisher Full Text